# Multiexcitons in semiconductor quantum dots

Maciej Molas

UNIVERSITÉ DE GRENOBLE

# THÈSE

Pour obtenir le grade de

## DOCTEUR DE L'UNIVERSITÉ DE GRENOBLE

Spécialité : **Physique de la Matiére Condensée et du Rayonnement**

Arrêté ministériel : 7 août 2006


Présentée par

**Maciej MOLAS**


Thèse dirigée par **Adam BABIŃSKI** et **Marek POTEMSKI**

préparée au sein du **Laboratoire National des Champs Magnétiques Intenses, CNRS, Grenoble, France** dans **l'École Doctorale de Physique de Grenoble** et au sein du **Faculty of Physics, University of Warsaw, Poland**

# Complexes multiexcitoniques dans des boites quantiques semiconductrices

Thèse soutenue publiquement le **14 Novembre 2014**,
devant le jury composé de :

**Professeur, José Manuel Calleja**
Universidad Autónoma de Madrid, Rapporteur
**Professeur, Piotr Kossacki**
Faculty of Physics, University of Warsaw, Rapporteur
**Directeur de recherche, Henri Mariette**
Institut NÉEL, CNRS, Grenoble, France, Examinateur
**Chercheur, Aurélien Nicolet**
LNCMI-CNRS, Grenoble, France, Examinateur
**Professeur, Arkadiusz Wójs**
Faculty of Fundamental Problems of Technology, Wroclaw University of Technology, Examinateur
**Professeur, Andrzej Wysmołek**
Faculty of Physics, University of Warsaw, Examinateur
**Professeur, Adam BABIŃSKI**
Faculty of Physics, University of Warsaw, Co-Directeur de thèse
**Directeur de recherche, Marek POTEMSKI**
LNCMI-CNRS, Grenoble, France, Directeur de thèse

University of Warsaw

Université de Grenoble

Maciej Molas

# Multiexcitons in semiconductor quantum dots



PhD thesis supervised by
dr hab. Adam Babiński and dr Marek Potemski

14.11.2014

*I dedicate this thesis to my mother*

# Acknowledgements

*The following PhD thesis was performed under the "co-tutelle" convention between the Université Joseph Fourier in Grenoble, France, and the University of Warsaw in Warsaw, Poland. First of all, I would like to thank my PhD supervisors - Adam Babiński and Marek Potemski, who were constantly guiding me during the years of my PhD. I would like to thank them for many encouraging words, invaluable support, every-day understanding and proofreading this manuscript. Their help cannot be overestimated.*

*The work presented in this thesis was carried out at the National High Magnetic Field Laboratory in Grenoble, in France, and at the Division of Solid State Physics of the University of Warsaw, in Poland. I thank all my colleagues from both research groups. In particular, I thank Aurélien Nicolet for the priceless help in the experimental work, fruitful discussions and the acceptance to participate in the jury for my defence. I also thank Katarzyna Gołasa for the great atmosphere in our Warsaw's group. I appreciate help of Ivan Breslavetz with all the scientific equipment in the laboratory.*

*It is my pleasure to thank Prof. José Manuel Calleja and Prof. Piotr Kossacki for the agreement to be the referees of my thesis and Prof. Henri Mariette and Prof. Andrzej Wysmołek for the acceptance to participate in the jury for my defence.*

*I would also like to thank all the administrative, IT, and technical staff in Grenoble and Warsaw. Here, I would like to distinctly express my gratitude to Olga Babicka, Alexandra Gasparini, Amélie Pic, Elisabeth Rochat, Aline Schwoob, and Małgorzata Trippenbach, who often helped me to go through all the administrative paperwork.*

*I would like to thank all the people from the University of Warsaw and the National High Magnetic Field Laboratory, who were not involved in my research, but with whom I have spent this great time: Marcin Białek, Clément Faugeras, Ignas Grigelionis, Younnes Heni, Maciej Koperski, Joanna Papierska, Paulina Perkowska, and Dominika Ziółkowska. I would also like to express my special gratitude to: Johannes Binder for nice time with a cup of coffee; Przemysław Leszczyński for long discussions about life; Karol Nogajewski for encouraging me to hike the mountains; Milan Orlita for interesting discussions during the lunch time; Barbara Piętka for the help in the first days in Grenoble and introducing me to the subject of quantum dots I was studying.*

*I kindly acknowledge the Foundation for Polish Science International PhD Projects Programme co-financed by the EU European Regional Development Fund and the National Science Center (decisions DEC-2013/08/T/ST3/00665 and DEC-2013/09/N/ST3/04237) for the financial support for my PhD.*

*Finally, I would like to thank my Father, my Brother, my Sister, my Aunt and my whole Family for their support and love.*

*Dear Marta, Thank you for your endurance over the last months, for your unfailing support and for your endless encouragement. We did this together. Thank you for sharing your life with me.*

***Dziękuję bardzo! Merci beaucoup! Thank you very much!***

# Abstract

In spite of about 25 years of intense research efforts, the semiconductor quantum dots remain to attract a relevant scientific interest and continue to surprise with new and interesting physical properties. Great part of this research has been devoted to optical studies of single objects, which also hold for the subject of this work. It is perhaps surprising, though the main body of optical studies of single quantum dots has been so far focused on emission spectroscopy (photoluminescence) and has been largely related to the recombination of rather simple electron-hole complexes such as excitons (neutral and charged) and biexcitons. Strongly confined quantum dots, such as those studied in this work, may, however, accommodate a large number of (photo-excited) carriers. The studies of energy levels and of recombination processes of single quantum dots, optically filled with up to four electron-hole pairs are the subject of this work. The dots used in the present experiments, formed out of the Ga(Al)As matrix, represent relatively strongly confined zero-dimensional systems, and display several, atomic-like *s*-, *p*-,...shells. The studied dots are fairly bright, their optical response is within a suitable spectral range covered by efficient CCD detectors and accessible with the Ti:Sapphire laser. Single dots can be easily selected in our structures as they exhibit an extremely low surface density ($\sim 10^6$ cm$^{-2}$). Experimental techniques applied in this work include the methods of single dot spectroscopy, polarization (when necessary linear or circular) resolved techniques, application of (high, up to 28 T) magnetic fields and photon correlation measurements. Distinct, below- and above-dot-barrier laser excitation has been used for photoluminescence experiments. Importantly, the photoluminescence excitations experiments (in magnetic fields) have been carried out, as well.

Depending on excitation conditions (power and wavelength of laser), the investigated dots show a multitude of relatively sharp lines, each dot

displaying the same, characteristic pattern of lines, grouped into distinct clusters corresponding to subsequent atomic-like shells. Spectral range covering the *s*- and *p*-shells region has been explored in the present studies. The assignment of spectral lines (identification of electron-hole complexes, carriers number and levels occupation, involved in the initial- and final-state of the recombination process) has been at large provided by the results of polarization (linear) resolved micro-photoluminescence and photon correlation experiments. Those experiments depict three distinct families of emission lines, each related to recombination of, correspondingly, neutral, positively charged and negatively charged electron-hole (excitonic) complexes. The emission lines observed within a four step cascade of a neutral quadexciton down to the recombination of a neutral exciton and two step cascades of positively charged biexcitons down to the recombination of a singlet and triplet state of positively charged excitons have been studied in details. The fine structure, induced by exchange interactions and preliminarily seen in (linear) polarization resolved emission experiment at zero magnetic field, has been studied for various emission lines (related to *s*- and *p*- shells). The evolution of this splitting has been then investigated as a function of the magnetic field. The results are interpreted in terms of the shape anisotropy of dots and an interplay between spin- and orbital-mediated effects, characteristic of different recombination processes. A significant portion of this work has aimed to compare the emission spectra measured at a relatively high excitation power (which include the recombination processes of up to quadexciton complexes) with photoluminescence excitation spectra (which probe the excited states of a single exciton). Such experiments have been also carried out as a function of the magnetic field. As expected the emission spectra of high order excitonic complexes are indeed greatly affected by Coulomb interactions between carriers and in consequence are in general very different from the photoluminescence excitation spectra (quasi absorption) of a neutral and charged exciton. Two types of the magnetic field evolution of detected absorption lines (resonant peaks), the *s*- and *p*-shell related, have been measured. The *s*-shell like resonant peaks were attributed to the transition between the excited hole levels in the valence band and the ground *s*-shell level in the conduction band. Nevertheless, there exists an emission line which is observed within the *p*-shell cluster, and which coincides with the absorption line. That "coinciding resonance" is concluded to be an excited excitonic state which recombines radiatively due to efficient blocking of its relaxation towards the ground state.

The manuscript is organized into 9 chapters.

- **Chapter 1** is thought as a very brief introduction to the subject of single semiconductor quantum dots and presentation of the motivation of this work.

- **Chapter 2** contains a description of general and most important properties of carriers confined in zero-dimensional systems - quantum dots. Simplified models of their energy structures including the effects of magnetic field are presented and basic description of the fine structure is given.

- Basic information on the sample and main characteristic properties of the dots studied in this work are presented in **Chapter 3**.

- In **Chapter 4** the experimental techniques applied in this work are presented. Micro-PL and the micro-PLE setups, including the one for the polarization-resolved measurements and operated in external magnetic field, are described. The setup dedicated to studies of photon correlations is also presented.

- An overview of emission spectra and basic classification of the observed lines is presented in **Chapter 5**. The effects of excitation conditions (laser power, below- or above barrier excitation) and application of magnetic fields are presented. Shell energy structure of the investigated dots is discussed. The identification of three different families of the observed emission lines, each related to neutral, positively charged and negatively charged excitons is provided from the results of photon correlation experiments.

- In **Chapter 6** the detailed properties of emission lines which belong to the neutral excitonic family are presented. The fine structure, the diamagnetic shift, and the Zeeman effect of these lines are studied. The magnetic-field-dependent micro-photoluminescence excitation spectra are presented, and the origin of resonant peaks is analysed.

- **Chapter 7** focuses on the identification and analysis of properties of positively charged states related to the $s$- and $p$-shell emissions. The magnetic-field-dependent micro-photoluminescence excitation spectra are also studied and the observed resonant peaks are identified.

- **Chapter 8** presents briefly the attribution and the fine structure of the negatively charged states. The origin of the emission lines is investigated.

- **Chapter 9** concludes the work. The most important results obtained in this work are listed.

# Résumé

Malgré vingt-cinq années d'intenses efforts de recherche, les boîtes quantiques semi-conductrices continuent de surprendre et de révéler de nouvelles propriétés physiques. Une partie importante de ces recherches s'est concentrée sur l'étude optique d'objets individuels, ce qui est aussi le cas de ce travail. Ces études ont jusqu'alors été axées sur la spectroscopie d'émission (photoluminescence) due aux recombinaisons de complexes électron-trou relativement simples – tels les excitons (neutres et chargés) et les bi-excitons. Les boîtes quantiques fortement confinées – comme celles examinées dans ce travail – peuvent accueillir un nombre beaucoup plus important de porteurs (photo-excités). Le présent travail se concentre sur l'étude des niveaux d'énergie et des processus de recombinaison de complexes excitoniques larges – jusqu'à quatre paires électron-trou – considérés au niveau d'une boîte quantique unique remplie optiquement. Les boîtes étudiées dans ces expériences, formées à partir d'une matrice de Ga(Al)As, représentent un système à zéro dimension avec un confinement relativement fort et peuvent en effet avoir plusieurs couches électroniques $s$, $p$, $d$, comme dans le cas d'atomes. Elles sont relativement lumineuses et leur réponse optique se situe dans un intervalle spectral adapté à la fois au domaine spectrale de sensibilité d'un détecteur CCD et à la gamme d'énergie accessible avec un laser titane:saphir. Les boîtes peuvent être facilement sélectionnées à l'état individuel du fait de la très faible densité de surface des structures considérées ($\sim 10^6$ cm$^{-2}$). Les techniques expérimentales utilisée dans ce travail comprennent : les méthodes de spectroscopie sur boîtes uniques, la détection optique résolue en polarisation (soit rectiligne, soit circulaire), l'utilisation de champs magnétiques intenses (jusqu'à 28 T) et des mesures de corrélation de photons. En ce qui concerne les expériences de photoluminescence, nous avons distingué les excitations en dessous de la barrière de celles se produisant en dessus. Finalement, des expériences de

spectroscopie d'excitation de la photoluminescence ont aussi été réalisées en champ magnétique.

En fonction des conditions d'excitation (longueur d'onde et puissance du laser), les boîtes étudiées présentent une multitude de raies relativement étroites, chaque boîte révélant un schéma caractéristique de raies groupées en amas distincts, similaires à une série de couches électroniques pour un atome. La présente étude s'est concentrée sur l'intervalle spectral correspondant aux couches électroniques $s$ et $p$. L'identification des raies spectrales (complexes électron-trou, nombres de porteurs et niveaux d'occupation participant aux états initiaux et finaux des processus de recombinaison) s'est principalement basé sur les résultats obtenus lors d'observations résolues en polarisation (rectiligne) ou bien lors de mesures de corrélation de photons. Ces expériences révèlent trois familles distinctes de raies d'émission, chacune étant respectivement reliée à un complexe électron-trou (excitonique) neutre, chargé positivement, ou bien négativement. Une attention particulière a été portée aux raies d'émission observées dans une cascade en quatre étapes partant d'un complexe à quatre excitons, jusqu'au niveau de la recombinaison d'un exciton neutre, ainsi que celles observées dans une cascade en deux étapes partant d'un bi-exciton chargé positivement, jusqu'à la recombinaison d'un état singulet ou triplet d'un exciton chargé positivement. La structure fine induite par les interactions d'échange – et préalablement observée lors des mesures résolues en polarisation (rectiligne) à champ magnétique nul – a été étudiée pour différentes raies d'émission (reliées aux couches $s$ et $p$). L'évolution de ce dédoublement de raies a été examiné en fonction du champ magnétique. Les résultats sont interprétés en terme d'anisotropie de forme des boîtes et d'une interaction avec les effets spin-orbite, caractéristiques des différents processus de recombinaison. Une partie importante de ce travail a été dévolue à la comparaison entre le spectre d'émission mesuré pour des puissances d'excitations relativement importantes (ce qui inclus les processus de recombinaison jusqu'aux complexes formés de quatre excitons) avec les spectres d'excitation de la photoluminescence (qui sonde les états excités d'excitons simples). De telles expériences ont aussi été conduites sous champ magnétique. Comme attendu, les spectres d'émission des complexes excitoniques d'ordres élevés sont particulièrement affectés par les interactions coulombiennes entre porteurs, et sont par conséquent très différents des spectres d'excitation de la photoluminescence (quasi-absorption) des excitons neutre et chargés. Deux types d'évolution en champ magnétique de raies d'absorption observées (résonance) – reliées aux couches $s$ et $p$ – ont été mesurés. Les résonances de

type $s$ sont attribuées à la transition entre un niveau excité de trou de la bande de valence et l'état fondamental de la couche $s$ dans la bande de conduction. Une raie d'émission, observée dans le groupement de la couche $p$, coïncide cependant avec la raie d'absorption. Nous concluons que cette résonance vient d'un état excitonique excité qui se recombine de manière radiative dû à un blocage efficace de sa relaxation vers l'état fondamental.

Le présent manuscrit est organisé en 9 chapitres.

- Le **Chapter 1** est vue comme une brève introduction aux boîtes quantiques semi-conductrices considérées à l'état individuel. Les enjeux et motivations d'une telle recherche sont présentés.

- Le **Chapter 2** se consacre aux propriétés générales ainsi qu'aux aspects fondamentaux des porteurs de charges confinés dans un système à zéro-dimension – la boîte quantique. Un modèle simplifié de leur structure en énergie prenant en compte les effets d'un champ magnétique est exposé. Une description élémentaire de la structure fine est aussi donnée.

- Le **Chapter 3** regroupe quant à lui les propriétés caractéristiques de l'échantillon et des boîtes étudiées.

- Le **Chapter 4** est dédié aux techniques et montages expérimentaux utilisés : photoluminescence et excitation de la photoluminescence, mesures résolues en polarisation, corrélation de photons, application de champs magnétiques.

- Dans le **Chapter 5**, nous présentons des spectres d'émission typiques et nous classifions les raies spectrales observées. Nous évoquons aussi les effets dus aux conditions d'excitation (longueur d'onde, puissance laser) et au champ magnétique. Nous discutons alors de la structure en énergie des différentes couches électroniques des boîtes étudiées. Les mesures de corrélation de photons nous permettent d'identifier trois familles distinctes de raies d'émissions, chacune reliée aux excitons neutres, positifs, ou négatifs.

- Le **Chapter 6** nous permet de détailler les propriétés des raies d'émissions relevant de la famille excitonique neutre. Nous étudions par la suite la structure fine de ces raies spectrales ainsi que les effets diamagnétiques et Zeeman. La dépendance en champ magnétique des spectres d'excitation de la photoluminescence nous conduit à analyser l'origine des différents pics résonants observés.

- Le **Chapter 7** traite de l'identification et de l'analyse des propriétés des états chargés positivement reliés aux couches $s$ et $p$. C'est à nouveau en considérant la dépendance en champ magnétique des spectres d'excitation de la photoluminescence que nous identifions les différents pics résonants observés.

- Le **Chapter 8** se concentre sur l'attribution des états chargés négativement ainsi que sur l'étude de leurs structures fine. Nous examinons l'origine de ces raies d'émissions.

- Le **Chapter 9**, dernier chapitre, conclut ce travail. Les principaux résultats sont alors résumés.

# Streszczenie

Pomimo około 25 lat intensywnych prac badawczych, półprzewodnikowe kropki kwantowe wciąż cieszą sią szerokim zainteresowaniem naukowym i nadal zaskakują nowymi oraz ciekawymi właściściami fizycznymi. Duża część przeprowadzonych na nich do tej pory badań została poświęcona pomiarom optycznym pojedynczych obiektów, które są również tematem tej pracy. Zdumiewające jest w pewnym stopniu to, że główny nurt badań optycznych pojedynczych kropek kwantowych był dotychczas skoncentrowany na spektroskopii emisyjnej (fotoluminescencji) i opierał się w dużej mierze na rekombinacji prostych kompleksów elektron-dziura, takich jak ekscyton (neutralny i naładowany) oraz biekscyton. Kropki kwantowe z silnym uwięzieniem kwantowym, takie jak te, którymi zajmowano się w ramach niniejszej pracy, mogą jednak pomieścić dużą liczbę (fotowzbudzonych) nośników. Badania poziomów energetycznych i procesów rekombinacji pojedynczych kropek kwantowych, wypełnionych optycznie maksymalnie czterema parami elektron-dziura są tematem bieżącej pracy. Będące przedmiotem rozważań kropki, wytworzone w matrycy GaAlAs, stanowią systemy zerowymiarowe o stosunkowo silnym potencjale wiążącym i ukazują kilka kwazi-atomowych powłok: $s$, $p$, $d$. Są one dość jasnymi obiektami, a ich emisja optyczna przypada na obszar widma promieniowania elektromagnetycznego, który pokrywa się z zakresem czułości wydajnych detektorów CCD oraz jest dostępny przy użyciu lasera tytan-szafir. Poszczególne kropki można łatwo wybrać w analizowanej strukturze, ze względu na ich bardzo niską gęstość powierzchniową ($\sim 10^6$ cm$^{-2}$). Stosowane w tej pracy techniki eksperymentalne obejmują metody spektroskopii pojedynczych kropek kwantowych wykorzystujące rozdzielczość polaryzacyjną (liniową lub w razie potrzeby kołową), zewnętrzne pola magnetyczne, w tym wysokie - do 28 T oraz pomiary korelacji fotonów. Wyróżnione są dwa obszary energii lasera pobudzającego kropki, poniżej oraz powyżej bariery, które mają

wpływ na wyniki eksperymentów fotoluminescencyjnych. Istotne są również przeprowadzone badania pobudzania fotoluminescencji (w polu magnetycznym).

W zależności od warunków pobudzania (mocy lasera i długości fali), w widmach badanych kropek pojawia się wiele ostrych linii, przy czym każda kropka ma bardzo charakterystyczny, identyczny układ linii, pogrupowanych w różne serie, odpowiadające kolejnym kwazi-atomowym powłokom. Prezentowane w niniejszej pracy badania obejmują zakres widmowy, ktory zawiera w sobie region powłok $s$ i $p$. Przypisanie linii widmowych (identyfikacja kompleksów elektron-dziura, liczby nośników oraz obsadzonych poziomów energetycznych, odpowiadających za stan początkowy oraz końcowy w procesie rekombinacji) zostało głównej mierze oparte na wynikach pomiarów mikroluminescencji przeprowadzonych z rozdzielczością polaryzacyjną (liniową) oraz eksperymencie korelacji pojedynczych fotonów. Wyniki tych badań ukazują trzy różne rodziny linii emisyjnych z ktŕych każda związana jest z rekombinacją odpowiednio: neutralnych, naładowanych dodatnio i naładowanych ujemnie kompleksów ekscytonowych (elektron-dziura). Szczegółowo badane są w tej pracy linie emisyjne, obserwowane w ramach czerostopniowej kaskady rekombinacji neutralnego kwadryekscytonu do neutralnego ekscytonu oraz w ramach dwuetapowych kaskad rekombinacji dodatnio naładowanych biekscytonów do stanu singletowego i trypletowego dodatnio naładowanego ekscytonu. Wynikająca z oddziaływania wymiennego struktura subtelna, która w eksperymencie ujawnia się jako (liniowo) spolaryzowana emisja w zerowym polu magnetycznym, jest analizowana dla różnych linii emisyjnych (związanych z powłoką $s$ i $p$). Badaniom poddany jest również wpływ pola magnetycznego na to rozszczepienie. Interpretacja wyników uwzględnia anizotropię kształtu kropek oraz oddziaływania związane z charakterystycznymi dla różnych procesów rekombinacji efektami spinowymi i orbitalnymi. Znaczna część pracy jest poświęcona porównaniu widm emisyjnych mierzonych przy stosunkowo dużej mocy pobudzania (które obejmują procesy rekombinacji aż z kompleksu kwadryekscytonowego) z widmami pobudzania fotoluminescencji (które próbkują stany wzbudzone pojedynczych ekscytonów). Tego rodzaju eksperymenty zostały przeprowadzone także w funkcji pola magnetycznego. Zgodnie z oczekiwaniami, widma emisyjne kompleksów wieloekscytonowych są modyfikowane przez oddziaływane kulombowskie między nośnikami, w związku z czym na ogół znacznie różnią się od widm pobudzania fotoluminescencji (kwazi-absorcji) neutralnego oraz naładowanego ekscytonu. Dwa rodzaje dyspersji linii absporcyjnych (rezonansów) w polu magnety-

cznym, charakterystyczne dla powłoki $s$ i $p$, zostały zaobserwowane. Rezonanse o dyspersji powłoki $s$ są przypisane przejściom między wzbudzonymi stanami dziurowymi w paśmie walencyjnym a podstawowym poziomem powłoki $s$ w paśmie przewodnictwa. Tym niemniej istnieje linii emisyjna, która jest obserwowana w zakresie emisji z powłoki $p$ i która pokrywa się z linią absorpcyjną. Ten "pokrywający się rezonans" jest identyfikowany jako wzbudzony stan ekscytonowy, który rekombinuje promieniście ze względu na efektywną blokadę jego relaksacji do poziomu podstawowego.

Praca jest podzielona na 9 rozdziałów.

- **Rozdział 1** jest krótkim wprowadzeniem do tematu pojedynczych półprzewodnikowych kropek kwantowych oraz prezentuje motywację pracy.

- **Rozdział 2** zawiera opis najważniejszych ogólnych właściwości nośników uwięzionych w zerowymiarowych systemach - kropkach kwantowych. Prezentowane są w nim ponadto uproszczone modele ich struktury energetycznej, w tym uwzględniające wpływ pola magnetycznego są, jak również podstawowy opis struktury subtelnej.

- Podstawowe informacje dotyczące próbki oraz główne charakterystyczne właściwości kropek badanych w tej pracy są zaprezentowane w **Rozdziale 3**.

- W **Rozdziale 4** omówione są techniki eksperymentalne, które zostały zastosowane w niniejszej pracy. Zawarty w nim opis obejmuje układy do pomiarów mikrofotoluminescencji oraz pobudzania mikrofotoluminescencji, w tym umożliwaniające prowadzenie badań z rozdzielczością polaryzacyjną oraz w zewnętrznym polu magnetycznym, a także przeznaczony do badań korelacji pojedynczych fotonów jest również zaprezentowany.

- Przegląd widm emisyjnych oraz podstawowa klasyfikacja obserwowanych linii jest przedstawiona w **Rozdziale 5** z uwzględnienem wpływu warunków pobudzania (mocy lasera, pobudzanie powyżej oraz poniżej

bariery) oraz zastosowania pola magnetycznego. Omówiona jest ponadto struktura energetyczna powłok badanych kropek. W rozdziale tym przedstawiono również trzy rodziny obserwowanych linii emisyjnych, związanych z neutralnymi oraz naładowanymi dodatnio i ujemnie ekscytonami.

- W **Rozdziale 6** są zaprezentowane szczegółowe właściwości linii emisyjnych, które należą do neutralnej rodziny ekscytonowej z uwzględnieniem ich struktury subtelnej, przesunięcia diamagnetycznego oraz efektu Zeemana. W tym rozdziale przedstawione są również widma mikro-PLE zmierzone w funkcji pola magnetycznego a pochodzenie linii rezonansowych jest poddane analizie.

- **Rozdział 7** koncentruje się na identyfikacji oraz analizie właściwości dodatnio naładowanych stanów związanych z emisją z powłoki $s$ oraz $p$. Zaprezentowana jest w nim dyskusja widm mikro-PLE zmierzonych w funkcji pola magnetycznego oraz identyfikacja zarejestrowanych linii rezonansowych.

- **Rozdział 8** krótko przedstawia przypisanie i strukturę subtelną ujemnie naładowanych stanów. Przedmiotem dyskusji jest w nim pochodzenie zaobserwowanych linii emisyjnych.

- **Rozdział 9** podsumowuje pracę. Są w nim wymienione najżniejsze wyniki, jakie zostały w jej ramach uzyskane.

# Contents

**Contents** xxi

**Symbols and abbreviations** xxiii

**1 Introduction** 1

**2 Quantum dot - a zero-dimensional object** 5
- 2.1 Quantum confinement . . . 5
- 2.2 Excitons in a quantum dot . . . 12
  - 2.2.1 Neutral exciton state . . . 13
    - 2.2.1.1 Fine structure splitting . . . 14
    - 2.2.1.2 Magnetic field dispersion . . . 14

**3 Investigated structure** 17
- 3.1 GaAs/AlAs type II double quantum wells . . . 18
- 3.2 GaAlAs quantum dots . . . 19

**4 Experimental techniques** 21
- 4.1 Micro-photoluminescence . . . 21
  - 4.1.1 Micro-PL setups . . . 21
  - 4.1.2 The setup for experiments in magnetic field . . . 23
- 4.2 Micro-photoluminescence excitation . . . 24
- 4.3 Single photon correlation . . . 25

**5 Optical response of the investigated structure - overall characteristic** 27
- 5.1 PL spectrum of the studied sample . . . 27
- 5.2 Above-barrier versus quasi-resonant excitation . . . 29
- 5.3 Excitonic shells . . . 31

5.4 Description of the excitonic families . . . . . 35
5.5 Changes of the QD charge . . . . . 41
5.6 Conclusions . . . . . 44

**6 Neutral excitonic states 45**
6.1 Micro-PL spectra vs the excitation power . . . . . 46
6.2 Fine structure splitting . . . . . 47
6.2.1 FSS of the X emission . . . . . 52
6.3 Magnetic field effects . . . . . 55
6.3.1 Diamagnetic shift . . . . . 55
6.3.2 Zeeman splitting . . . . . 56
6.4 Photoluminescence excitation . . . . . 60
6.4.1 PLE spectra in a magnetic field . . . . . 64
6.4.2 Origin of PLE peaks . . . . . 70
6.5 Conclusions . . . . . 73

**7 Positively charged excitonic states 75**
7.1 Optical recombination of the positively charged excitons . . 75
7.2 The effect of magnetic field . . . . . 80
7.3 Photoluminescence excitation . . . . . 84
7.3.1 PLE spectra in magnetic field . . . . . 88
7.3.2 Origin of PLE peaks . . . . . 95
7.3.3 The resonant peak corresponding to the emission line 97
7.4 Conclusions . . . . . 103

**8 Negatively charged excitonic states 105**
8.1 Identification and properties of emission lines . . . . . 105
8.2 Photoluminescence excitation . . . . . 107
8.3 Conclusions . . . . . 109

**9 Conclusions 111**

**A List of publications 113**

**Bibliography 115**

**List of Figures 129**

**List of Tables 138**

# Symbols and abbreviations

| Abbreviation | Description |
|---|---|
| MBE | molecular beam epitaxy |
| PL | photoluminescence |
| PLE | photoluminescence excitation |
| CW | continuous wave |
| $\lambda$ | wavelength |
| M | magnification |
| NA | numerical aperture |
| g/mm | grooves/mm |
| CCD | charge-coupled device |
| FWHM | full width at half maximum |
| $P_{exc}$ | excitation power |
| $E_{exc}$ | excitation energy |
| 2D | two-dimensional |
| 0D | zero-dimensional |
| QW | quantum well |
| QD | quantum dot |
| HH | heavy hole |
| LH | light hole |
| $ee$ | electron-electron |
| $hh$ | hole-hole |
| $e$-$h$ ($eh$) | electron-hole |
| SP | single-particle |
| 2D | two-dimensional |
| FD | Fock-Darwin |
| FSS | fine structure splitting |
| X | neutral exciton |
| $X^-$ | negatively charged exciton |

| Abbreviation | Description |
|---|---|
| $X^+$ | positively charged exciton |
| 2X | biexciton |
| LO | longitudinal optical phonon |
| $e_s$ ($h_s$) | $s$-shell electron (hole) |
| $e_p$ ($h_p$) | $p$-shell electron (hole) |
| $\tau_r$ | relaxation time of carrier |
| $\tau_s$ | spin flip time |

# Chapter 1

# Introduction

For many years, semiconductor ***quantum dots*** (QDs) have been at the heart of intensive research driven by their potential for practical applications as well as an input to the nanoscale physics they provide [1–3]. A worldwide interest they arouse is deeply connected with their "atomic-like" nature and the compatibility with modern semiconductor-based microelectronics and optoelectronics. The combination of these features makes QDs very promising candidates for building blocks of future devices, such as, for example, highly desirable single-photon emitters [4]. Moreover, the predicted suppression of carrier relaxation rates in semiconductor QDs as compared to quantum wells has motivated the study of the QDs carrier relaxation mechanisms and stimulated the development of the QD-based optoelectronic devices that are capable of operating over a broad range of wavelengths [5]. In particular, QDs are considered as an active medium for emitters and detectors of THz radiation [6, 7].

The fact that QDs are often called "artificial" atoms is due to the discrete nature of their energy levels, which is a result of zero-dimensional degree of freedom for carriers [8, 9]. Because of the small volume they are confined to, all carriers in a QD (electrons and holes) strongly interact with each other via Coulomb interaction. A single electron-hole pair, confined in a dot and bound by Coulomb interaction is referred to as an *exciton*. In contrast to atoms, QDs may accommodate different number of carriers, forming multiple $e$-$h$ pairs states also known as **multiexcitons** [10, 11].

Like in atoms, the electrons and holes in the QD occupy the confined electronic shells. These shells, which are usually degenerate due to geometrical and dynamical symmetries are often referred to as $s$, $p$, $d$ ... shells [12]. The shells can be populated with carriers according to Pauli principle. In the spectra, a number of distinct emission and characteristic features appear, which correspond to the re-

combination of multiexcitons from various confined shells. In each degenerate shell, the electrons and holes quickly relax into a quasi-equilibrium state in which they represent a spatially confined many-particle system. It resembles the situation met in atoms, however, the advantage is that the eventual radiative decay of this state offers a convenient way to probe the complexity of multi-particle correlations. The most known example is a biexciton - neutral exciton cascade considered also as a source of an entangled photon pair [13, 14].

A detailed understanding of the energy levels of confined carriers in the QDs, as well as the interactions between them, is essential for implementing the potential applications mentioned above. In connection with this, the present PhD thesis has been aimed at studying the excited states of excitonic complexes, such as the neutral and charged exciton, by means of the comparison of results of two types of basic optical experiments: the photoluminescence (PL) and the photoluminescence excitation (PLE) spectroscopy.

The project has been divided into a number of steps. In the first part it was focused on investigating the main optical properties of the QDs through the identification and analysis of the excitonic complexes giving rise to the occurrence of particular lines in the emission spectra. Next, an attempt to identify the excited states has been undertaken. A few types of experiments have been performed to accomplish this task: the polarization-resolved PL and PLE measurements as a function of the laser intensity and in the presence of external magnetic field, and the polarization-resolved photon-correlation experiments.

The essential question addressed concerns the fundamental difference between the information provided by the PL and PLE experiments.

The PL is an obvious method that has been applied for years to investigate the optical emission of the $e$-$h$ complexes confined in a single QD [9, 15]. Due to the capability of a dot to accumulate numerous $e$-$h$ pairs, the measurement of the micro-PL spectrum as a function of the laser power can provide information about the number of $e$-$h$ pairs forming multiexciton. However, there is a fundamental limitation of such a method: it only allows to probe the states which are occupied by charge carriers. For example, the ground state ($s$-shell) emission can be studied when the QD is filled with 1, 2, 3,... $e$-$h$ pairs. The emission of the first excited state ($p$-shell) can be measured if the dot is populated with more than two $e$-$h$ pairs (the ground state can accommodate only two $e$-$h$ pairs), *e.g.*, the excitonic complex consisting of three $e$-$h$ pairs. It is evident that the presence of two $e$-$h$ pairs occupying the $s$-shell level in the QD has a significant impact, through the Coulomb interaction, on the energy of a whole complex of three $e$-$h$ pairs. As discussed later on in this thesis, the PL experiment gives no information about the energetic structure of levels in the valence and conduction bands. It is particularly true for the excited states of a single $e$-$h$ pair, *i.e.* a neutral exciton.

On the other hand, the PLE has rarely been used to study the energetic structure of the $e$-$h$ states in a single QDs [16]. In this experiment, the laser energy is tuned (whereas the laser power is kept at a constant power). These spectra provide information about the excited states of basic excitonic states. A proper analysis of the PLE data is complex, due to three subsequent processes: absorption, relaxation and recombination, which underlie the PLE spectrum. A solution to this problem may be provided by the comparison of results of both types of optical experiments: the PL and the PLE. The former one probes the ground energy states of the $e$-$h$ complexes in the dot, whereas the latter one gives an access to their excited states.

The physical system under study are GaAlAs/AlAs QDs, formed in a GaAs/AlAs double quantum well structure. Despite the fact that their emission is typical for QDs, they posses many properties which distinguish them from all other systems that have been investigated up to now. The distinct properties of our dots are:

- an extremely low surface density, which goes down to $\sim 10^6$ cm$^{-2}$,
- a relatively strong three-dimensional confinement providing conditions to display several atomic-like $s$-, $p$-, ... shells,
- an optical response that falls within a suitable spectral range covered by efficient CCD detectors and can be accessed with the Ti:Sapphire laser.

As already mentioned, this work is mainly focused on the excited states of the neutral and charged excitons. Because of numerous multiexcitonic lines observed within the $s$- and $p$-shell region, a detailed analysis of the emission spectra represents a challenging task of high level complexity. The characteristic optical properties of single QDs are as follows:

- The energy (below or above the barrier) of the excitation laser strongly affects the lineshape of the PL spectra of single QDs (Section 5.2).
- The emission lines observed are grouped in clusters, which are identified as the $s$-, $p_-$-, and $p_+$-shell in terms of the Fock-Darwin model (Section 5.3). However, the shells emission does not follow a typical Fock-Darwin-like evolution in a magnetic field. This results from a significant anisotropy of the confinement potential (in lateral directions) as well as from Coulomb interaction which we expect are more pronounced in our dot as compared to the case of dots with the strong quantum confinement.
- The emission lines are also related to one of the three families (the neutral, positively and negatively charged one), due to respective charge states of a QD (Section 5.4).

- The cascades resulting from a few-step recombination of multiexcitons occupying both the *s*- and *p*-shell are observed (refer to Chapters 6, 7 and 8 for details), *e.g.*, a four-step cascade starting from a neutral quadexciton and ending with recombination of a neutral exciton.

The formation process of QDs studied here is not yet well understood. Those dots appear as inclusions (defects) in a structure, originally designed as a GaAs/AlAs type II bilayer. However, it is important to stress that all the optical properties indicate that these objects display all characteristic attributes of semiconductor QDs, typically of tens of nanometers in a lateral diameter and deep potential traps (see Chapter 3 for further discussion).

# Chapter 2

# Quantum dot - a zero-dimensional object

A semiconductor quantum dot is an object of nanometer size made of a material with a narrower band gap than the band gap of the material surrounding it. This allows QDs to confine/trap charge carriers (electrons and/or holes). The energy spectrum of such confined carriers is discrete, reflecting the (quasi)-zero-dimensional nature of these objects. Due to the analogy with the energy spectrum of atoms, QDs are often called "artificial atoms".

## 2.1 Quantum confinement

The confining potential - $V(r)$ of the QD can be written as the sum of two parts:

$$V(r) = V(x, y) + V(z) \tag{2.1}$$

where $V(x, y)$ describes the confining potential in the plane $xy$, and $V(z)$ refers to the motion along the $z$-axis. The potential profile $V(z)$ can be well described by rectangular shape (characteristic a single quantum well). The in-plane confining potential $V(x, y)$ is worth more comments. In a number of cases, following the photoluminescence [10, 17], capacitance, far-infrared absorption measurements [18–20], and numerical calculations [8, 21, 22], the $V(x, y)$ potential is described by an effective two-dimensional parabolic potential, having a formula:

$$V(x, y) = \frac{1}{2} m_e^* \omega_{e,0}^2 (x^2 + y^2) \tag{2.2}$$

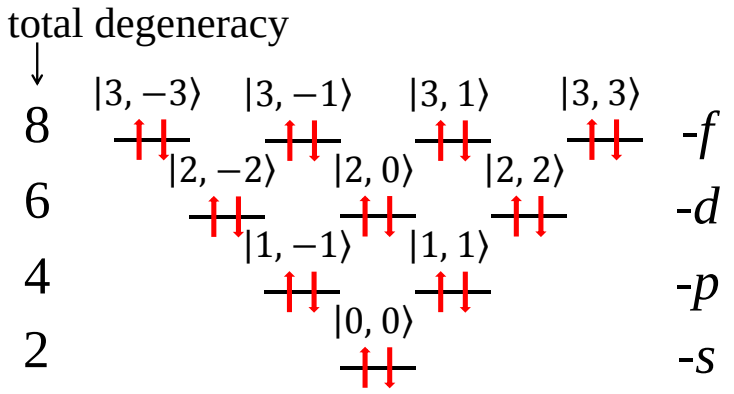


Figure 2.1: Shell structure of the SP energy spectrum, and associated total degeneracies including the angular momentum and spin.

where $m_e^*$ is the electron effective mass, and $\omega_{e,0}$ is the confinement frequency.

The discrete and energetically equidistant single-particle levels of such a dot are obtained as a simple solution of the 2D harmonic oscillator of a characteristic confinement frequency $\omega_{e,0}$ (the potential asymmetry is neglected), with a characteristic SP energy ladder given by:

$$\epsilon(n) = \hbar\omega_{e,0}(n+1) \tag{2.3}$$

These levels are referred to as $s$, $p$, $d$,..., (atomic-like) shells. The levels are numbered by an orbital quantum number $n = 0, 1, 2, 3, \ldots$ and an angular orbital quantum number $m_z = -n, -n+2, \ldots, n-2, n$. In the $|n, m_z\rangle$ representation, the $|0, 0\rangle$ state accounts for the ground state ($s$-shell), the $|1, -1\rangle$ and $|1, 1\rangle$ states for the first excited state ($p$-shell), the $|2, -2\rangle$ and $|2, 0\rangle$ and $|2, 2\rangle$ states for the second excited state ($d$-shell), and so on. The angular momentum number for the $s$-shell equals 0, but for excited shells equals: -1 and 1 for the $p$-shell, -2, 0, and 2 for $d$-shell, .... The SP shells are degenerate due to both electron quantum numbers: the angular momentum number with their characteristic onefold, twofold, threefold,..., degeneracy, respectively, and the twofold spin degeneracy of each SP level.

The parabolic profile of the $V(x, y)$ potential is certainly a rough approximation. Calculation of energy levels of dots with a more realistic potential shapes show clear departure from simple, rectangular $V(z)$ and parabolic $V(x, y)$ modelling.

For example, a comparison of the SP levels in a lens shaped InAs QD, presented in Fig. 2.2(a), and a disk shaped InAs QD, shown in Fig. 2.2(c) leads to important conclusions related to the shell degeneracy, especially in the case of hole levels. Figure 2.2(b) shows the charge distribution and energies corresponding to a few electron and hole levels in a lens shaped dot. It can be seen

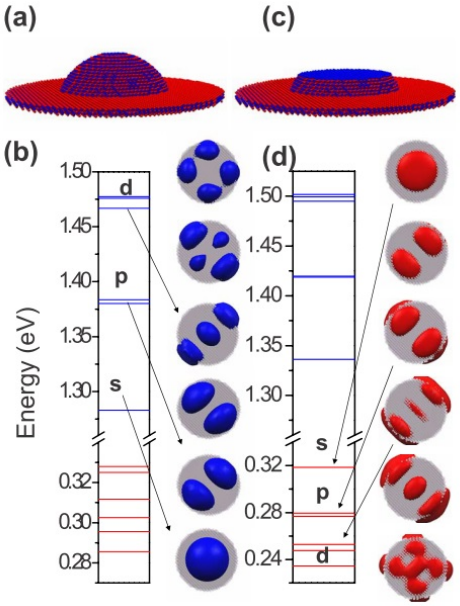


Figure 2.2: (a) lens shaped InAs QD embedded in GaAs matrix, (b) Electron probability density isosurfaces and electron and hole energies for dot (a), (c) disk shaped InAs QD (grown by the indium-flush method [23]), (d) Hole probability density isosurfaces and electron and hole energy shells for dot (c). From Ref. 22.

that the energies and envelope wave functions of electronic states are well described by the $s$, $p$, and $d$ energy shells of a 2D harmonic oscillator. However, the hole energy levels cannot be grouped anymore into quasidegenerate shells.

Figure 2.2(d) shows the energetic structure of the same dot but grown using the indium-flush technique [23], manifested in a disk shape. It is seen that the energies and envelope wave functions of electronic states are again well described by the $s$, $p$, and $d$ energy shells of a two-dimensional harmonic oscillator. In these structures, the hole energy levels can be grouped into quasidegenerate shells. This example points to the non-trivial role of a shape, composition, strain, and spin-orbit interaction in designing electronic properties of QDs. Especially, it must be keep in mind, that for hole levels, the grouping into shells might be observed only in very particular cases.

The illustration example of "simple dots" are self-assembled InGaAs/GaAs QDs. Their typical, characteristic of ensemble, micro-PL spectra (refer to Chapter 4.1 for more information) are shown in Fig. 2.3. At low excitation powers, the emission from the ground, $s$-shell as well as from the 2D wetting layer is observed. The $s$-shell is two-fold spin-degenerate, and can be occupied by not more than two excitons. Increasing the excitation power results in complete $s$-shell filling and saturates its emission. Simultaneously, the emission from the $p$-shell appears.

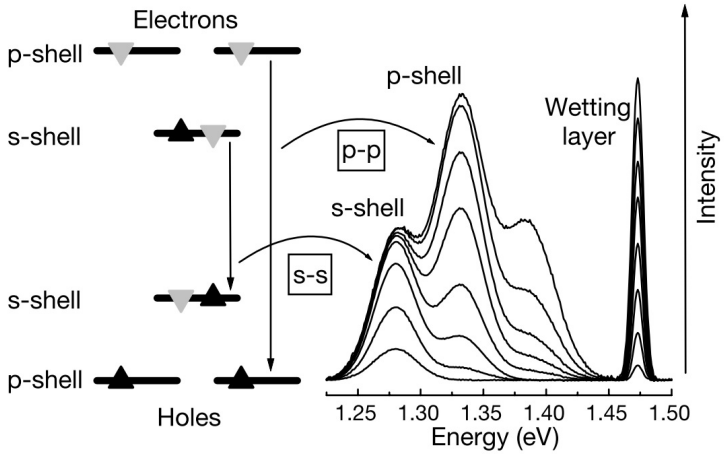


Figure 2.3: On the left-hand side is a scheme of the dot energy levels, their occupation by carriers and the radiative transitions. Spin orientations of electrons and holes: grey triangles, spin-down; black triangles, spin-up. On the right-hand side are typical photoluminescence spectra as a function of excitation power of an ensemble of $In_{0.60}Ga_{0.40}As$ QDs. From [9].

Further increasing the excitation intensity leads to the appearance of the emission of the next excited state - *d*-shell (approx. 1.39 eV, not labelled in Fig. 2.3).

The quantum confinement and electron-electron interactions in QDs can be effectively modified by the application of a magnetic field. The magnetic field applied perpendicularly to the initial 2D plane lifts the orbital degeneracy of a single harmonic oscillator, resulting in the Fock-Darwin diagram [24,25]. Notably, in the presence of the anisotropic confining potential, the shells degeneracy is also lifted both in the conduction and valence band [26,27]. The evolution of the electronic SP levels confined in the harmonic potential in the presence of the magnetic field $B$ normal to the dot plane can be expressed as:

$$\epsilon(n, m_z) = \hbar\Omega(n+1) - \frac{1}{2}\hbar\omega_c m_z \tag{2.4}$$

$$\Omega^2 = \omega_0^2 + \frac{1}{4}\omega_c^2 \tag{2.5}$$

where $\omega_0 = \omega_{e,0} + \omega_{h,0}$ is the harmonic frequency describing the strength of the in-plane parabolic confinement of an electron $\omega_{e,0}$ and a valence band hole with similarly defined frequency $\omega_{h,0}$; $\omega_c = eB/\mu^*$ is the cyclotron frequency and $\mu^*$ is the effective reduced mass of the exciton $1/\mu^* = 1/m_e^* + 1/m_h^*$.

The evolution of the energy spectrum with the magnetic field is illustrated in Fig. 2.4 (spin splitting has been neglected).

In high magnetic field, *i.e.* when $\omega_c \gg \omega_0$, the confinement of carriers into cyclotron orbits is so strong that carriers "do not feel" the confining potential

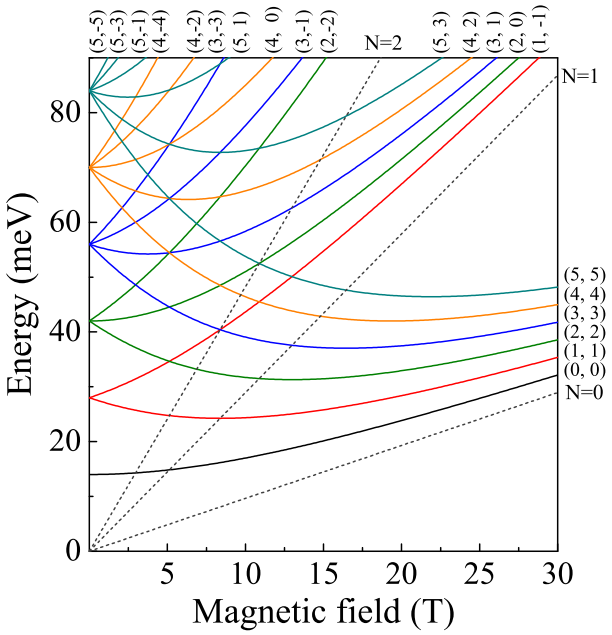


Figure 2.4: Simulated FD spectrum of the first five states in magnetic field for $\hbar\omega_0$=14 meV and $\mu^*$=0.06 $m_0$. The pairs of values in brackets correspond to the $(n, m_z)$ quantum numbers. Dashed lines present the evolution of the first three Landau levels (see Eq. 2.6).

anymore, thus behave as free carriers in a magnetic field and form Landau level bands. The energy of the Landau levels is given by:

$$\epsilon(N) = \hbar\omega_c(N + \frac{1}{2}) \tag{2.6}$$

The quantum number, N=0,1,2,..., indexes the infinite set of Landau levels.

In some specific cases, the evolution of the emission spectra of the QD with the magnetic field may resemble the SP Fock-Darwin diagram. This is in spite of the fact that the recombination processes in the dot imply significant effects of Coulomb interactions between carriers (electrons, holes) which form the complexes (multiexcitons) characteristic (in general) of the states prior and after the recombination event. Among systems which demonstrate this fortuitous agreement, are InAs QDs - see Fig. 2.5. Roughly speaking, the diagram of the Fock-Darwin type (referred to as excitonic Fock-Darwin diagram) can be used to model the field evolution of the single dot spectra in the limit of strongly confined dots, *i.e.* when the quantum confinement energy largely exceeds the electron-hole Coulomb interaction. More comments on applicability of Fock-Darwin diagrams to describe the magneto-PL spectra of QDs is discussed in Section 5.3, following the arguments presented in Ref. 10.

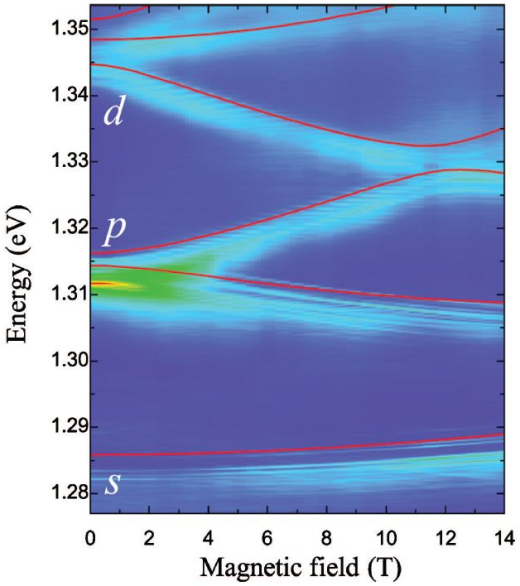


Figure 2.5: Luminescence from the $s$-, $p$-, and $d$-shell of the single InAs/GaAs QD at magnetic field up to 14 T. Red lines represent the simulation based on the excitonic Fock-Darwin diagram. From Ref. 10.

The SP wavefunctions of electrons confined in the harmonic potential can be parametrized by an effective length:

$$l_{eff} = \frac{l_0}{(1 + \frac{1}{4}(\Omega_{e,c}/\Omega_{e,0})^2)^{\frac{1}{4}}}. \tag{2.7}$$

with $l_0 = \sqrt{\frac{\hbar}{m_e^* \Omega_{e,0}}}$.

The electronic wavefunction related to the SP ground state as a function of radial distance, $r$ in the QD plane ($r^2 = x^2 + y^2$) is:

$$\psi(r)_s^e = \frac{1}{\sqrt{\pi} l_{eff}} \exp(-\frac{r^2}{2l_{eff}^2}). \tag{2.8}$$

The SP eigenstates $\psi(r)_s^e$ and energies $\epsilon(n, m_z)$ do not describe the excitations of an interacting system because they do not account for the electron-electron interactions. The Hamiltonian for the interacting electrons and holes can be written as [8, 22, 28]:

$$\begin{aligned} H = &\sum_i \epsilon_i^e c_i^+ c_i + \sum_i \epsilon_i^h h_i^+ h_i + \frac{1}{2} \sum_{ijkl} V_{ijkl}^{ee} c_i^+ c_j^+ c_k c_l \\ &+ \frac{1}{2} \sum_{ijkl} V_{ijkl}^{ee} h_i^+ h_j^+ h_k h_l - \sum_{i,j,k,l} V_{ijkl}^{eh,\mathrm{dir}} c_i^+ h_j^+ h_k c_l - \sum_{i,j,k,l} V_{ijkl}^{eh,\mathrm{exch}} c_i^+ h_j^+ h_k c_l \end{aligned} \tag{2.9}$$

The $c_i^+$ ($c_i$) and $h_i^+$ ($h_i$) operators create (annihilate) the electron or valence-band hole in the state $|i\rangle$ with the SP energy $\varepsilon_i^\beta$, with $\beta = e, h$. The two-body Coulomb matrix elements $V_{ijkl}^{ee}$, $V_{ijkl}^{hh}$, and $V_{ijkl}^{eh,\mathrm{dir}}$ describes an electron-electron, hole-hole, and electron-hole scattering, respectively. The electron-hole exchange interaction is defined by the $V_{ijkl}^{eh,\mathrm{exch}}$ element.

In the limit of symmetric interactions (a typically smaller confining potential for holes can be compensated for by their heavy mass), which corresponds to equal spatial extent of electron and hole wavefunctions [29]:

$$m_e^* \omega_{e,0} = m_h^* \omega_{h,0}, \tag{2.10}$$

The Coulomb matrix elements corresponding to carriers in the SP ground state are equal to: $V_{ijkl}^{ee} = V_{ijkl}^{hh} = V_{ijkl}^{eh,\mathrm{dir}} = V_0$, for the $ee$, $hh$, and $eh$ respectively. The matrix element $V_0$ can be found analytically then: $V_0 = Ry^* a_B^* \sqrt{2\pi}/l_0$, with the effective Rydberg $Ry^*$ and the effective Bohr radius $a_B^*$.

The order of energy scales for different energy terms changes significantly. Based on the calculations presented in Ref. 30 for InAs/GaAs QDs the energy separation between SP levels equals approximately 30 meV. The energy scale of Coulomb scattering is twice smaller (∼15 meV). The comparison values presented above with the electron-hole exchange energy (from tens to hundreds of μeV) permits neglect the last one in the most studied cases. The correction of the configuration mixing (correlation energy) due to the electron-hole scattering is substantially smaller than other energy terms. The effect of the interaction between carriers on a triexciton state (three $e$-$h$ pairs confined in a dot) is illustrated in Fig. 2.6.

QDs can be divided on two groups, due to the ratio between the radius of the dot $R$ (a lateral size) and the effective Bohr radius of the bulk exciton $a_B^*$ (a confinement):

$$a_B^* = \frac{\varepsilon}{\mu^*/m_0} a_0 \tag{2.11}$$

where $\varepsilon$ is the relative electric constant, $m_0$ is the mass of an electron, $a_0$=0.0529 nm is the Bohr radius.

For $R \gg a_B^*$ the electron and hole form a Coulomb-bound $e$-$h$ pair, a neutral exciton, whose centre-of-mass motion becomes localized and quantized in presence of the quantum confinement. The regime referred to as the weak confinement regime, and is manifested typically at monolayer fluctuations in the thickness of a semiconductor quantum well [31,32].

In the case $R \ll a_B^*$, called the strong confinement regime, confinement effects dominate over the Coulomb ones, and give rise to electron-hole states with dominant SP character. Well known representatives for III-V semiconductors are structures with self-assembled InAs/GaAs QDs [9,10,33].

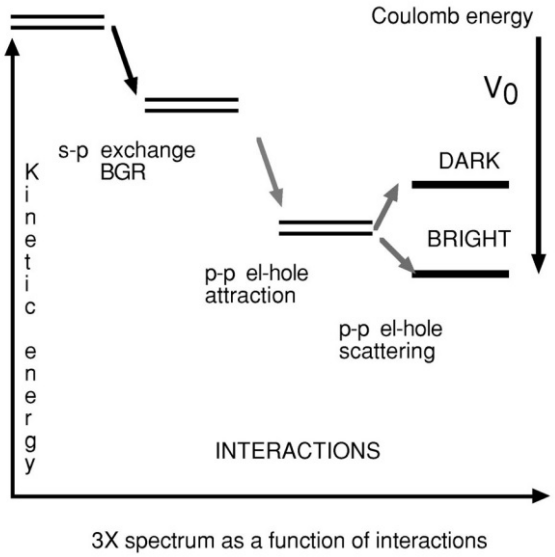


Figure 2.6: Contributions to energy levels and oscillator strength of the triexciton complex. The $s$ and $p$ letters describe the electron and hole on the $s$- and $p$ shells, respectively. From Ref. 8.

Notably, the dots investigated in the present work do not fulfil the above condition. In a case of "our dots" we estimate (see Section 3.2) that $\mu^*$=0.058 $m_0$ and $\varepsilon$=12.85, following Eq. 2.11, conclude $a_B^*$ ∼10 nm for the exciton Bohr radius. The latter value is comparable or even smaller than the lateral size of the dot, estimated ∼50 nm. Manifestations of Coulomb interaction effects are therefore expected to be more pronounced in the present systems as compared to the case of InAs QDs. Accurate description of multiexcitons in our system is more complex. Electron-electron interactions may therefore significantly deform the ladder of multiexcitons in our dots, as compared to expectations invoking the parabolic, lateral confinement. These interactions in addition to pronounced shape-anisotropy of our dots, which equally decides on non-applicability of parabolic (isotropic) potential models. One consequence of this fact is failure of the simple Fock-Darwin model to describe the magneto-PL spectra of the dots studied here (see Fig. 5.4).

## 2.2 Excitons in a quantum dot

The elementary excitonic complex is a single $e$-$h$ pair, a neutral exciton, described in details in the next Section. If the barrier of confining potential is high enough, other more complex excitonic states might be also formed in the dot. Those include charged excitons (two electrons and one hole or two holes and one electron), neutral biexcitons (two $e$-$h$ pairs), neutral triexcitons (three $e$-$h$ pairs), and so on (see Fig. 2.7). In the case of excitonic states (X, $X^+$, $X^-$, XX, ...), related to

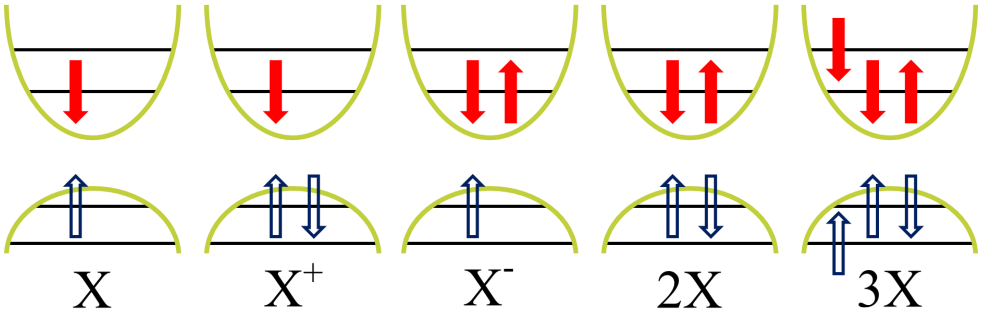


Figure 2.7: A schematic diagram of a few charge states in QD: neutral exciton (X), charged excitons ($X^+$ and $X^-$), neutral biexciton (2X) and neutral triexciton (3X). Red full and blue empty arrows represent electrons and holes, respectively. Horizontal lines in the confining potential represent two lowest energy shells.

the same ground level - $s$-shell, the energies of states are slightly different, due to the Coulomb interaction between carriers. The energy of the 3X state (which implies carriers occupying of the excited level - $p$-shell) is significantly different, due to the energy separation between the $s$ and $p$ shell levels.

### 2.2.1 Neutral exciton state

As it was mentioned before, the basic excitonic complex in the QD is the neutral exciton. In this Section, the description and typical properties of the X state, such as: the fine structure splitting, the diamagnetic shift, and the Zeeman splitting, are presented and discussed.

In QDs, due to the strain and confinement, the valence band degeneracy is lifted and heavy- and light-hole states are split in energy by at least several meV. This splitting is considerably larger than the fine structure interaction energies, and the light hole states can be neglected in most situations (compare with experimental results presented in Chapters 6 and 7). The SP states of excitons in QDs consists of an electron with spin $S_e = 1/2$, $S_{e,z} = \pm 1/2$, and a heavy hole with angular momentum $J_h = 3/2$, $J_{h,z} = \pm 3/2$.

From these states four excitons are formed, which are degenerated when the spin of carriers is neglected. These states are characterized by their total angular momentum $|M| = S_e + J_h$ and projection $M = S_{e,z} + J_{h,z}$. Two of these states, with the electron and hole spins oriented antiparallely, are optically active ($|M| = 1$). These states are called bright neutral excitons. The other two states, with the parallel spin projection of the carriers in $e$-$h$ pair, are usually not optically active ($|M| = 2$) and called dark excitons. They might be optically observed when their wave function is mixed with bright states and this can be achieved, *e.g.*, by the use of in-plane magnetic field which mixes the heavy and light hole

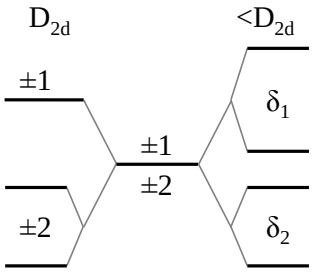


Figure 2.8: Scheme of the neutral exciton fine structure at zero magnetic field. The central part of the figure illustrates the situation when the *eh* exchange interaction is neglected ($M = \pm 1$ and $M = \pm 2$ are degenerate). The left panel shows the excitonic fine structure for QDs with $D_{2d}$ symmetry, while the right panel accounts for dots with a symmetry lower than $D_{2d}$.

states [34,35].

#### 2.2.1.1 Fine structure splitting

The fine structure of a neutral exciton at zero magnetic field arises from the exchange interaction. The general form of the spin Hamiltonian for the *eh* exchange interaction in the X state, composed of a hole with spin $J_h$ and by an electron with spin $S_e$, is given by [36,37]:

$$\mathcal{H}_{exchange} = -\sum_{x,y,z}(a_i J_{h,i} S_{e,i} + b_i J_{h,i}^3 S_{e,i}) \tag{2.12}$$

Then, due to the *eh* exchange interaction, when the confining potential is isotropic in-plane (the QD with an in-plane rotational invariance - $D_{2d}$ symmetry), the bright and dark excitons are hybridized and the splitting is described by an isotropic $\delta_0$ parameter - see the left panel of Fig. 2.8. Moreover, the bright excitons are degenerated, and the dark excitons are split into two components ($\delta_2$) independently of the QD symmetry. The dark exciton splitting is small (of the order of a few μeV) [34,38–40], and is usually neglected.

In structures with an anisotropy of the confining potential (symmetry lower than $D_{2d}$, *e.g.* $C_{2v}$ or $C_2$, when the dot shape is ellipsoidal), the splitting of the bright excitons appears and it is described by anisotropic $\delta_1$ parameter - see the right panel of Fig. 2.8. The fine structure splitting of the X state is intensively studied in view of possible application of biexciton-exciton cascade as a source of the entangled photon pair [13].

#### 2.2.1.2 Magnetic field dispersion

The application of an external magnetic field to the X state in the QD leads to the observation of two effects: a diamagnetic shift and a Zeeman spin splitting.

The magnitude of the diamagnetic shift is determined by the spatial extension of the X state wave function in the direction perpendicular to the external magnetic field. In the configuration when the magnetic field is oriented along the heterostructure growth direction ($B\|z$) the applied field confines the $e$-$h$ pairs in the $x$-$y$ plane (in-plane). A typical, flat shape of QDs implies a stronger confinement along $z$ direction (crystal growth axis) than in the lateral, in-plane directions. The application of the magnetic field, even of small magnitude in this configuration, causes additional (magnetic) confinement with significant effect.

In the limit of low magnetic fields, the energy of the X state increases quadratically with the applied magnetic field. This diamagnetic shift is characterized by a coefficient, $\gamma$, given by [41–43]:

$$\gamma = \frac{e^2}{8\mu^*}\langle\rho^2\rangle \tag{2.13}$$

where $\langle\rho^2\rangle$ is the mean square of the in-plane electron-hole separation, $\langle\rho^2\rangle = \langle\rho_{eh}^2\rangle$ in the weak-confinement limit, or the mean-square of the extent of the SP wave functions assuming equal values for the electrons and holes, $\langle\rho^2\rangle = \langle\rho_e^2\rangle = \langle\rho_h^2\rangle$ in the strong-confinement limit. In a general case, there is a competition between the lateral confinement and the Coulomb interaction. The expectation value $\langle\rho^2\rangle$ can be expressed by [43,44]:

$$\langle\rho^2\rangle = \lambda(\langle\rho_{eh}^2\rangle) + (1-\lambda)^2\langle\rho_e^2\rangle \tag{2.14}$$

where the parameter:

$$\lambda = 1 - \frac{\rho_{eh}^2}{2\langle\rho_e^2\rangle} \tag{2.15}$$

serves to characterize the relative strength of the lateral confinement and the Coulomb interaction.

Different regimes of the strength of the magnetic field can be distinguished by comparing the effective Bohr radius $a_B^*$ (see Eq. 2.11) and a magnetic length given by:

$$l = \sqrt{\frac{\hbar}{eB}} \tag{2.16}$$

As long as the magnetic length is significantly smaller than the effective Bohr radius ($l \ll a_B^*$), it is the low-field regime. Otherwise ($l \gg a_B^*$), the evolution of excitonic states in high magnetic field follows Landau levels.

Another, field induced effect, called the Zeeman spin splitting, is related to the interaction of the spins of particles with the magnetic field. In the case of neutral exciton, the initial state consists of one $e$-$h$ pair, with angular momentum projection $M{=}\pm1$, as presented in Section 2.2.1.1. The amplitude of the

Zeeman splitting ($\Delta E_Z$) in QDs is characterised by an effective Landé factor $g^*$, ($\Delta E_Z = g^* \mu_B B$) which is usually independent on magnetic field. For the bright exciton of the X state, the $g^*$ factor is given by:

$$g^* = g_e + g_h \tag{2.17}$$

where $g_e$ and $g_h$ are the Landé factor of an electron and a hole, respectively.

It must be noted that this oversimplified model of the $g^*$ factor can be broken, when a HH-LH mixing is affected by magnetic field - see Chapter 6.

When combining the orbital and spin effects, the magnetic field evolution of the X state can be written as [34]:

$$E_{\mathrm{X}}(B) = E_0 \pm \frac{1}{2}\sqrt{\delta_1^2 + g^* \mu_B B^2} + \gamma B^2 \tag{2.18}$$

where $E_0$ is the exciton energy at zero magnetic field, $\delta_1$ is the FSS of two bright X components (see Section 2.2.1.1), $g^*$ is the effective Landé factor of the X state, $\mu_B$ is the Bohr magneton and $\gamma$ is the diamagnetic coefficient.

Eq. 2.18 also implies that in low magnetic field, where $\delta_1$ is comparable with the magnitude of the Zeeman splitting, the non-linearity appears. At higher fields the dependence is linear as function of the external magnetic field.

# Chapter 3

# Investigated structure

This Chapter contains a general description of the sample with GaAlAs quantum dots, which was used for the investigations presented in this work. Dots appear in our sample as unintentional defects" in a type II GaAs/AlAs structure.

Section 3.1 describes the GaAs/AlAs double quantum well system, the position of the energy states and the symmetry of the bands. Next, the detailed description of the potential distribution and symmetry of the bands in QDs is presented in Section 3.2.

The studied sample was grown at the Laboratoire de Microstructures et de Microélectronique, CNRS, in Bagneux, France by R. Planel by the MBE method. The nominal structure of the investigated sample is presented in Fig. 3.1.

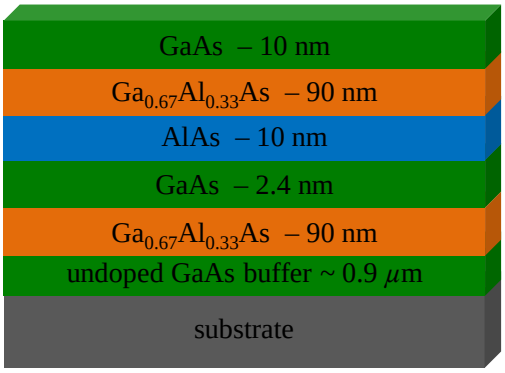


Figure 3.1: The nominal structure of the investigated sample.

## 3.1 GaAs/AlAs type II double quantum wells

A type II quantum well, in the configuration of spatially separated electron and hole, can be achieved in GaAs/AlAs double layer structures by the appropriate choice of the width of the GaAs and AlAs layer [45, 46]. The energies of the $X$ and $\Gamma$ conduction band in GaAlAs layer strongly depend on the composition of Al atoms [47]. The symmetry of the lowest energy band for GaAs is $\Gamma$-type and for AlAs is $X$-type. In the GaAs/AlAs QW system, due to the confinement, the $\Gamma$ band minimum of the GaAs conduction band can be pushed up in energy in comparison with the GaAs bulk material by reducing the width of the GaAs layer. Therefore, the lowest energy level of the conduction band is the $X$-band eigenstate in the AlAs layer. The upper energy level of the valence band is always of $\Gamma$-symmetry, in GaAs. As a result, the spatially separated electron and hole system can be achieved. An additional effect is the splitting of the $X$-band eigenstate in the AlAs layer into $X_{XY}$- and $X_Z$-symmetry eigenstates related to the strain that is induced by a small lattice mismatch [48]. In a case, when both the $X_{XY}$ and $X_Z$ eigenstate energies are below the $\Gamma$ eigenstate energy, the structure is called indirect - both in real and momentum space (see Ref. 49 for more details).

The evolution of energy bands in GaAs/AlAs type II double QWs and a characteristic photoluminescence spectrum of the investigated sample are presented in Fig. 3.2 and 3.3, respectively.

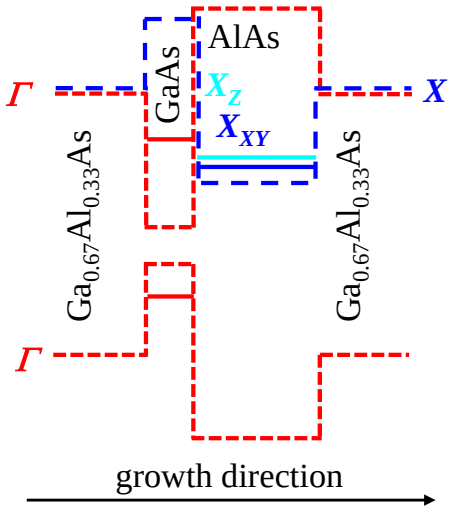


Figure 3.2: Distribution of the energy bands and the position of the confined levels, characteristic of the GaAs/AlAs type II QW structure. Red dashed line - $\Gamma$-symmetry band; blue dashed line - $X$-symmetry band. The positions of the $\Gamma$- and $X$-symmetry states in the QW are marked in red and yellow colours, respectively.

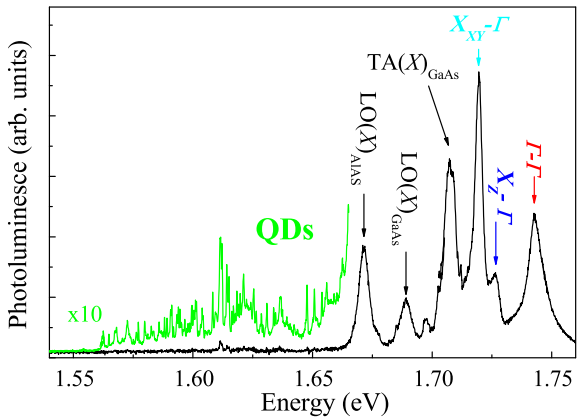


Figure 3.3: A characteristic macro-PL spectrum (∼1 mm$^2$ of the laser spot) of the investigated sample.

## 3.2 GaAlAs quantum dots

Together with broad and expected emission lines of a "2D character", our sample show other emerging features: an ensemble of sharp emission peaks [50,51]. The measurements of the PL spectra have proven that the observed discrete lines are related to single QDs [49,52–55] - see Fig. 3.3. Moreover, time-resolved micro-PL measurements showed that the lifetimes of the emission lines are in the range of ∼1 ns, characteristic for direct-gap recombination processes [49,52,56].

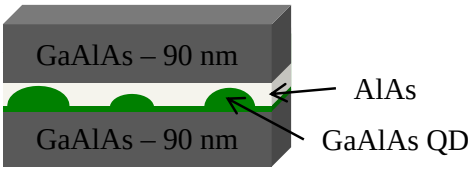


Figure 3.4: General scheme of the main part of the sample structure.

In our opinion, the imperfections in the growth process presumably led to formation of gallium droplets (see Fig. 3.4). In these gallium-rich islands the nominal GaAs/AlAs structure is replaced by a $Ga_{1-x}Al_xAs$, where $x < 0.33$. The emission from the dots is observed in the broad energy range (up to 150 meV) below the main quantum well transitions. On the other hand, the characteristic low energy cut-off of the photoluminescence is observed at approx. 1.56 eV (see Fig. 3.3). This, likely corresponds to the situation when a pure GaAs dot replaces the whole GaAs/AlAs bilayer and thus has a height of 12.4 nm [49]. The estimated lateral extent of the confining potential is around 50 nm. The surface density of dots is estimated at $10^6$ cm$^{-2}$ - see Fig. 3.5. Additional informations about the origin of the QDs are presented in Chapter 5.

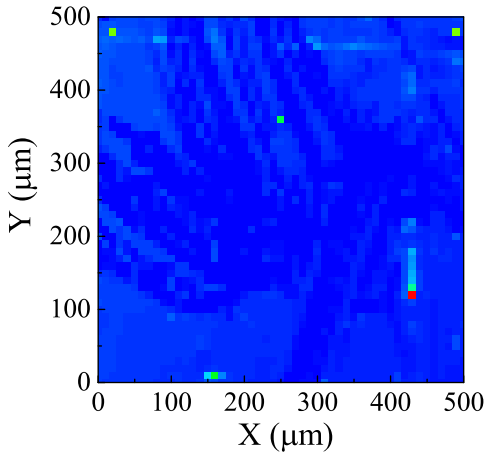


Figure 3.5: The micro-PL map of the emission from the QDs in the energy range: 1.58-1.70 eV. The mapping step was the same in both direction and equal 10 μm. The map was measured using the setup presented on part (b) in Fig. 4.1.

The shape of the potential distribution in the quantum dot deduced from the optical experiments is presented in Fig. 3.6.

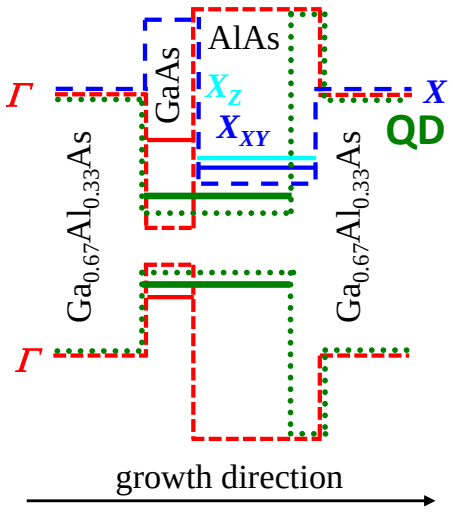


Figure 3.6: Potential distribution through the GaAlAs QD formed in the GaAs/AlAs type II QW structure is marked schematically on the potential distribution of double QW structure. Red dashed line - $\Gamma$-symmetry band; blue dashed line - $X$-symmetry band; and green dotted line - distribution of the potential through the dot in the growth direction. The positions of the ground state in QD are marked in green colour. The energy of $\Gamma$- and $X$-symmetry states in the QW are marked in red and blue colours, respectively.

# Chapter 4

# Experimental techniques

In this Chapter, the experimental techniques applied in this work to study the optical properties of QDs are presented. The micro-PL and the micro-PLE setups, including the one for polarization-resolved measurements and operated in external magnetic field, are described. The setup used to study single photon correlations is also presented.

## 4.1 Micro-photoluminescence

The purpose of the micro-photoluminescence experiments is to detect the emission light from the smallest possible sample region. In the case of QDs investigated in this work (low surface density - see Chapter 3.2), it allowed to study a single QD. The excited spot diameter is limited by the diffraction limit of the laser and depends on the objective and the geometry of the experimental setup. A typical spot diameter in the presented systems was around 1 $\mu m^2$.

### 4.1.1 Micro-PL setups

Two similar experimental setups available in the Faculty of Physics University of Warsaw and at the Grenoble High Magnetic Field Laboratory were used to measure micro-photoluminescence spectra. The schemes of both systems are presented in Fig. 4.1.

In the case of Warsaw setup, presented in Fig. 4.1 (a), an $Ar^+$ CW laser was used as an excitation source. This source ($\lambda$=488 nm was selected by an interference filter placed in the laser beam) was used for an excitation above the band-gap of the type-II GaAs/AlAs bilayer (detailed informations in Section 3.1). The in-

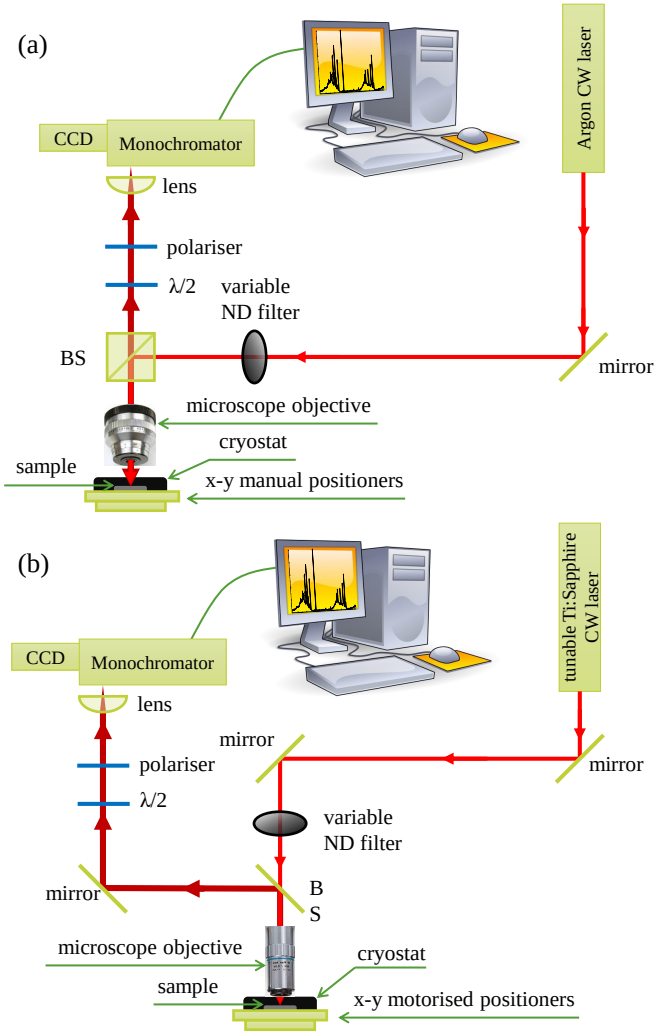


Figure 4.1: Scheme of micro-photoluminescence setups available in: (a) Faculty of Physics, University of Warsaw, (b) Grenoble High Magnetic Field Laboratory.

vestigated sample was located on a cold finger of a continuous flow cryostat at liquid helium temperature ($T$=4.2 K). The cryostat was mounted on the $x$-$y$ manual positioners. The excitation light was focused by means of an adjustable reflective objective (M=36X, NA=0.5). The spot size was around 1 $\mu m^2$. The micro-PL was collected via the same microscope objective, and sent through a monochromator. The light was dispersed by a 1 m monochromator equipped with 1200 g/mm grating. The signal was detected by a CCD camera cooled down with liquid nitrogen.

In the Grenoble setup, presented in Fig. 4.1 (b), a tunable Ti:Sapphire CW laser was used as an excitation source. The Ti:Sapphire laser set at $\lambda$=725 nm provides the excitation light below the band-gap. The investigated sample was

located on a cold finger of a continuous flow cryostat at liquid helium temperature ($T$=4.2 K). The cryostat was mounted on the $x$-$y$ motorized positioners. The excitation light was focused by means of an infinity corrected objective (M=50X, NA=0.5). The spot size was also around 1 $\mu m^2$. The micro-PL was collected via the same microscope objective, and sent through a monochromator. The light was dispersed by a 0.5 m monochromator equipped with 1800 g/mm or 600 g/mm. The signal was detected by a CCD camera cooled down with liquid nitrogen.

Polarization-resolved experiments were implemented using a motorized rotating half-wave plate combined with a fixed linear polarizer in front of the monochromators in order to avoid detection artifacts related to the anisotropic response function of the setup [57].

### 4.1.2 The setup for experiments in magnetic field

Application of an external magnetic field reveals the relevant energy shell structure by progressively lifting degeneracies and shifting the transitions associated with different angular-momentum channels as the field is increased [10, 34, 58]. There are two magnet systems available in the Grenoble High Magnetic Field Laboratory:

**(a)** a superconducting magnetic coil producing field up to 14 T,

**(b)** a 20 MW resistive magnet capable of producing field up to 28 T.

A especially designed probe with optical fibers (see Fig. 4.2) was used in both systems. The probe was constructed for measurements in the Faraday configuration.

The sample was placed on top of the $x$-$y$-$z$ piezo-stage in the bath cryostat and kept in gaseous helium at $T$=4.2 K [59]. The laser light from the tunable Ti:Sapphire CW laser was coupled to one branch of a Y-shaped single mode fiber. The photoluminescence signal was separated from the laser beam by a fiber-based dichroic beam splitter in the ratio of 10/90% for the transmission of the excitation/detection light. The microscope objective was located above the sample and provided the spot size around 1 $\mu m^2$. The micro-PL was collected via the same objective, and sent through the monochromator with the CCD camera (see Section 4.1.1 for details).

Such a setup makes the polarization-resolved measurements very difficult on account of the fibers. The both branches of a single mode fiber are about 10 m long and they act as a high order wave plate. Moreover, high magnetic field results in a strong Faraday effect in the fibers. However, if the measured micro-PL emission is circularly polarized (it takes place for emission lines of single QDs), it permits to compensate the effect of the fiber on polarization of transmitted light in the detection beam. It is done by the rotation of the quarter-wave or half-wave

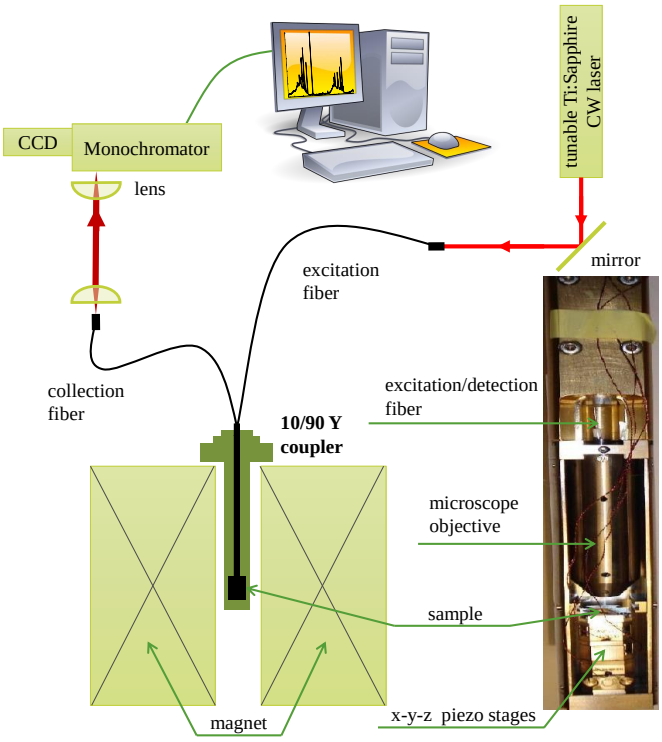


Figure 4.2: The scheme of the micro-PL setup used for measurements in magnetic fields. An inset photo comprising of a microscope objective and piezoelectric x-y-z stages with the sample.

plate or both at the same time during the measurements in the magnetic field. The compensation of both effects on the excitation beam is much more difficult, and it is described in the next Section.

## 4.2 Micro-photoluminescence excitation

One of the fundamental properties of electron-hole pairs captured in the dot is their energetic structure. The structure can be retrieved by studies of the excitation spectrum of such a complex, *e.g.*, in an experiment of photoluminescence excitation of one of the basic excitonic lines [16,60,61].

The micro-PLE setups are based on the experimental arrangements presented before (for measurements of micro-PL spectra: the details described in Section 4.1). The main difference is related to the basis of the PLE experiment, which is to detect changes of the intensity of the studied signal (excitonic emission line) as a function of the excitation energy. To measure and control the wavelength and the intensity of the laser light, the wavemeter, the noise eater and the motorized micrometer stepper were added to the setup. The injection of a few percent of

the excitation light to the wavemeter, combined with the software, allowed us automatically measure the micro-PLE spectra. The noise eater, known also as the laser intensity stabilizer, provided a stable excitation intensity when the laser wavelength is tuned.

It is more difficult to measure and control the polarization of the excitation light than the polarization of the PL signal (see Section 4.1.2). One of the reasons is the expected splitting of the excited state into two components in a magnetic field. The splitting is similar to the one observed in the case of the X state, both those states are related to the specific spin projection of the excitonic state onto the axis given by the magnetic field (+1 or -1). This means that they are resonantly coupled to oppositely (circularly) polarized light in Faraday configuration. Therefore, the energy of the resonant excitation is strictly related to the circular polarization of light due to the fact that Faraday effect is wavelength dependent.

Of great importance for the quality of studies of the excited states in single QDs is the accurate determination of the laser wavelength. The available states in dots exist only at discrete energies (can be represented by delta functions). Therefore, the excitation laser wavelength should be changed with very small steps (in the case of the present study the minimum step was 0.01 nm$\sim$21 µeV at $\lambda$=760 nm). It was observed, that the laser light wavelengths as measured by the wavemeter were encumbered with errors. During measurements, when the laser wavelength was tuned, the intensity variation of the laser light was noticed. The small intensity of the laser light, injected to the wavemeter, affects on the accuracy of the measured wavelength by the wavemeter. The additional fitting procedure was carried out to obtain the proper laser wavelength (the Gaussian function was fitted to the each laser peak, which was detected in the same spectrum window as the micro-PL signal).

## 4.3 Single photon correlation

Measurement of single photon correlations is a very powerful technique which allows investigation of time-dependent phenomena occurring in light emitting structures. In the case of QDs, it has been successfully used to study the cascade pathways (*e.g.* photons emitted in a biexciton-exciton cascade) and attribute the observed emission lines to excitonic states [62–65].

The correlation measurements were performed in a Hanbury-Brown and Twiss configuration type setup with additional spectral filtering [66,67]. The excitation part of the setup is described in Section 4.1. The micro-PL signal was separated into two beams by a 50/50 beamsplitter. Each beam was sent through a 0.5 m monochromator and either detected by a CCD camera in case of micro-PL or by an avalanche photodiode (APD) after selection of the line of interest. APDs were triggering a "Start"-"Stop" measurement, and were coupled to a time-

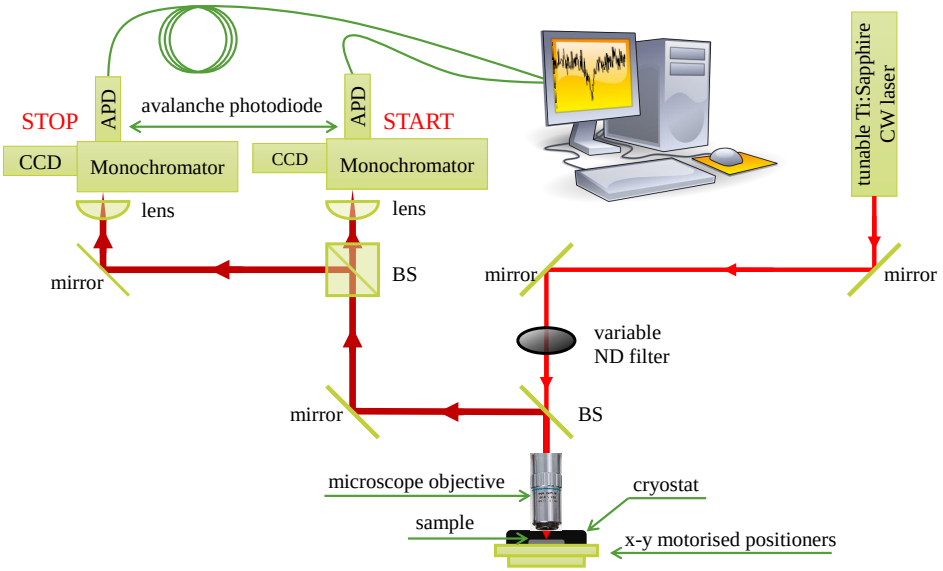


Figure 4.3: Scheme of the photon correlation experimental setup.

correlated coincidence counter (*PiqoQuant TimeHarp 300*). The overall temporal resolution of this system was equal to about 250 ps. A schematic diagram of such experimental setup is shown in Figure 4.3.

The correlation system generates histograms of correlated photon detection events versus the delay-time between detected photons. The use of a delay line, made of a long coaxial cable, at "Stop" input of the correlation electronics allowed to record events with a negative delay between photons, *i.e.*, the events when the photon at "Stop" detector arrived before the photon arrival at the "Start" one.

After normalization, the recorded histograms are equivalent to the normalized second-order correlation function:

$$g^{(2)}(\tau) = \frac{\langle I(t)I(t+\tau)\rangle}{\langle I(t)\rangle^2} \tag{4.1}$$

where $\langle \ldots \rangle$ denotes the time average and $I(t)$ is the light intensity at time $t$. $g^{(2)}(\tau)$ gives the probability of detecting a second photon at time $\tau$, under the condition that a photon has been already detected at time $t$=0.

The polarization-resolved correlation experiments were implemented using a motorized rotating half-wave plate combined with a fixed linear polarizer in front of the monochromators - see Section 4.1.

# Chapter 5

# Optical response of the investigated structure - overall characteristic

The possibility to optically generate cold, tunable-density, two-dimensional electron-hole gas has stimulated studies of double quantum well structures, such as the type-II GaAs/AlAs QW investigated here. The PL spectra of such systems are known to exhibit a number of properties which have been interpreted as the observation of a precursor of the Bose condensate of excitons [68] or alternatively are assigned to effects of trapping carriers in the potential fluctuations caused by the interface roughness, named natural QDs [31].

In this Chapter, main optical properties of the investigated sample are presented and discussed. Emerging broad features attributed to the transition in the type-II GaAs/AlAs QW are described and the effect of the excitation regimes are explained. Most of all, however, the general optical properties of single QDs present in our sample are discussed. Excitonic shells, the identification and changes of the charge state of excitonic lines are presented.

## 5.1 PL spectrum of the studied sample

At first glance, the photoluminescence spectrum of our structure (Fig. 5.1) displays six, well pronounced, but rather broad emission peaks. The appearance of these peaks ("QW-like") is accounted by the nominal design of our sample, as a type II double quantum well. The peak at $E_{\Gamma-\Gamma}$ ~1.743 eV corresponds to the direct $\Gamma - \Gamma$ transition in GaAs QW. The next two peaks $E_{X_Z-\Gamma}$ ~1.726 eV,

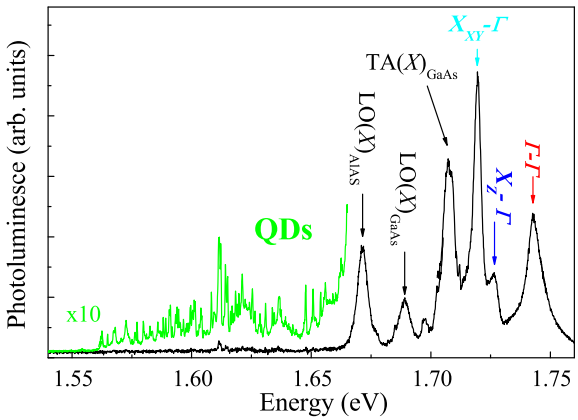


Figure 5.1: The PL spectrum of a 1 mm size area of the investigated sample measured at $T$=4.2 K.

$E_{X_{XY}-\Gamma}$ ~1.719 eV are related to a detect allowed indirect recombination of the $e$-$h$ pair between the $X$-symmetry state in the conduction band and the $\Gamma$ state in the valence band. Moreover, three phonon replicas $TA(X)_{GaAs}$, $LO(X)_{GaAs}$, and $LO(X)_{AlAs}$ are seen in the spectrum [46, 49–52, 69].

Apart the broad, "QW-like" emission peaks, the PL spectrum of our sample shows a large ensemble of sharp emission line. As shown in Fig. 5.1, these sharp emission lines appear in a wide spectral range between 1.56 eV and 1.72 eV) [49, 52]. At first sight, the appearance of sharp emission lines in PL spectra of (narrow) QWs might be not surprising. Such narrow lines are usually attributed to well width fluctuations leading to the formation of potential traps in lateral direction, which can be seen as shallow QDs [31, 70]. Typical localization energies related to well width fluctuations are however of the order of few meV, only [31, 32]. Well width fluctuations can account for the appearance of narrow lines in our sample but only in the high energy range, in a vicinity of "QW-like" emission peaks. The presence of sharp emission lines in a very broad (160 meV) energy range must imply the presence of another type of trapping centres in our structures. Those "new" traps are assumed to be the result of growth imperfection, (Ga droplets and/or Ga diffusion [71–73]) which results in Ga-rich islands ($Ga_{1-x}Al_xAs$, $x < 0.33$) which replace the original GaAs/AlAs double layer (for a details see Chapter 3.2). Notably, the lowest possible emission energy among such objects would correspond to the case when GaAs/AlAs double layer is entirely replaced by a pure GaAs layer. This is in agreement with the observation of a clear low energy onset, at 1.56 eV, for the appearance of narrow lines in the investigated structure. The recombination processes related to the objects raising sharp emission lines are studied in this work.

## 5.2 Above-barrier versus quasi-resonant excitation

The issue of excitation mechanism at the level of a single QD has been studied for many years, *e.g.*, in Ref. 67,74. The observed effects are related to the excitation energy with respect to the energy of the barrier confining the captured carriers in the QD [75–77]. The measured micro-PL spectra of our sample related to the *s*- and *p*-shell of a single QD as a function of the excitation power for both excitation regimes are presented in part (a) and (b) of Fig. 5.2.

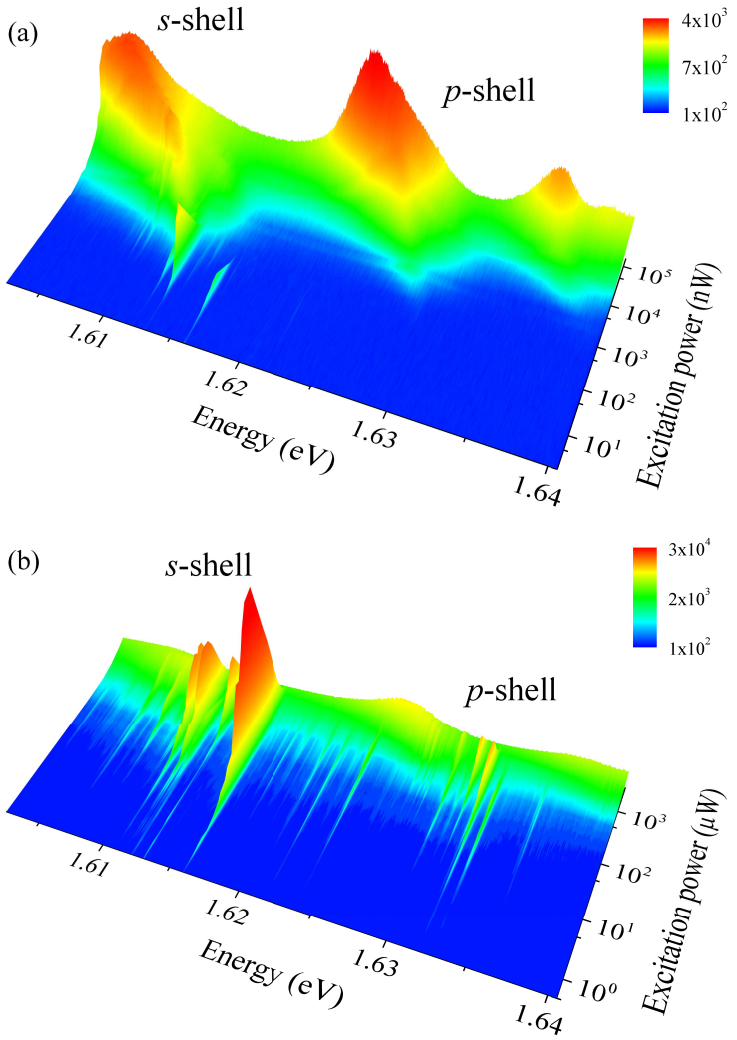


Figure 5.2: The micro-PL spectra of a single GaAlAs/AlAs QD as a function of the excitation power at (a) the above-barrier ($E_{exc}$=1.759 eV) and (b) the quasi-resonant excitation regime ($E_{exc}$=1.71 eV).

The above-barrier excitation regime (the excitation energy is above the barrier band-gap) provides the simplest way to excite single QDs. The $e$-$h$ pairs are created in the indirect quantum well and, subsequently, carriers (electrons and holes) are preferentially independently captured in the QD. In this excitation regime, due to, *e.g.*, the difference in the depth of the confinement potential of the QD and the relaxation time of electrons (holes) in the conduction (valence) there is no preference for capturing the neutral or charged states. The second excitation regime is called (quasi-)resonant (depending on the energetic distance between the exciting laser light energy and the ground state of the dot). In this regime, the laser energy is tuned below the barrier energy and carriers are preferentially captured in pairs (electron-hole) directly in the QD, favouring the formation of neutral states. Notably, the energy realised to the lattice (number of emitted phonons) is larger in the case of high energy (above-barrier) excitation than in the case of the quasi-resonant excitation. The difference between the excitation mechanisms are reflected in the micro-PL spectral shape, as it is shown in Fig. 5.2. In the above-barrier regime, a set of sharp lines is observed only at moderate excitation powers of the laser. At higher laser intensities, when the emission related to the $p$-shell emerges, only a broad emission attributed to the multiexcitons appears (no discrete lines are observed). On the other hand, in the quasi-resonant regime, the micro-PL spectra have a more complex structure of sharp lines (the line of the highest intensity is related to the transition of the neutral exciton). For higher excitation powers the excitonic lines related to the charged states can also be detected [55, 78]. Clearly, however, larger charge fluctuation effects and high carrier/lattice temperature are characteristic of above-

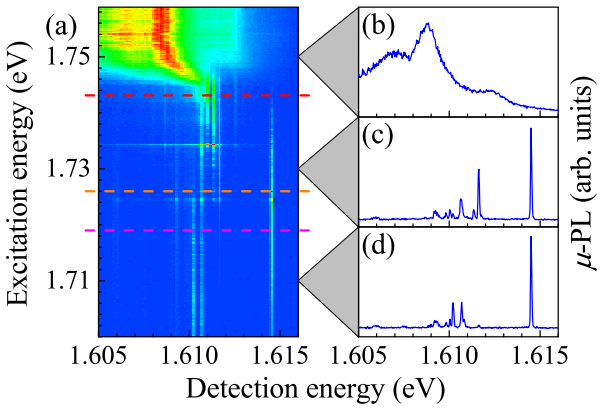


Figure 5.3: a) Color plot of the micro-PL spectra recorded as a function of the excitation energy while keeping the excitation power at approximately constant level. Dashed horizontal lines indicate the energies of the $\Gamma - \Gamma$ (red), $X_Z - \Gamma$ (orange), $X_{XY} - \Gamma$ (pink) transitions in the QW; (b)-(d) Three micro-PL spectra excited at energies equal to 1.75 eV, 1.73 eV and 1.71 eV, respectively.

barrier excitation regime.

It is worth noticing, that there is a three orders of magnitude difference between the emission line intensities excited with the same laser power in the two excitation regimes (see 5.4) - Fig. 5.2. The above-barrier excitation (see Fig. 5.1) leads to the creation of long lifetime carriers in the QW structure and efficiently supply QDs with the carriers [49,52]. On the other hand, in the quasi-resonant regime, the $e$-$h$ pairs are directly created in the dot, and the overlap between the dot and the excitation spot is crucial. The diameter of the laser spot is around 1 µm whereas the spatial extend of the QDs is estimated to be 50 nm (see Chapter 3 and 4). The ratio of these areas amounts approx. 400, which agrees well with the proportion of the used excitation powers. This proportion might be additionally affected by different strength of the absorption.

The progressive decrease of the excitation energy leads to the significant change in the micro-PL spectra related to the $s$-shell of the single QD - see Fig. 5.3. As long as the excitation energy is above the $\Gamma - \Gamma$ transition, a broad spectrum of the highly excited $s$-shell (Fig. 5.3(a)) is observed. Below this transition, the QD is less efficiently populated by carriers from the QW and the spectra comprise a set of discrete lines (Fig. 5.3(b)). The comparison of the Fig. 5.3(c) and (d) shows smaller number and the intensity change of the excitonic lines. The results presented in Fig. 5.3 confirm facts discussed in paragraphs above.

## 5.3 Excitonic shells

Single particle levels and interactions between carriers in a QD can be effectively modified using a magnetic field. The magnetic field lifts the spin degeneracy and the orbital degeneracy of single-particle levels. This results in the excitonic Fock-Darwin spectrum of multiexcitonic emission observed, *e.g.*, in self-assembled InAs/GaAs QDs [10,33]. The excitonic shell structure (the $s$, $p$, $d$,... shells) has been presented [9,10], in such QDs. The magneto-spectroscopic measurement of single QDs in the investigated structure were performed and a typical ensemble of micro-magneto-PL spectra are presented in Fig. 5.4. The spectra were excited quasi-resonantly. Such measurements represent a significant challenge. The difficulty, intrinsic of quasi-resonant excitation regime, is due to a large input laser power as compared to relatively low emission intensities. Then, the extra emission of optical fibers (partially kept at low temperatures) appears as a relevant background. The micro-PL signal of the QD appears on the top of the PL of the fibers and an additional procedure must be carried out to extract the clean micro-PL spectra of the single dot.

The evolution, with the magnetic field, of the multiexcitonic spectra of highly excited GaAlAs/AlAs QD can be compared to the similar dependence previously

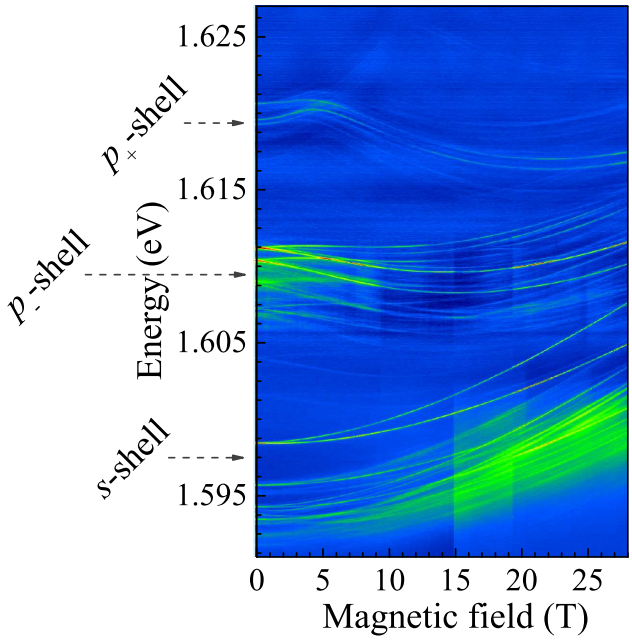


Figure 5.4: The evolution of the micro-PL spectrum of the highly excited GaAlAs/AlAs QD ($E_{exc}$=1.71 eV) in the magnetic field up to 28 T. The background intensity variation is an artifact resulting from the procedure described at the beginning of this Section.

observed in InGaAs/GaAs QDs (see Fig. 2.5) The analysis leads to the following conclusions:

- The set of lines ∼1.595 eV can be easily ascribed to the emission from the ground state, the *s*-shell by analogy with the InGaAs dot (compare Fig. 2.5 and 5.4).
- The attribution of the two next groups of lines (around 1.61 eV and 1.62 eV) requires more precise analysis - see Fig. 5.4. In the case of QDs with an in-plane isotropy and neglecting the electron-electron interactions, the two *p*-like-levels, the $p_x$ and $p_y$ states are degenerate. The SP *p*-level is characterized by $p_- = p_x + ip_y$ and $p_+ = p_x - ip_y$ states which have the same spatial function differing only by a phase factor [8, 26, 27]. In the presence of an in-plane anisotropy, the degeneracy between the SP $p_-$ and $p_+$ states is lifted. The magnitude of the observed splitting between the *p*-like-levels is of the order of a few meV. Because of the two set of lines are related to the $p_x$ (∼1.61 eV) and $p_y$ (∼1.62 eV) states, which are labelled as the $p_-$ and $p_+$ states (to make it easier with reference to the Fock-Darwin diagram). It is important to mention that the splitting of the excitonic states, *e.g.* the neutral exciton, as a result of the *eh* exchange interaction in

the in-plane anisotropy is of the order of tens of μeV (refer to Section 6.2.1 for more information).

- The additional argument, which supports our description of the $p_-$ and $p_+$ states (Fig. 5.4) is a sudden change of the magnetic shift slope of the $p_+$ state at approx. 5 T. This effect is related to previously presented anticrossing of the $p_+$ and $d_-$ states in the magnetic field [10,33].

- The Zeeman splitting of the excitonic lines is evidently observed, which suggests larger value of the effective $g^*$ factors than in the case of the InGaAs dots (see Section 2.2.1.2). This effect is analysed in details in Chapter 6.3 and 7.2 for emission lines attributed to the neutral and positively charged states.

Despite the fact that our dots are not fabricated in a well-controlled process and that their characteristic emissions are spread in a broad spectral, each single dot show very similar pattern of the recombination lines. This we illustrate in Fig. 5.5, with emission spectra measured for a selection of 10 different (single) dots. For each spectrum, the excitation was chosen below the dot barriers, and the laser power was kept at the same, moderate level, to reassure the observation of (sharp) emission lines related to both $s$- and $p$-shells. The emission lines related to the $s$-shell emission are horizontally scaled with respect to the neutral exciton X line and all $p$-shell emission lines are scaled with respect to the triexciton 3X line (associated to the $p$-shell). The assignment of X and 3X lines is discussed in the Chapter 6. Similar arrangement of emission lines can be seen in each of ten spectra presented in Fig. 5.5, though the energy spacing between the emission lines is different for each dot. In particular, the energy difference between the 3X and X lines varies from dot to dot, in the range from ∼10 to 20 meV (see also Fig. 5.6). In a rough approximation, this energy difference is taken as a measure of the inter shell ($s$- and $p$-) separation of SP states in the dot:

$$\Delta_{s\text{-}p} = E_{3\mathrm{X}} - E_{\mathrm{X}} \tag{5.1}$$

It is worth noticing that all attempts to correlate the amplitude of $\Delta_{s\text{-}p}$ with the apparent energy of neutral exciton X, representative of the characteristic spectral range of the emitting dot, have failed. This likely implies that the spectral range characteristic of each individual dot is primarily determined by Al composition of the GaAlAs island forming the dot, whereas the amplitude of $\Delta_{s\text{-}p}$ reflects the apparent lateral extension of this island.

A histogram of $\Delta_{s\text{-}p}$ for a large number of the investigated individual dots is presented in Fig. 5.6. The amplitude of $\Delta_{s\text{-}p}$ spreads in the range of 10 to 20 meV, and the most frequent values for the estimation of the $s$-$p$ inter shell separation in our dots are concentrated around 13.5 meV. Notably, this value is of

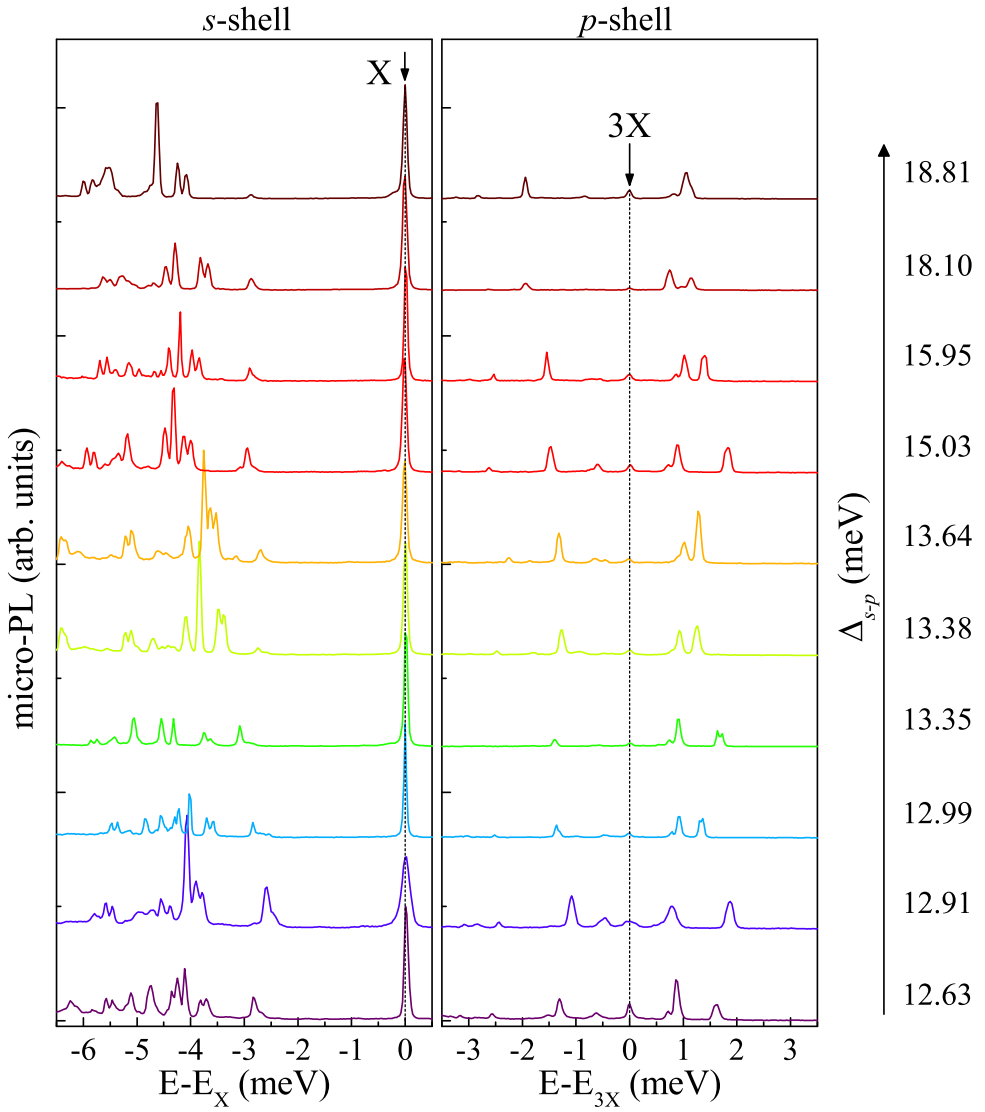


Figure 5.5: The micro-PL spectra of different single QDs excited with about the same excitation power. The spectra are normalized to the most intense emission lines and vertically shifted for clarity purpose.

about three times smaller as compared to the representative case of self-assembled InGaAs/GaAs QDs ($\Delta_{s\text{-}p} \sim 30$ meV). Since the strength of Coulomb interactions in both systems (investigated here and in InGaAs/GaAs dots) are expected to be similar (binding energies of 2D, QW excitons of the order of $\sim 10$ meV), the optical properties of InGaAs/GaAs dots may quantitatively follow the rules of SP approach (SP spacing exceeds the Coulomb binding). On the other hand, the effects of spatial confinement and Coulomb interactions are of the same magnitude in our dots, what implies a more complex description of multiexcitonic

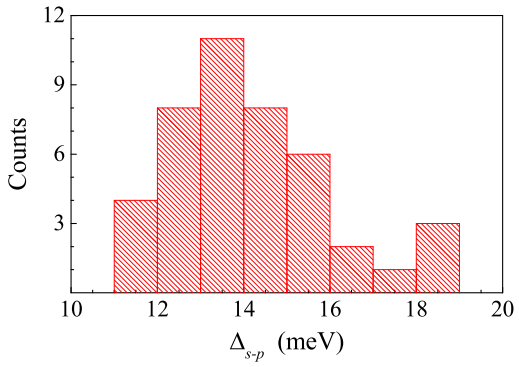


Figure 5.6: The histogram of the $\Delta_{s\text{-}p}$ value for the series of QDs.

states in the present case. In contrast to the case of InGaAs/GaAs dots, the pronounced interplay between the spatial confinement and the Coulomb interaction effects is likely at the origin of the significant departure of the magneto-Pl spectra of our dots from the models which refer to simple Fock-Darwin diagrams of SP states. Moreover, the effects of the shape anisotropy may be another source of the complexity. Indeed all our attempts in this direction were not successful. In particular, the set of magneto-PL spectra presented in Fig. 5.4 cannot be consistently modelled with a simple Fock-Darwin diagram (compare Fig. 2.5 and 5.4). Firm description of our magneto-Pl diagrams requires thorough theoretical studies, which are beyond the scope of this work. Nevertheless some efforts towards understanding of our magneto-PL spectra (particular lines) are presented in the next Sections of this manuscript.

## 5.4 Description of the excitonic families

Multitude of emission lines, which exhibit single semiconductor QDs including those studied in this work, is a known experimental fact [34, 61, 79]. Identification/assignment of these lines is, in general, not an easy task. Semiconductor dots, in contrast to atoms, are embedded into solid state environment which, in particular, is sensitive to electric charge fluctuation effects. The dot can be neutral (in particular empty) or can be negatively or positive charged, *i.e.*, filled with (additional) electrons or holes, respectively. The presence of a charged carrier in the dot (predominantly a single electron or hole in nominally undoped structures) may fluctuate (typical time scale of $\sim$ 10 ns) whereas a typical emission spectrum is averaged over $\sim$ 1 s time interval. The charge state of the dot may also vary with respect to optical excitation regime - as a function of the laser power and/or depending whether the laser excitation is set above or below the barrier of the dot (photo-created electron and holes captured separately or, preferentially, in

pairs). Obviously, all, neutral and charge dots may be optically filled with one, two, three, etc., $e$-$h$ pairs, each complex rising distinct emission lines - this finally accounts for the complexity of emission spectra of single dots.

Despite their large complexity, a number of emission lines of our dots can be identified and markedly classified into three characteristic families of lines, representative of neutral, positively charged, and negatively charged QDs. This classification and identification is based on the analysis of the results of different measurements and the following argumentation:

(a) Comparison of spectra measured with above-barrier and quasi-resonant excitations [55, 78, 80]. Emission due to charged dots is favoured in the spectra measured with above-barrier excitations, since in this case the photoexcited electrons and holes are, preferentially, separately trapped in the dot.

(b) Emission as a function of the excitation power [64,65,81]. Obviously, neutral excitons and/or charge excitons are observed at low excitation powers, higher complexes, biexcitons, triexcitons, appear at higher excitation power

(c) Analysis of the fine structure splitting (splitting of emission lines in polarization experiments at zero magnetic field) [11, 34, 38, 79]. This splitting, due to the anisotropic $eh$ exchange interaction, is primary characteristic of spin-paired, *i.e.*, neutral exciton, and absent in case of spin-singlet state of singly charged excitons.

(d) Photon correlation measurements and analysis of the shape of correlation diagrams, for different lines and different pairs of lines [65,81]. This is one of the central methods in identification of emission lines of single QDs, discussed more in details for our dots in this Section.

Our ultimate assignment of a number of emission lines with their characteristic grouping into three ("blue", "green" and "red") distinct excitonic families is shown in Fig. 5.7, for our representative dot (largely studied with photon correlation measurements). The sets of lines recognized are related to various charge states of the QD in a following manner:

- **neutral** - the excitonic states are occupied by equal number of electrons and holes. Four emission lines belonging to this collection are: X, 2X, 3X and 4X.

- **positively charged** - a given number of $e$-$h$ pairs and an extra hole are captured in the QD. Five emission lines: the $X^{+}$, $X^{+*}$, $2X^{+}$, ${}^{p}X^{+*}$ and ${}^{p}2X^{+*}$, are ascribed to the recombination of excitonic complexes belonging to this group.

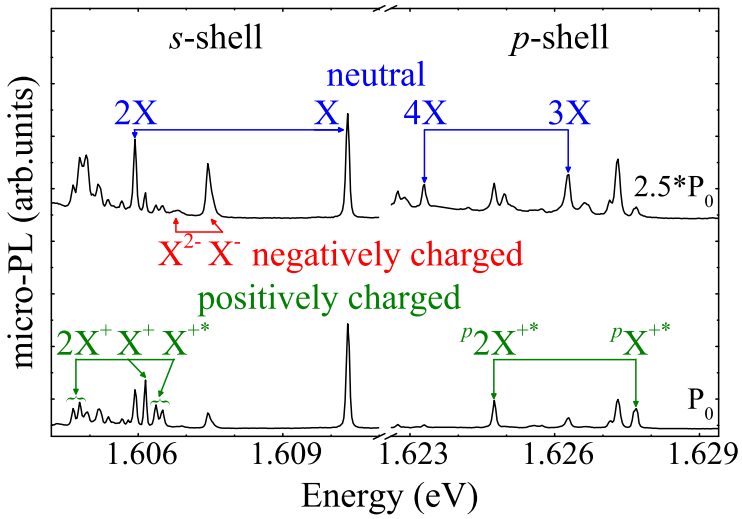


Figure 5.7: The micro-PL spectra of a single GaAlAs/AlAs QD, excited quasi-resonantly at $E_{exc}$=1.71 eV and measured at $T$= 4.2 K for two different excitation powers: $P_0$=200 µW and 2.5*$P_0$. The spectra are normalized to the intensity of the X emission line and vertically shifted for clarity purpose.

- **negatively charged** - a specific number of $e$-$h$ pairs and an extra electron are confined in the dot. This family comprises only two emission lines - the $X^-$ and $X^{2-}$.

Please, note that other dots display similar pattern of emission lines (see Fig. 5.5), thus the assigned peaks can be easily recognized in any other single QD characteristic of the present structure.

The assignment of emission peaks presented in Fig. 5.7 follows the ensemble of experiments and arguments, (a) to (d), which are listed above. Experiments and arguments pointed out in (b) to (d) are discussed in separate Chapters devoted to each characteristic excitonic family of emission lines.

Here we focus on arguments supporting our peak assignments, which follow from photon correlation experiments. Typical shapes of correlation diagrams which can be found for our dots are presented in Fig. 5.8 (see also Fig. 5.9). Majority of them (all four in Fig. 5.8) display the processes characteristic of rather long time scale, of the order of 10 - 20 ns, on the top of which the short scale (<1 ns) processes are seen in some configurations (see, *e.g.*, Fig. 5.8 (a) and (b). The long-scale processes reflect the charge fluctuation effects in the QD excited quasi-resonantly [55, 78, 80]. On the other hand, no signatures of such effects are observed for the above-barrier mode of QDs excitation [67,82–84]. It is related to different mechanisms of carriers trapping in the dot which are specific to a given regime of excitation (see Section 5.2 for details). Accordingly, these long time scale processes appear as bunching peaks within the same family of

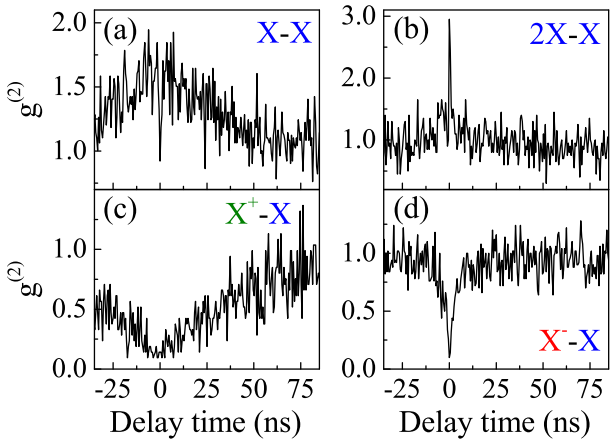


Figure 5.8: A set of correlation histograms: (a) an auto-correlation on the X emission line, (b)-(d) cross-correlations between the 2X and X, the $X^+$ and X, and the $X^-$ and X emission lines, respectively. The histograms (a) and (c) were measured at $P_{exc}$=50 µW whereas (b) and (d) at $P_{exc}$=500 µW.

the emission lines (see, *e.g.*, Fig. 5.8 (a) and (b)), but as the anti-bunching peaks in crossed-correlation diagrams of different families members (see, *e.g.*, Fig. 5.8 (c) and (d)). Sharp peaks around zero delay time (characteristic of processes on the scale of the radiative recombination time) reflect the single-photon-source character of our QDs [4, 85, 86]. Sharp antibunching peaks are seen in autocorrelation diagrams (see, *e.g.*, Fig. 5.8 (a)). Positive, sharp peaks are signatures of the sequential (cascaded), one after another, photon emission processes. Accordingly, this cascaded emission is seen in the cross-correlation diagrams, for pairs of members of the same family (see, *e.g.*, Fig. 5.8 (b)). An ensemble of correlation histograms, all measured for the same dot (the spectra of which are presented in Fig. 5.7) is shown in Fig. 5.9. Inspection of this figure, in reference to the above discussion of the characteristic features of the correlation histograms, provides a key support in the identification of the emission lines characteristic of our QDs.

The above discussion of photon correlations histograms characteristic of our dots is definitely not complete, though accounts for the main features relevant for the identification of our emission lines. More on our photon correlation experiments can be found in other Sections of this work, though some additional comments may appear appropriate at this point. The shape of a typical cross-correlation histogram between photons associated with two emission lines, which are emitted one after another, *e.g.* a 2X-X cascade, displays a particular asymmetry around zero delay time, the antibunching and bunching peaks occur [14]. As it is presented in Ref. 14, the intensity of both peaks is comparable. In the case of studied dots, however, the bunching peak is large an the antibunching

peak is hardly seen (see Fig. 5.8(b)). The effect, the asymmetry in the intensity of the bunching ans antibunching peaks, has been previously observed in the case of the cross-correlation between the 2X and X emission lines [55, 78, 83]. The highly pronounced bunching peak for small positive times in the 2X-X correlation reflects the expected higher probability of X photon emission directly after 2X photon emission. The observation of the antibunching peak for small negative delay times occurs because the QD needs to be repopulated with two electrons and two holes and the time has to pass after emission of the X photon before the 2X photon can be emitted. The similar effect appears in all cross-correlation histograms for which the sharp bunching peak is observed (sse Fig. 5.9) and the analogous line of reasoning can be applied.

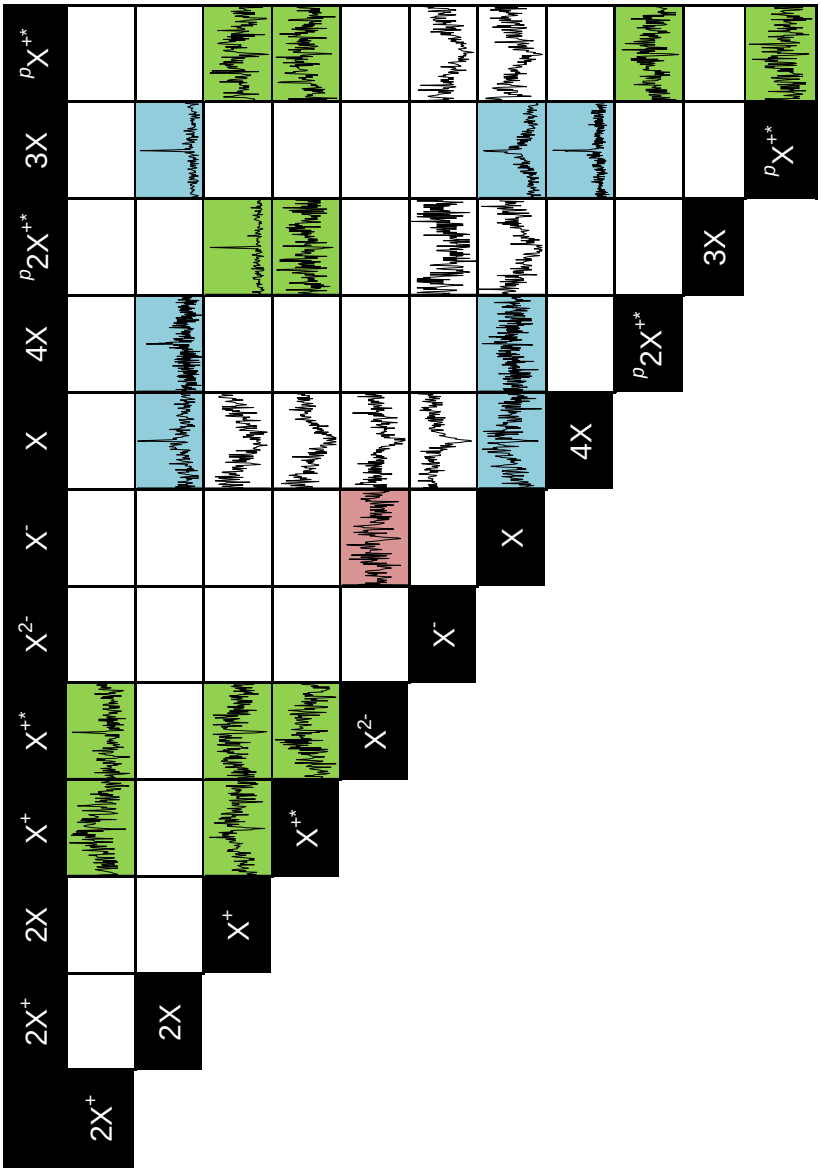


Figure 5.9: The photon auto- and cross-correlation histograms of the excitonic lines related to the *s*- and *p*-shell of the single QD under quasi-resonant excitation. Colours of background indicate the cross-correlations between emissions from the same family: blue - neutral, green - positively charged, red - negatively charged.

## 5.5 Changes of the QD charge

The subtle issue of the identification of emission lines is their assignment to a specific charge state of a QD: **n**egative or positive). The charge state of a dot can not be determined with the aid of the polarization-resolved micro-PL measurements because the *eh* exchange interaction influences neither the initial (in which the two carriers form the spin-singlet state) nor the final state (only one carrier left) of the emission line ascribed to the recombination of the singlet-state of the charged excitons. An external electric field is typically used to create extra electrons or holes inside the QD in a controllable way [87]. However, in order to apply this method, a sample needs to contain a doped layer with electrical contacts [87,88] or has to be prepared in a form of a Schottky diode [89,90]. Since in the case of the present work there was no possibility to performing the measurements on such type of structures, our attribution of the sign, "+" or "-" , for two distinct families of charged excitons, is, to this end, at the speculative level. Notably, however, inverting the attribution of the sign for those two families does not influence any relevant conclusions of this work. The logic and arguments which favour our specification of "+" and "-" families are as follows:

- The doping background in very likely p-type in our sample. Other, intentionally undoped GaAs/GaAlAs samples grown with the same MBE machine were showing the same feature. We presume this is due an unintentional contamination of the MBE growth with carbon impurities, indeed

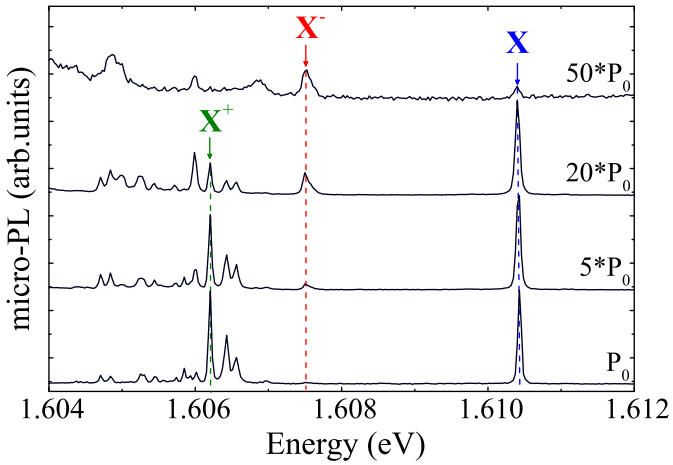


Figure 5.10: The excitation-power evolution of the micro-PL spectra of a single GaAlAs/AlAs QD measured at $T$= 4.2 K. The spectra are excited quasi-resonantly ($E_{exc}$=1.71 eV). $P_0$=10 µW and indicates the excitation power. The spectra are normalized to the intensity of the X emission line and vertically shifted for clarity purpose.

often polluting the MBE growth of III/V compounds (Ref. 91). The growth process of our structure implied a number of stop events for the deposition of III/V elements sources (to smooth the interface) what likely resulted in the accumulation of carbon impurities, acting as acceptors in our sample.

- With the above supposition, we expect that our dots may be positively charged even in the absence of optical excitation, whereas negatively charged dots appear as a consequence of trapping of optically pumped electrons, which are usually more mobile than holes and effectively diffuse to the dots.

A number of experimental trends are in accordance with the above assumptions:

- Under quasi-resonant excitation, and in the limit of low excitation power, the $X^+$ emission line dominates the $X^-$ one. This is because optically excited carriers are preferentially trapped in pairs (electron-hole) but positively charged dots exist even without optical excitation.

- The observation of $X^-$ emission line is favoured in the regime of the above-barrier excitation [49]. And in any case $X^-$ intensity is sub-linear with the excitation power, whereas, at the same time the relative decrease of the $X^+$ intensity is usually observed. Indeed, negatively charged dots appear as a result of trapping of photoexcited electrons which easily diffuse to the dots. This process can also neutralize the positively charge dots, what partially accounts for the relative decrease of $X^+$ intensity. In the extreme case, but under above barrier excitation, some dots do not show the $X^+$ emission line at all (see Section 6.2.1) [69].

- The micro-PLE spectra detected on the $X^-$ and $X^+$ emission lines, which are the subject of discussion in Sections 7.3 and 8.2, look extremely different. Notably, the micro-PLE spectrum measured at the energy of the recombination of the negatively charged exciton, because the related emission line is absent in the used range of excitation powers, does not exhibit any resonant peak (see Fig. 7.8) while in the micro-PLE spectrum of the positively charged excitons a number of resonant peaks is observed (see Fig. 8.3). These results imply that each of the charged excitonic complexes mentioned above has a different origin.

Based on the arguments presented above, one can conclude that the emission lines, labelled $X^+$ and $X^-$ in Fig. 5.10, are ascribed to the recombination of the singly positively and negatively charged excitons, respectively. Although the logical structure of this reasoning cannot be questioned, it also has some weak points (for instance, typically the emission energy of the positively charged exciton

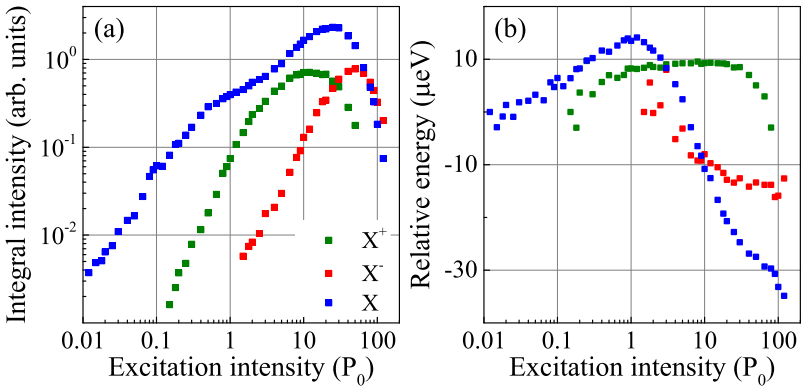


Figure 5.11: The excitation-power dependence of the integrated intensity (a) and the relative energy (b) of three main emission lines: X, $X^-$, and $X^+$. The plots are drawn in the log-log and the semi-log scale, respectively.

is bigger than the negatively charged one [11,38,58,92]). Therefore, the opposite attribution of the emission lines cannot be absolutely rejected.

Fig. 5.11 displays the excitation-power dependence of the integrated intensity and the relative energy of three main emission lines: X, $X^-$, and $X^+$. The intensities of these lines, depicted in Fig. 5.11 (a), exhibit a super-linearity. In particular, the intensity of the X emission line changes the slope when the $X^-$ emission emerges. Moreover, the relative energies of those lines increase and/or decrease with the increase in the excitation power (see Fig. 5.11 (b)). Similar effects has already been observed in the past and are related either to the presence of background impurities [77,93] or to the band-gap renormalization [49,94,95].

As is discussed above, GaAs layers exhibit a p-type background doping (the most likely impurity is carbon). This means that acceptor centres may be located near and/or within the QDs. In the low excitation power range, most of the residual impurities are ionized. Due to the presence of an acceptor centre, the ionized atom will give rise to an electric field and hence to the Stark shifts in emission energies for the exciton states [77,93]. Under higher excitation power, such a charged impurity starts to be neutralized by the photogenerated carriers, thereby eliminating the Stark shifts. It leads to the blue-shift in the energies of the X and $X^+$ emission lines and the recombination of the negatively charged exciton ($X^-$ line) occurs (see Fig. 5.11 (b)). Therefore, when the excitation power goes across ∼1 μW, the direction of the shift in the X energy becomes opposite (it changes from the blue- to the red-shift). The energies of two other emission lines, $X^-$ and $X^+$, are affected as well, but the slopes of shifts are different in every case. In this range of the excitation power, the effects related to the exchange-correlation interaction in a highly excited QD, known as the band-gap renormalization, are activated. [49,94,95].

## 5.6 Conclusions

In this Chapter, a brief introduction to the optical properties of the investigated GaAlAs/AlAs QDs is presented. The most probable origin and the morphology of the dots is shortly described. Two excitation regimes, the above-barrier and the quasi-resonant, are identified and the respective mechanisms of carrier trapping active in both of them are discussed. The effect of the excitation regime on the lineshape of the micro-PL spectra of a single QD is also shown. The magnetic-field dispersion of the multiexcitonic emission from a highly excited QD is analysed in terms of the Fock-Darwin model. Despite the fact that the shells emission does not follow a typical Fock-Darwin-like evolution in a magnetic field, three groups of emission lines are attributed to the $s$-, $p_-$-, and $p_+$-shell in the QD. Three families of excitonic lines (the neutral, positively and negatively charged ones) are identified on the basis of respective charge states of a QD. The number of electrons and holes confined in the dot in a particular configuration was found using the single photon correlation experiment. The attribution of the $X^+$ and $X^-$ emission lines to the recombination of the singly positively and negatively charged excitons is discussed. Moreover, a non-typical behaviour of the intensity and the energy of three basic emission lines, X, $X^+$ and $X^-$, as a function of the excitation power is ascribed to the presence of the p-type impurities in the vicinity or even within the QDs.

# Chapter 6

# Neutral excitonic states

The best-known example of a confined neutral state in a QD, is a single $e$-$h$ pair, called a neutral exciton [8,9,34]. The trapping of one additional $e$-$h$ pair in a dot leads to the formation of a complex of two $e$-$h$ pairs, referred to as a biexciton. The photons are emitted consecutively by these two excitonic complexes in a cascade process. The biexciton-exciton cascade has been considered as a promising source of entangled photon pairs [13,62,63] for the quantum cryptography [96] and teleportation [97]. However, its practical applications are limited by the fine structure of the intermediate bright exciton state, which is due to the anisotropic $eh$ exchange interaction [34,98–101]. Moreover, the possibility of the multiexciton formation in single QDs significantly increase the probability of the observation of correlated photons. In particular, it has been presented, that the emissions of the quadexciton and triexciton (four and three $e$-$h$ pairs confined in a dot, respectively) are also correlated and can be considered as an equivalent to the biexciton-exciton cascade [65]. It should be noted that while the latter process involves the carriers from the $s$-shell levels, the former cascade is related to the transitions of carriers between the $p$-shell levels.

In this Chapter, the properties of four emission lines attributed to the recombination process of the neutral charge states between the $s$- and $p$-shell levels are discussed. Especially, the fine structure splitting, the diamagnetic shift and the Zeeman splitting of these lines are studied. Moreover, the magnetic-field-dependent photoluminescence excitation spectra of the neutral exciton are presented and analysed.

## 6.1 Micro-PL spectra vs the excitation power

The micro-PL spectra of the single dot, excited quasi-resonantly (see Section 5.2) and measured as a function of the excitation power are shown in Fig. 6.1. At low excitation powers (below $P_0$=10 µW), a single emission line, labelled X, is dominant. This line is attributed to the recombination of a single *e*-*h* pair - the neutral exciton. At higher excitation power, several peaks appear on the low energy side of X. They are related to the emission of the multiexcitons in the QD. Among those peaks, the 2X line occurs which is identified as originating from the emission of two *e*-*h* pairs forming a spin-singlet state, *i.e.*, the biexciton. A broad group of features, which include X and 2X emission lines, is associated with the recombination of *e*-*h* pairs occupying the *s*-shell levels.

A further increase of the excitation power leads to emergence of another set of lines at higher energies (∼12 meV above the energy of the X line), ascribed to the emission that takes place within the *p*-shell (see Fig. 6.1). Two emission lines denoted by 3X and 4X occur in this energy range and are recognized as resulting from the recombination of a triexciton (a complex consisting of three *e*-*h* pairs) and a quadexciton (a complex formed by four *e*-*h* pairs), respectively.

The attribution of these four lines to the recombination of a given excitonic complex has been confirmed by the polarization-resolved measurements and the photon correlation experiments [34], and is the subject of detailed discussion in what follows. The emission lines which are not labelled in Fig. 6.1 are linked to either positively or negatively charged states and will be analysed to a larger

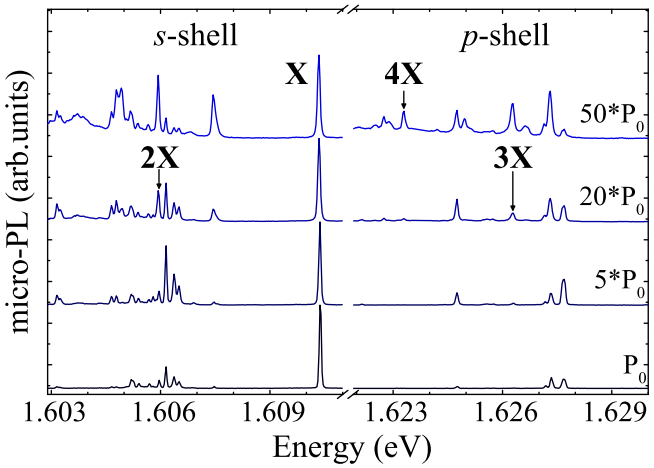


Figure 6.1: The excitation-power evolution of the micro-PL spectra of a single GaAlAs/AlAs QD measured at $T$= 4.2 K. The spectra are excited quasi-resonantly ($E_{exc}$=1.71 eV). $P_0$=10 µW indicates the excitation power. The spectra are normalized to the intensity of the X emission line and vertically shifted for clarity purpose.

extent in Chapters 7 and 8.

## 6.2 Fine structure splitting

Polarization-resolved µ-PL measurements have been performed to study the fine structure of excitonic states, involved in the emission lines, whose identification was the subject of the previous Section. The µ-PL spectra measured in two perpendicular polarizations with respect to the [110] crystallographic direction are presented in Fig. 6.2. As can be seen, all investigated lines related to the *s*- and *p*-shell emission are split and the splitting components exhibit the linear polarizations in mutually perpendicular directions. The energy separation between them is of the order of tens µeV. As mentioned in the introductory part of this manuscript, the phenomenon that underlies the emergence of the above components is the fine structure splitting of excitonic states, which will be analysed in detail in what it follows.

The FSS is a result of the *eh* exchange interaction and it has intensively been studied in the literature [34]. The origin of the fine structure of a neutral exciton is precisely described in Section 2.2.1.1. In this case, the FSS arises from the anisotropic part of the exchange interaction between an electron and

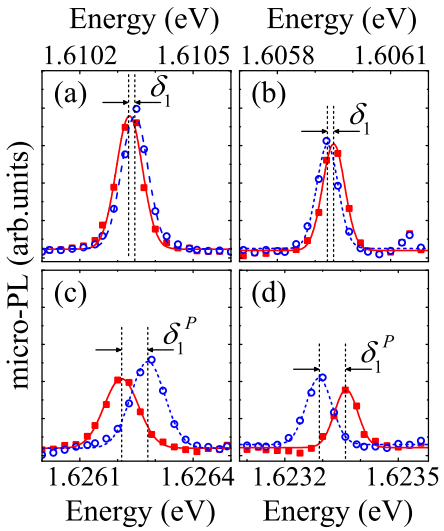


Figure 6.2: High-resolution polarization-resolved micro-PL spectra of the emission lines attributed to neutral exciton (a), biexciton (b), triexciton (c) and quadexciton (d) in a single GaAlAs QD measured in two polarizations: parallel (red) and perpendicular (blue) to the [110] crystallographic direction. The open circles and closed squares indicate the experimental data. The curves drawn with solid and dashed lines represent the results of fitting the data with the Gaussian function.

a hole forming the neutral exciton. The magnitude of FSS can be defined as $\delta_1 \equiv |E_{X_\parallel} - E_{X_\perp}|$ [34, 99–101]. The splitting observed between polarised components of the X emission line provides the value of $\delta_1$. The biexciton state is spin-degenerate, as a consequence of the spin-singlet state of the $e$-$h$ pairs it is composed of. The splitting of the 2X emission line is therefore related to the FSS of the neutral exciton. This in turn means that the splitting of the 2X and X emission lines have the same magnitude but different polarization axes which extend over mutually perpendicular directions [63] (see Fig. 6.2(a) and 6.2(b)). The anisotropy axis can be defined as an angle of a polarization analyser at which the intensity of the low-energy component of the X emission line is maximized while its high-energy component of it disappears. This angle can easily be ascribed to the crystallographic direction of studied sample. The FSS magnitude and the anisotropy axis of the neutral exciton state are discussed in detail in Section 6.2.1. It is worth noting that the anisotropy axis of the neutral exciton state is preferentially oriented along the [110] crystallographic direction [69].

The emission lines associated with the $p$-shell, the 3X and the 4X, are also split into two linearly polarized components, as it is shown in Fig. 6.2(c) and 6.2(d). The magnitudes of the FSS measured for those lines are equal and their polarization axes are oriented along mutually perpendicular directions. Moreover, the polarization axes of the neutral exciton and triexciton as well as of biexciton and quadexciton states are parallel, respectively. It means that the triexciton state has a non-zero FSS similarly like the neutral exciton state. On the other hand, the quadexciton state does not exhibit the FSS similarly to the case of the biexciton state. In consequence, the FSS of the triexciton state can be defined as $\delta_1^p \equiv |E_{3X_\parallel} - E_{3X_\perp}|$. Nevertheless, it must be taken into account that the fine structure of the triexciton states is related to the exchange interaction between the electron and the hole occupying the $p$-shell levels in a QD with the anisotropy of the confining potential.

A theoretical description of the triexciton state is more complex than for the neutral exciton state due to a difference between the $p$- and $s$-shell levels. In QDs with symmetrical confining potential, there are two degenerate SP states with a $p$-like envelope function: a $p_+$ and a $p_-$. This leads to the formation of four (lowest-energy optically active excitonic configurations of the triexciton) excitonic configurations of the triexciton which posses the lowest energy and are optically active [8]. The electron-hole Coulomb interaction splits them into two configurations: an optically active (bright) and an inactive (dark), similarly to the neutral exciton (for details see Section 2.2.1.1). The asymmetry of the confining potential affects the two degenerate bright states of the triexciton and splits them into two linearly polarized components, as it has been predicted on a theoretical ground [102] and experimentally demonstrated [103]. In the case of the quadexciton, there are two configurations regarding the spin of carriers: the spin-singlet

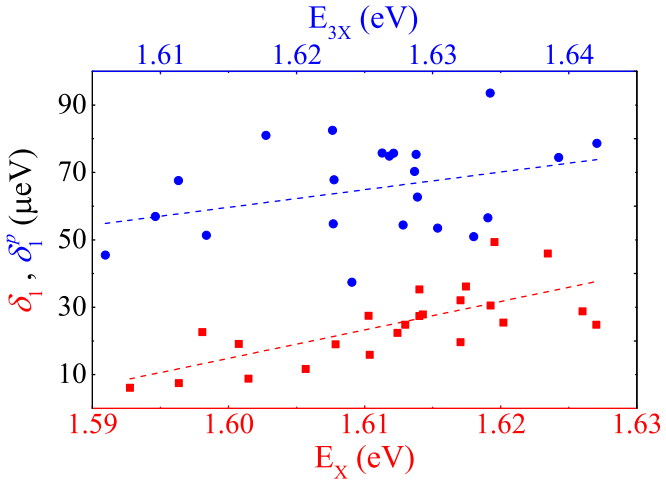


Figure 6.3: Fine structure splitting $\delta_1$ ($\delta_1^p$) as a function of the X (3X) emission energy for a series of single QDs, respectively. Dashed lines are a guide to the eye.

states (with a total spin for electrons and holes: $S_e = S_h = 0$) and the spin-triplet states (with a total spin for electrons and holes: $S_e = S_h = 1$) [8]. In the former case, the anisotropy of the confining potential increases the number of bright excitonic states from two to five, while in the latter case the basis set consists of one configuration only, in which there are two spin-parallel electrons and two spin-parallel holes distributed on two $p$-shell levels and there is no qualitative difference between the isotropic and anisotropic confinement [102]. Due to large splitting between the $p_+$- and $p_-$-shells levels observed in the dots under investigation at zero magnetic field (see Section 5.3), the description of the quadexciton state becomes more complex than discussed above. In spite of that, based on the polarization pattern of the 4X emission line, it can be concluded that the quadexciton state is not split in the studied case.

The FSS of the neutral exciton and triexciton states has been measured for a number of single QDs (more than 20) and it is presented in Fig. 6.3. The $\delta_1$, which describes the FSS of the neutral exciton, varies from 5 μeV up to 50 μeV (10 times in the whole energy range). In the case of triexciton, $\delta_1^p$ changes (2 times) by a factor of 2 in the whole energy range (from 35 μeV up to 95 μeV). The $\delta_1^p$ always exceeds the $\delta_1$. Fig. 6.4 displays a $\delta_1^p/\delta_1$ ratio as a function of the energy separation between the $s$- and $p$-shell levels, $\Delta_{s\text{-}p}$ (see Eq. 5.1). This ratio changes monotonically from ~1 for $\Delta_{s\text{-}p}$=9 meV up to ~9 for $\Delta_{s\text{-}p}$=17 meV. In our opinion, this relationship can be understood in terms of different spatial extent of the $s$- and $p$-shell orbitals, but additional theoretical studies are necessary to support such a supposition.

The polarization properties of the investigated emission lines can be explained within a simple model of the ladder of neutral excitonic states in an asymmetric

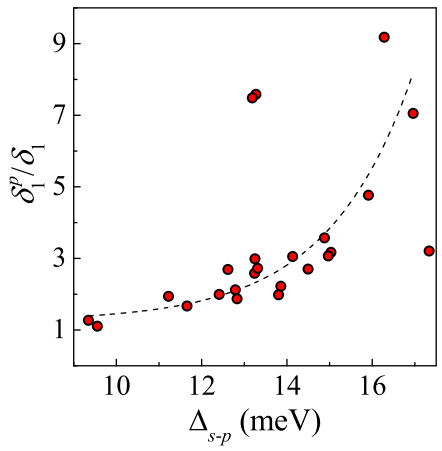


Figure 6.4: The ratio ${\delta_1}^P/\delta_1$ as a function of the energy separation $\Delta E_{s-p}$. Dashed line is a guide to the eye.

confining potential of a QD, presented in Fig. 6.5. Two steps in the quadexciton recombination can be distinguished. The polarizations of photons of the 4X $\rightarrow$ 2X and the 2X $\rightarrow$ 0 cascade are preserved within each of them but no correlation effects can be observed (a random choose of the recombination pathway resulting from the spin-degenerate state of a biexciton).

To verify the proposed model, which is schematically depicted in Fig. 6.5, the polarization-resolved single photon correlation experiment has been performed. The histograms of all the possible photon correlation measurements between the emission lines ascribed to the neutral excitonic states are shown in Fig. 6.6 (a)-(f).

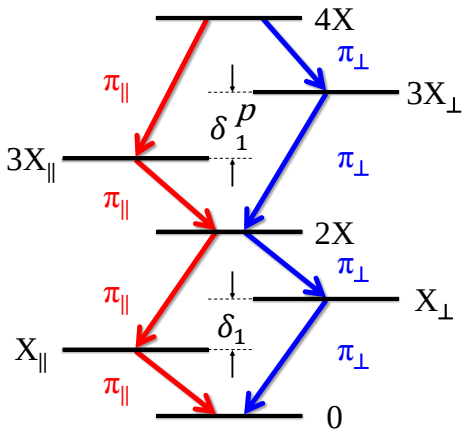


Figure 6.5: Schematic diagram of the cascade decay of a quadexciton in a single QD. The solid blue (red) arrows denote the radiative transitions in two perpendicular polarizations. The $\pi_\parallel$ and $\pi_\perp$ are the parallel and perpendicular linear polarizations with respect to [110] crystallographic direction, respectively.

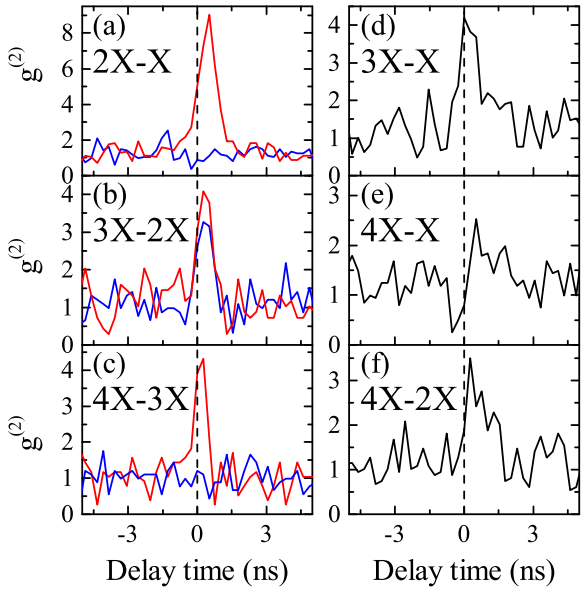


Figure 6.6: The histograms of all the possible photon correlation measurements between the X, 2X, 3X and 4X emission lines. The red and blue curves correspond to the $\pi_{\parallel}$-$\pi_{\parallel}$ (co-polarized) and $\pi_{\parallel}$-$\pi_{\perp}$ (cross-polarized) configurations of the experiment, respectively. $\pi_{\parallel}$ ($\pi_{\perp}$) stands for the linear polarization that is parallel (perpendicular) to the [110] crystallographic direction. The black curves represent the data obtained without the polarization resolution. A zero delay time between the start and stop beam is indicated in each panel with a black dashed line.

All measurements were carried out with the use of the same excitation power. Each cross-correlation histogram reflects the relation between photons of analysed emission lines (in other words, the relation between the photons of the start and stop beams - refer to Section 4.3 for details). During the experiment, the polarization of each beam was adjusted individually.

It is shown in Section 5.4 that a histogram of the X autocorrelation exhibits a sharp antibunching peak, which proves the single-photon character of light emitted from the investigated dots. The co-polarized cross-correlation measurements ($\pi_{\parallel}$-$\pi_{\parallel}$) of the 2X and X photons display a bunching peak around a zero delay time (see Fig. 6.6(a)). This peak is slightly shifted towards positive delay times what confirms that the emission of 2X-photon always precedes the X-photon emission. In the case of the cross-polarized configuration, a very weak antibunching peak appears around the zero delay time. This result can be interpreted in terms of the excitonic ladder presented in Fig. 6.5. Due to the fine structure of the neutral exciton state, the emission of the X-photon can only occur after the 2X-photon in the co-polarized configuration and the emission of photons in the 2X-X cascade shows an antibunching peak in the cross-polarized configuration [104].

The cross-correlation measurement between the 3X- and 2X-photons displays a different effect (see Fig. 6.6 (b)). The obtained results are independent of the polarization configuration. It is a consequence of the spin-degenerate state of a biexciton which causes the polarization of the 2X-photon to be chosen randomly (with the probability around 50%) when the biexciton state is reached after the emission of the 3X-photon.

In the case of a quadexciton (see Fig. 6.6 (c)), the polarizations of the 4X- and 3X-photons are correlated similarly like in the 2X-X cascade. The results of photon correlation experiment combined with the polarization-resolved micro-PL measurements imply that the 4X-3X cascade can also be a good candidate for a source of entangled photon pairs, if the FSS of the triexciton state is substantially reduced.

A combination of other correlation histograms recorded without a polarization resolution (Fig. 6.6 (d)-(f)) with the polarization-resolved correlation histograms (Fig. 6.6 (a)-(c)), fully supports the ladder of the neutral excitonic states shown in Fig. 6.5.

### 6.2.1 FSS of the X emission

This Section is devoted to meticulous studies of the fine structure of the neutral exciton state in single GaAlAs/AlAs QDs, based on the micro-PL experiment performed as a function of the excitation power and with the polarization resolu-

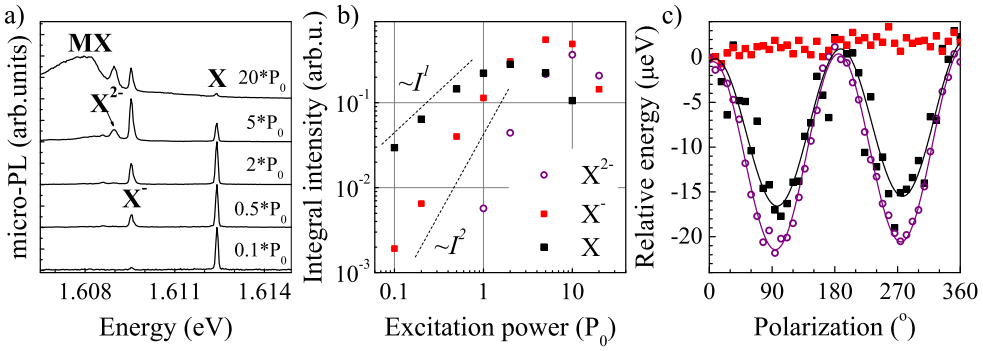


Figure 6.7: (a) The excitation-power evolution of the micro-PL spectra of a single GaAlAs QD measured at $T$= 4.2 K. The spectra are excited above the barrier ($E_{exc}$=2.54 eV). $P_0$=1 μW and indicates the excitation power. The spectra are normalized to the intensity of the X emission line and vertically shifted for clarity purpose. (b) The dependence of the X, $X^-$, and $X^{2-}$ intensities on the excitation power. The dashed lines indicate the linear and quadratic behaviours as guides to the eye. (c) The energy of the X, $X^-$, and $X^{2-}$ lines as a function of the angle of a polarization analyser (points). The FSS of the X and $X^{2-}$ emission lines is determined by means of fitting the cosine-squared function (solid curves).

tion.

The micro-PL spectra of a single dot, excited above the barrier (see Section 5.2), as a function of the excitation power are shown in Fig. 6.7(a). In the lowest excitation power range only one emission line, labelled with X, is observed. It is attributed to the recombination of the neutral exciton state. The increase in the excitation power results in the occurrence of two emission lines, the $X^-$ and $X^{2-}$, on the lower side of the X line. These lines are ascribed to the emission of negatively charged excitons (see Chapters 5 and 8 for detailed information). The intensities of the emission lines are the linear (for X) and quadratic (for $X^-$ and $X^{2-}$) functions of the excitation power (Fig. 6.7(b)). At the highest excitation power, a broad emission band, denoted by MX in Fig. 6.7(a) emerges in the lowest energy range, which is attributed to the emission of multiexcitons confined in a single dot.

In order to identify the observed emission lines, the polarization-resolved micro-PL experiment was performed. The FSS of the X and $X^{2-}$ lines were determined by means of fitting the experimental data plotted as a function of the polarization angle with the Gaussian curve (see Fig. 6.7(c)). It can be seen that both X and $X^{2-}$ lines comprise two linearly polarized components. Their polarization axes are equal within the experimental error and the respective FSS of the X and $X^{2-}$ lines can be considered as equal too. The $X^-$ emission line is not split. The X line is ascribed to the recombination of the neutral exciton (the fine structure of it is described in detail above). The $X^-$ emission line is attributed to the singly negatively charged exciton since the *eh* exchange interaction influences neither the initial (in which the two electrons form the spin-singlet state)

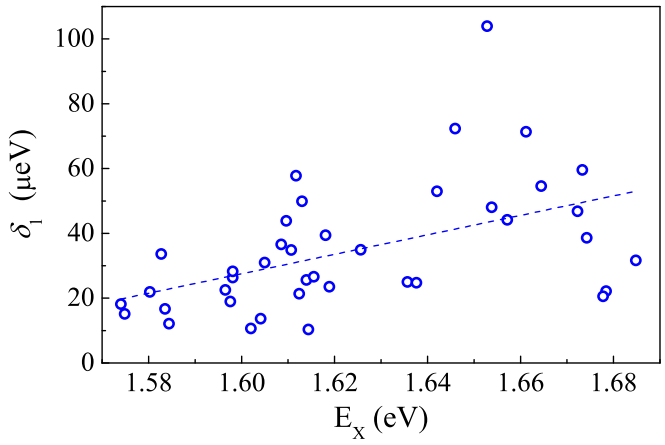


Figure 6.8: The $\delta_X$ as a function of the X emission energy for a series of single QDs, measured in a broad energy range. Blue (dash) dashed line is a guide to the eye.

nor the final state (only one electron left). The $X^{2-}$ emission line is tentatively identified as originating from the recombination of a doubly negatively charged exciton.

The FSS of the neutral exciton was measured for a number of single dots (Fig. 6.8). The X energy ranges from 1.57 eV to 1.69 eV, which suggests a substantial dispersion of QDs size and/or the Ga composition inside them. Moreover, the magnitude of the FSS of the neutral excitons confined in the QDs is distributed over a very broad range (from about 10 µeV to 100 µeV).

In the case of III-V QDs, *e.g.* InAs/GaAs, the FSS of the neutral exciton state usually decreases as a function of the X emission energy (when the size of QDs is connected with the energy of the X line, the FSS of this state is smaller for larger dots). This effect is a result of the piezoelectric field and has already been discussed in Ref. 105. The trend observed in the QDs investigated within the framework of the present thesis is opposite (the FSS increases with the increasing energy of the X line), and it can be related to the effect of the elongation of the QD shape [106].

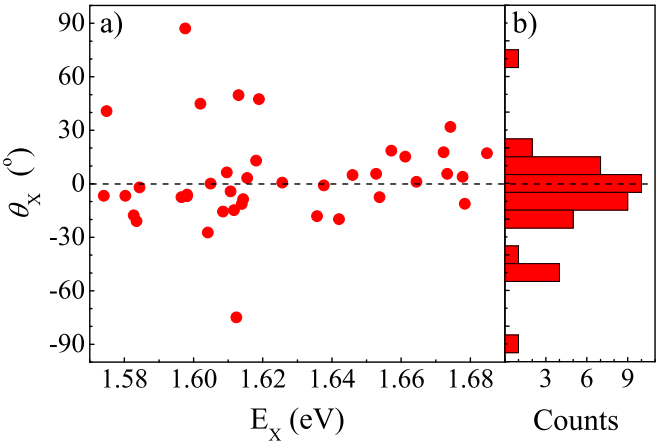


Figure 6.9: (a) The anisotropy axis, $\theta_X$, of the neutral exciton state as a function of its energy. (b) A histogram of the $\theta_X$ obtained for a number of single dots under investigation. $0^o$ indicates the [110] crystallographic direction.

The anisotropy axis of the neutral exciton state (defined in the previous Section) measured for a number of single dots is presented in Fig. 6.9. It can be seen that for most of the dots under study, the anisotropy axis is preferentially oriented along the [110] crystallographic direction. The orientation of the anisotropy axis of the fine structure along the [110] crystallographic axis of the substrate suggests that the origin of the anisotropy is mainly due to the elongated shape of the dots. Such an elongation most likely results from different diffusion rates of Al atoms along the direction parallel and perpendicular to atomic steps at the GaAlAs/AlAs interface.

## 6.3 Magnetic field effects

The application of an external magnetic field to the system consisting of QDs has two effects on the energy structure of the multiexcitons. The first one is the diamagnetic shift, which introduces an inter-play between the spatially and magnetically induced confinement. The second one is the Zeeman splitting related to the spin of electrons and holes.

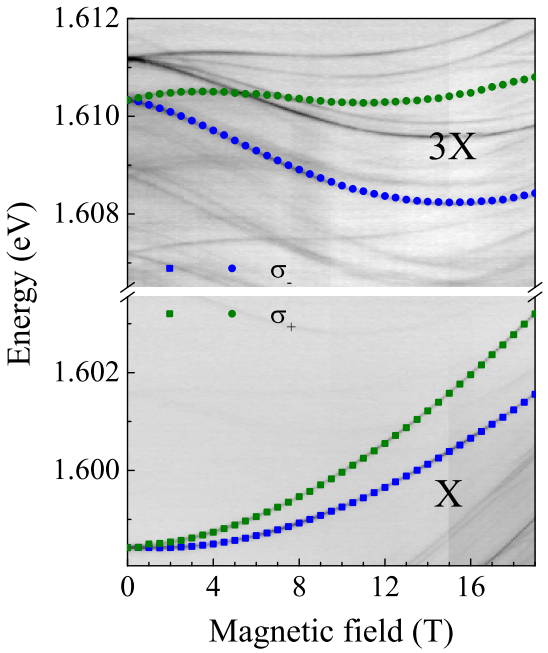


Figure 6.10: The energy evolution of the X (solid squares) and 3X (solid circles) emission lines highlighted on the gray-scale map of the QD emission in the magnetic field up to 19 T. The green and blue points illustrate the $\sigma_+$ and $\sigma_-$ polarizations, respectively.

In this Section, the magnetic field evolution of the X and 3X emission lines associated with the *s*- and *p*-shell and presented in Fig. 6.10 with the blue- and green-coloured points, is studied. In the next two Sections, the effect of both the diamagnetic shift and the Zeeman splitting are analysed in detail.

### 6.3.1 Diamagnetic shift

The diamagnetic shift describes the effect of the magnetic field on the carriers SP levels and on the Coulomb interaction between those carriers. It results from an additional confinement they experience due to the presence of the external magnetic field. In the case of the neutral exciton state, an *e*-*h* pair occupies the ground *s*-shell levels. These levels are characterised by zero angular mo-

mentum (see Chapter 2 for details). As a consequence, the magnetic moment is induced in a direction opposite to the external magnetic field direction. This phenomenon is called diamagnetism. Based on Eq. 2.18, describing the evolution of the neutral exciton state in the magnetic field, the diamagnetic shift can be defined as $\Delta E_d = (E(\sigma_+) + E(\sigma_-))/2$. It represents a quadratic function of the magnetic field and is characterized by a single coefficient $\gamma$. The triexciton consists of three $e$-$h$ pairs, out of which two form a spin-singlet state on the $s$-shell and only the third one occupying the $p$-shell can be affected by the magnetic field. However, the angular momentum of the $p$-shell levels is non-zero ($\pm 1$) what means that they should experience the energy shift which is a linear function of the magnetic field. Although the origin of this shift is not related to the diamagnetism, it is also called diamagnetic in what follows.

Fig. 6.11 displays the evolution of the diamagnetic shift ($\Delta E_d$) of the X and 3X emission lines in the magnetic field. In accordance with Eq. 2.18 and the discussion presented above, it can be written as:

$$\Delta E_d = E_0 + \gamma B^2 \tag{6.1}$$

In the case of the X emission line, a simple description relying on a single-valued $\gamma$ coefficient equal to $\sim$11.5 $\mu$eV/T$^2$ nicely reproduces the experimental data up to $\sim$14 T (refer to the black solid curve in Fig. 6.11). At higher magnetic fields, due to an additional confinement induced by the external field, the evolution of the diamagnetic shift of the X emission line differs from the quadratic behaviour resulting from Eq. 6.1 and becomes a linear function of the field strength (follows the first Landau level - see Sections 2.1 and 2.2.1.2 for details).

The magnetic-field evolution of the diamagnetic shift of the 3X line is more complex, due to the non-zero angular momentum. The effect of Coulomb interaction between the carriers modifies the predicted linear dependence [107] and in the small magnetic field range (up to $\sim$8 T), this evolution can also be described by Eq. 6.1. The $\gamma$ coefficient equals $\sim$-12.3 $\mu$eV/T$^2$ in this case. It is worth pointing out that the absolute values of $\gamma$ are nearly the same for the X and 3X lines, but differ in respect of the sign. At $B \sim$14 T, the slope of the diamagnetic shift changes (see Fig. 6.11). It means, that at higher magnetic fields, the magnetic-field induced confinement becomes larger than the lateral confinement of the dot and, as a result, the evolution of the diamagnetic shift of the 3X line also approaches the first Landau level (further details can be found in 2.2.1.2).

### 6.3.2 Zeeman splitting

Based on a simple theory for the neutral exciton (Section 2.2.1.2), the Zeeman splitting, defined as $\Delta E_Z = E(\sigma_+) - E(\sigma_-)$, is a linear function of the magnetic

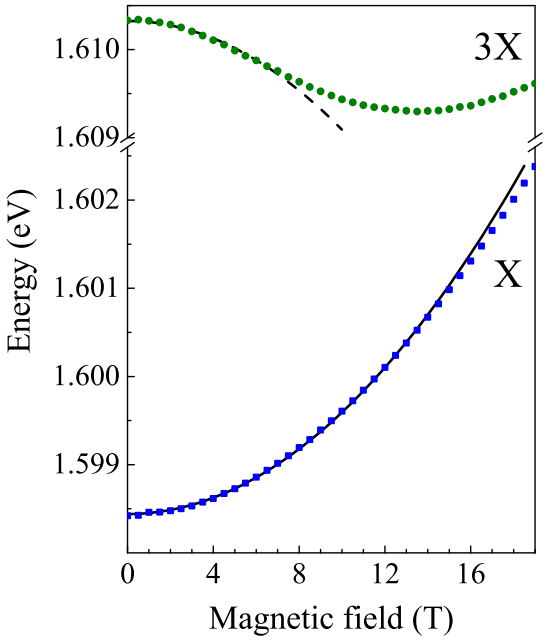


Figure 6.11: The evolution of the diamagnetic shift of the X (blue squares) and 3X (green circles) emission lines in the magnetic field up to 19 T. The solid and dashed black curves result from fitting the experimental data with Eq. 6.1.

field with the magnitude determined by the effective Landé factor $g^*$. When including the effect of FSS splitting, it can be expressed as:

$$\Delta E_Z = \sqrt{\delta_1^2 + g^* \mu_B B^2} \tag{6.2}$$

The measured Zeeman splitting of the X and 3X emission lines in the magnetic field is presented in Fig. 6.12. As can be seen, its evolution for both lines is highly non-linear. In spite of this non-linearity, Eq. 6.2 can sufficiently well describe the experimental results in the low-magnetic-field range (up to ~8 T). As shown with straight lines draw in Fig. 6.12, the approximate values of $g^*$ parameter are then $g^*$=1.12 and 3.28,correspondingly for the X and 3X emission lines. The fact that the Zeeman splitting of the 3X emission line is ~3 times bigger as compared to the X line is unexpected. As mentioned at the beginning of Section 6.3.1, only one *e*-*h* pair forming the triexciton and occupying the *p*-shell level, has a non-zero momentum. Thus, the splitting of the triexciton and the neutral exciton states should be similar. The observed effect can be explained in terms of the HH-LH mixing induced by the magnetic field (see Section 2.2.1) [10, 108, 109], which is discussed below. It is important to stress that the attribution of the electron and hole Landé factors in the effective $g^*$ factor is a difficult task due to unknown percentage of the Al atoms in the whole GaAlAs QDs. The electron $g_e$ factors in a GaAlAs alloy are relatively small and vary from -0.4 to 0.4 depending on

Table 6.1: The $z$ projections ($m_{h,z}$) of the envelope angular momentum and the charge density weights associated with each $J_{h,z}$ component of the three lowest-lying SP hole states at $B$=0. Only the states with positive $F_{h,z}$ are shown. States with negative $F_{h,z}$ have reversed order of weights and $m_{h,z}$, as well as the opposite sign of $m_{h,z}$. All the values collected in the table are taken from Ref. 111.

| | | $J_{h,z}=3/2$ | $J_{h,z}=1/2$ | $J_{h,z}=-1/2$ | $J_{h,z}=-3/2$ |
|---|---|---|---|---|---|
| $F_{h,z}=3/2$ | $m_{h,z}$ | 0 | 1 | 2 | 3 |
| | weight | 0.975 | 0.018 | 0.006 | 0.001 |
| $F_{h,z}=1/2$ | $m_{h,z}$ | -1 | 0 | 1 | 2 |
| | weight | 0.868 | 0.047 | 0.072 | 0.013 |
| $F_{h,z}=5/2$ | $m_{h,z}$ | 1 | 2 | 3 | 4 |
| | weight | 0.928 | 0.041 | 0.029 | 0.002 |

the alloy composition [110]. Therefore, the effective excitonic Landé factor in the investigated dots mostly depends on the hole $g_h$ factor. Big amplitudes and pronounced nonlinearities in the observed excitonic Zeeman splittings point out towards relevant effects of the heavy and light hole mixing for the valence band levels of our dots [10,108,109]. On the qualitative level, this can be accounted by the following arguments.

As a result of the HH-LH mixing, the $J_h$ and $m_h$ are no longer proper quantum numbers for holes. Owing to this fact, it is necessary to define a new quantum number - the total angular momentum $F_h = J_h + m_h$, which is the sum of the Bloch angular momentum $J_h$ ($J_{h,z}$=$\pm 3/2$ and $\pm 1/2$ for the heavy and light holes, respectively) and the envelope angular momentum $m_h$ ($m_{h,z}$=0,$\pm$1,$\pm$2,...) [111–113].

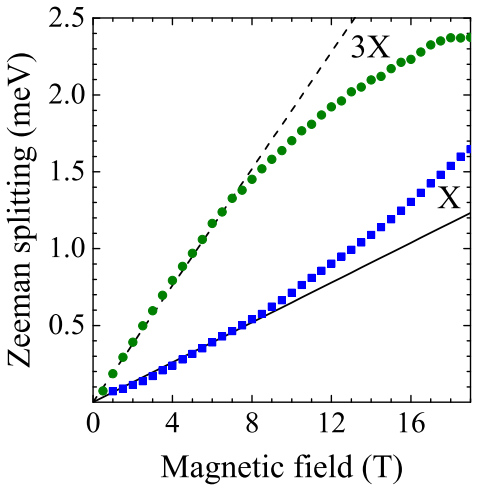


Figure 6.12: Zeeman splitting of X (blue squares) and 3X (green circles) emission lines in the magnetic field up to 19 T. The solid and dashed black curves result from fitting the experimental data with Eq. 6.2 in the range 0<B<8 T.

The $z$ projection of $F_h$ reads $F_{h,z} = J_{h,z} + m_{h,z}$. For each $F_{h,z}$, various combinations of $J_{h,z}$ and $m_{h,z}$ are possible. For the ground $s$-like hole level, a predominant component of the $F_h$=3/2 state at zero magnetic field is that of $J_h$ =3/2 (about 97.5% of the charge density in the case of the InGaAs QDs presented in Tab. 6.1 [111]), which corresponds to $m_h$=0. The $p$-like hole levels, labelled with $F_h$=1/2 and 5/2, split up in the presence of the magnetic field, leading to a characteristic emission pattern that stems from the optical selection rules: $\Delta m_z$=0 and the spin conservation $S_{e,z} + J_{h,z} = \pm 1$. To determine the allowed transitions, only the dominant $m_z$ contribution to each $F_z$ level is used. The diagram of the three lowest-lying SP hole states of the InGaAs dots from Ref. 112 is shown in Fig. 6.13.

The analysis of Fig. 6.13 leads to the conclusion that the $p$-like levels (*e.g.* $F_h$=1/2 and 5/2) have much bigger Zeeman splitting than the $s$-like levels (*e.g.* $F_h$=3/2), what results from the HH-LH mixing. This effect explains the huge Zeeman splitting observed in this work for the 3X emission line, which is ∼3 times bigger than the splitting of the X line, as mentioned at the beginning of the present section.

The Zeeman splitting of the X emission line displays a quadratic $\propto B^2$ contribution. This effect has also been explained on the basis of the HH-LH mixing by redefining the hole $g_h$ factor [109]. The hole Landé factor is described as the sum of the linear ($g_h$) and the quadratic components. The second one appears due to the HH-LH mixing in the valence band.

At high magnetic fields, the Zeeman splitting of the 3X emission line exhibits a nonlinear behaviour and becomes proportional to $\sqrt{B}$. The origin of this effect is not entirely understood but it can be related to the change of the hole level

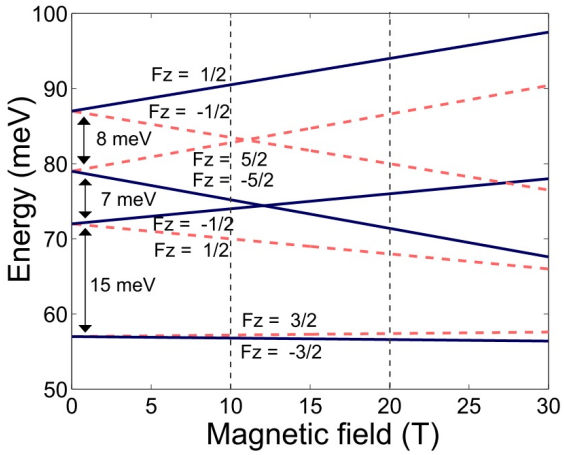


Figure 6.13: The magnetic field evolution of the single-particle hole energy levels as obtained from the photoluminescence experiment. The diagram adapted from Ref. 112..

by a given hole (forming a $e$-$h$ pair, which occupies the $p$-shell), as a result of the anticrossing they experience in the high magnetic field range [10,30].

## 6.4 Photoluminescence excitation

The photoluminescence excitation spectroscopy is often used to study the excitation spectra of various excitonic complexes confined in a QD [11,16,60,61,114–116]. As a consequence this method has been carried out on several dots. We refer to those dots according to the energy distance $\Delta_{s\text{-}p}$ between their characteristic X ($s$-shell) and 3X ($p$-shell) emission lines. Dots with $\Delta_{s\text{-}p}$=12.24, 14.30 and 16.97 meV have been measured in magnetic fields. Mostly discussed are the results obtained for the dot with 14.30 meV. The PLE spectroscopy and magneto-spectroscopy of single dot excitons is one of the relevant themes of this work. First to be inspected are the PLE spectra of the basic excitonic state: neutral exciton. micro-PLE spectra are represented here as a function of the energy distance between the detection energy fixed at the X position and the actual energy of the laser excitation. Mostly explored is the range of excitation energies which extends from 10 meV to 20 meV (above the X emission line). This range covers the expected resonance energies of the excited, $p$-shell related states. A possibility to observe in this range the resonant peaks due to transitions involving the $s$-shell of the conduction band and a sequence of different levels in the valence band should be also considered [11,16]. It results from the symmetry breaking, possibly related to mixing with other bands [61,114].

The analysis begins with presentation of the characteristic micro-PLE spectra

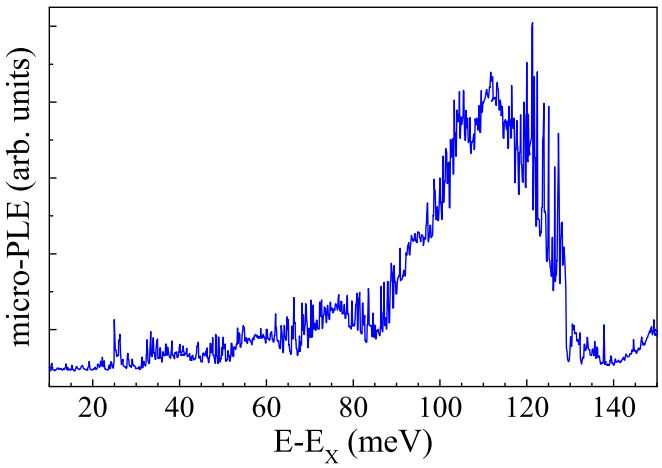


Figure 6.14: Micro-PLE spectrum of a single dot detected on the X emission line (dot with $\Delta_{s\text{-}p}$=12.63 meV). The scale of the horizontal axis is set by the energy relative to the X emission line.

of the neutral exciton, measured in a relatively broad spectra range (∼10 - 150 meV, above the X emission line) - see Fig. 6.14. Perhaps to some surprise, this spectrum is pretty complex, consist of huge amount of sharp lines which appear together with some broader bands. A broad feature of the highest intensity, seen in this spectrum around 110 meV, is related to the crossover between the quasi-resonant and the above the barrier excitation regimes. Reduction of the PLE intensity above 120 meV is due to substantial change in the shape of Pl spectra when keeping the same excitation power but fixing the excitation energy well above the dot barrier (see Fig. 5.2). At energies below 90 meV, one may recognized some modulated structure in this spectrum, appearance of four bands centred, correspondingly at ∼26, ∼39, ∼57, ∼76 meV. We speculate that those bands may be related to the excited states of the neutral exciton, involving the subsequent, electronic shells of the dot, but each band involving a number of hole levels. Notably, those absorption bands appear at energies which are considerable higher than those of the corresponding sequence of bands observed in emission spectra. This underlines the essential difference between the excitation spectra of the neutral exciton and the emission spectra due to multiexcitons (involving Coulomb binding of additional carriers). The micro-PLE spectrum, such as shown in Fig. 6.14, is however very difficult to be accurately interpreted in its whole, broad energy range.

In what follows, the studies are focused on the low energy parts (∼10 – ∼30 meV) of the micro-PLE spectra, where the resonant peaks appear as better resolved. An example of such a spectrum is shown in Fig. 6.15, for the dot with $\Delta_{s\text{-}p}$=14.30 meV. We suspect that the strongest resonant peak ob-

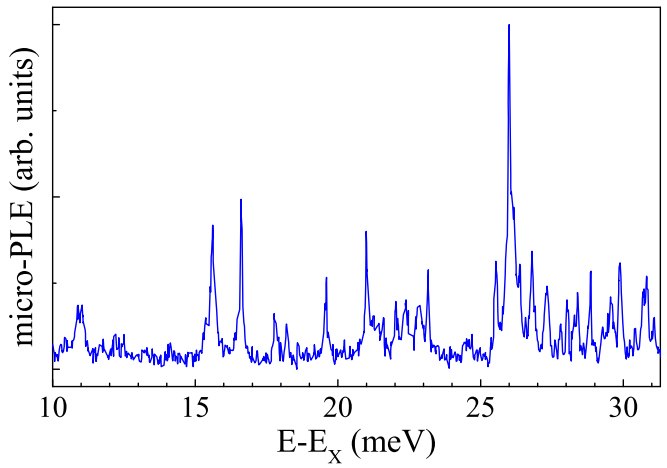


Figure 6.15: Micro-PLE spectrum of a single GaAlAs QD detected on the X emission line (dot with $\Delta_{s\text{-}p}$=14.30 meV). The scale of the horizontal axis is set by the energy relative to the X emission line.

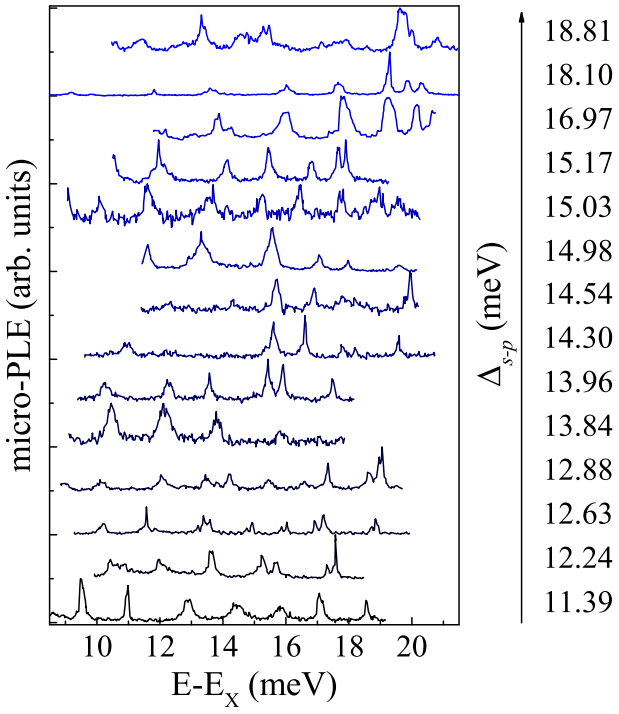


Figure 6.16: Micro-PLE spectra detected on the X emission line, measured for a series of QDs characterized by different amplitude of $\Delta_{s\text{-}p}$. The scale of the horizontal axis is set by the energy relative to the X emission line. The spectra are normalized to the most intense peaks and vertically shifted for clarity purpose.

served in this spectrum at ∼26 meV is related to the onset of absorption involving the electronic $p$-shell.

Now, we concentrate on peaks at lower energies, and show that they appear due to absorption process to the electronic $s$-shell but from different confined hole levels of the dot. Low energy (10 – 20 meV) micro-PLE spectra detected on the X emission line for a series of dots (characterized by different $\Delta_{s\text{-}p}$ splitting) are shown in Fig. 6.16. It is also important to remember, that the spectral width of the resonant peaks is extremely small (the "atomic" nature of QDs) and, as a result, the micro-PLE spectra need to be measured with a high resolution (steps on the level of ∼5-10 µeV) of the excitation energy (see Fig. 6.15 and 6.16). As can be seen, a general sequence of the resonant peaks associated with the neutral exciton is similar for each single dot and corresponds to the specific pattern of the micro-PL spectra of different QDs (see Fig. 5.5). It means that the position of a given excitonic state changes with $\Delta_{s\text{-}p}$, but the ladder of levels is, to some extend, preserved. Notably, no systematic relationship between the shift of the resonant peaks and the value of $\Delta_{s\text{-}p}$ can be established.

The energy separation between individual peaks is rather small and varies

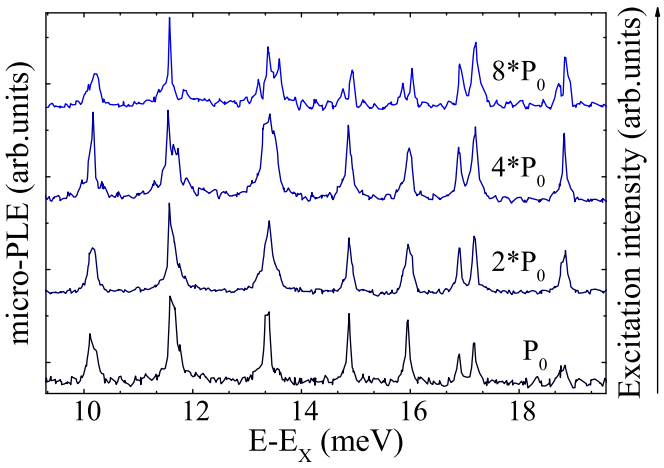


Figure 6.17: The excitation-power evolution of micro-PLE spectra detected on the X emission lines (dot with $\Delta_{s\text{-}p}$=12.63 meV). The scale of the horizontal axis is set by the energy relative to the X emission line. The spectra are normalized to the most intense peaks and vertically shifted for clarity purpose.

from 0.5 meV to 2.5 meV. Such a small energy separation can only be found in the valence band, where the distance between the hole levels has been previously postulated to fall within a similar range [49]. Due to the HH-LH mixing, an absorption process from the excited hole levels, the *p*-, *d*-, ... shells, to the ground electron level, the *s*-shell, is allowed [11,16] and can be responsible for the resonant peaks.

Fig. 6.17 displays the micro-PLE spectra of the neutral exciton as a function of the excitation power. A little effect of the excitation power on the lineshape of the micro-PLE spectra can be seen. This suggests that the resonant peaks in the spectra can be ascribed to the absorption of a single *e*-*h* pair in an empty QD. It is worth noticing that in a more complex case, *e.g.* an *e*-*h* pair excited in the presence of another *e*-*h* pair in a dot, the intensity of resonant peaks should be more affected by the excitation power to much larger extent, similarly like for the emission lines attributed to the recombination of the multiexcitons (the 2X emission line shows the power dependence with the exponent above one) [116,117].

A number of discrete and energetically resolved resonant peaks has been observed in the micro-PLE spectra of the neutral exciton. The energy separation between them is on the order of a few meV, suggesting the transitions between the levels of different symmetries, *e.g.* the *s*- and *p*-like. Since attributing the resonant peaks to the specific transitions is a challenging task, the measurements of the micro-PLE spectra in the presence of an external magnetic field have been performed. The results of those experiments are presented and discussed in the next Section.

### 6.4.1 PLE spectra in a magnetic field

Fig. 6.18 shows the magnetic field evolution of the micro-PLE spectra of the neutral exciton measured in the excitation energy range between ∼10 to 30 meV above the X-emission energy. At high energies, in the range above ∼21 meV, the observed pattern of resonance peaks is extremely complex and the resonances can be hardly followed with the magnetic field. Nevertheless in this energy range, some of the observed resonances may be presumed to lower their energies with the magnetic field, see *e.g.*, the evolution of peaks originating from structures around ∼26 meV at B=0. This characteristic behaviour confirm our previous conjecture that the resonant peak around ∼26 meV is indeed due to the excited states of the neutral exciton involving the electrons from the *p*-like conduction band levels.

The transitions observed at lower energies, below ∼21 meV can be analysed more accurately. The magnetic-field evolution of the micro-PLE spectra

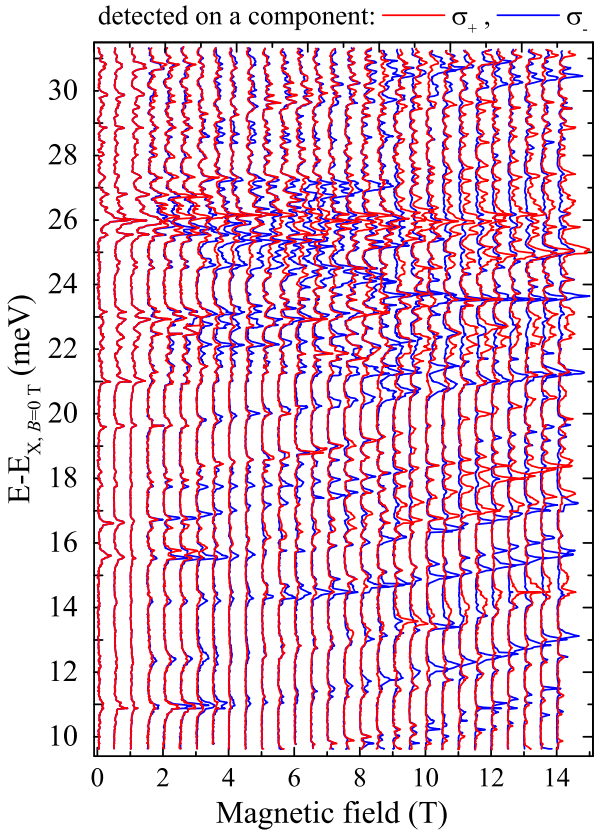


Figure 6.18: The magnetic-field evolution of micro-PLE spectra detected on the X emission line (dot with $\Delta_{s\text{-}p}$=14.30 meV). The scale of the horizontal axis is set by the energy relative to the X emission line. The spectra are normalized to the most intense peaks and shifted for clarity purpose.

of the neutral exciton is presented in Figs 6.20, 6.19 and 6.21 for three single QDs.

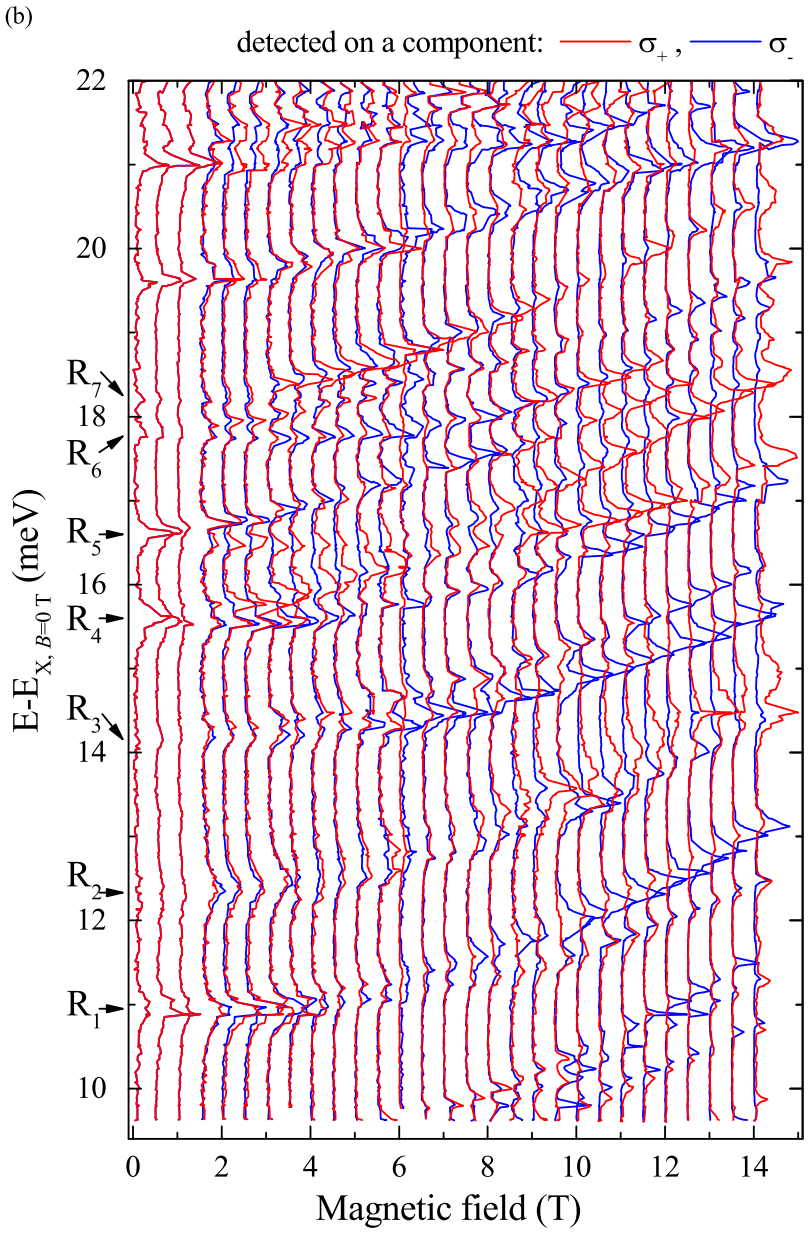


Figure 6.19: The magnetic-field evolution of micro-PLE spectra detected on the X emission line (dot with $\Delta_{s\text{-}p}$=14.30 meV). The scale of the horizontal axis is set by the energy relative to the X emission line. The spectra are normalized to the most intense peaks and shifted for clarity purpose.

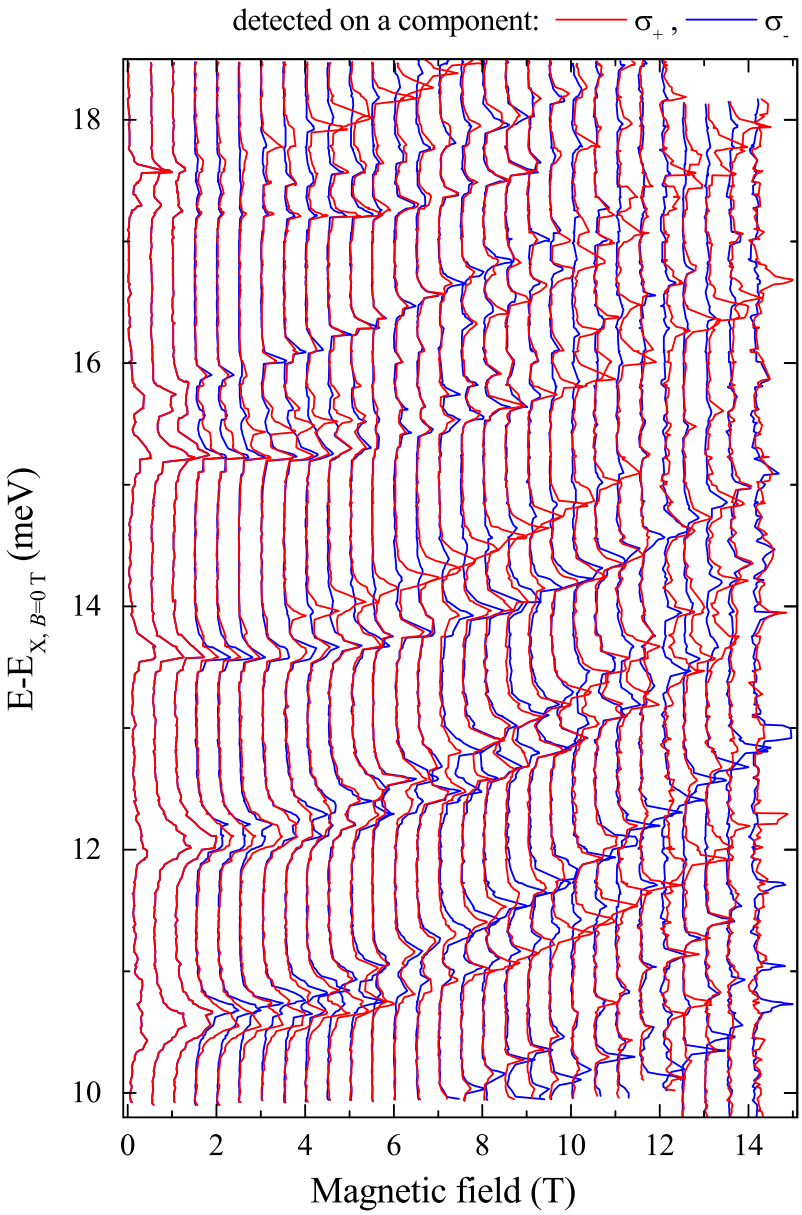


Figure 6.20: The magnetic-field evolution of micro-PLE spectra detected on the X emission line (dot with $\Delta_{s\text{-}p}$=12.24 meV). The scale of the horizontal axis is set by the energy relative to the X emission line. The spectra are normalized to the most intense peaks and shifted for clarity purpose.

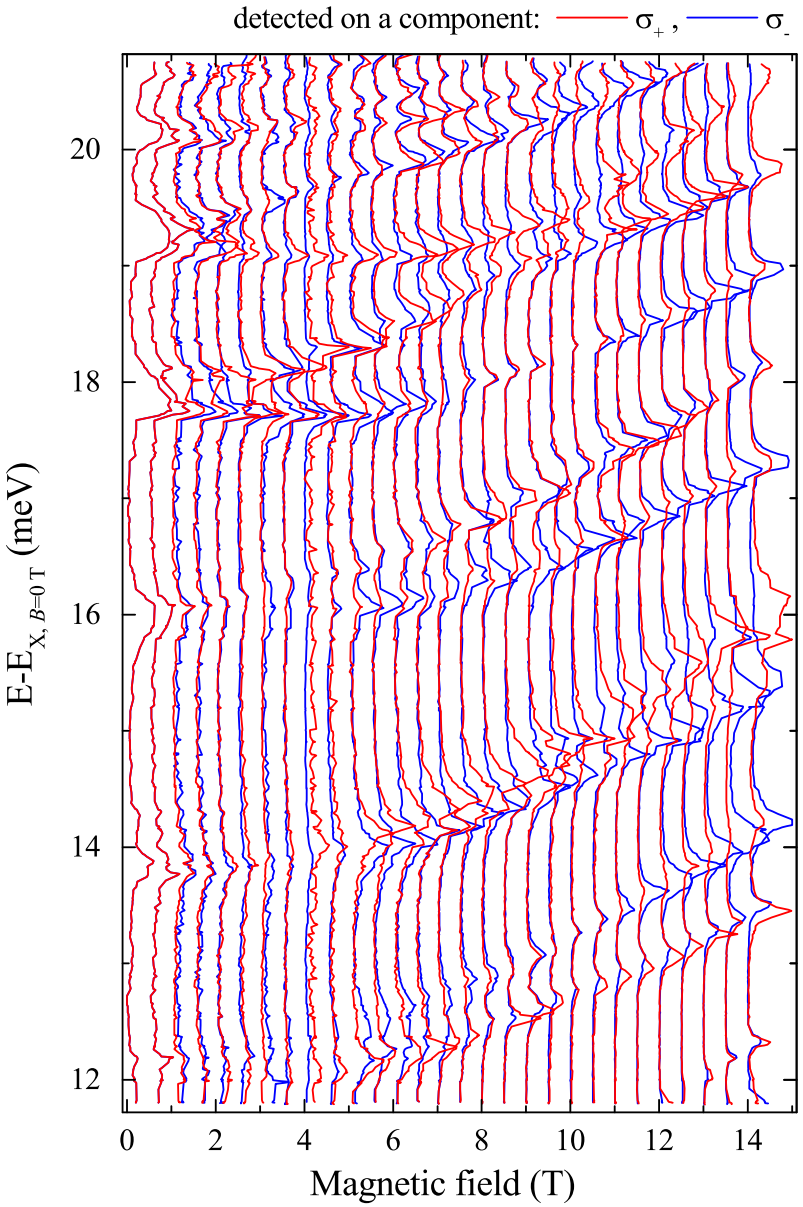


Figure 6.21: The magnetic-field evolution of micro-PLE spectra detected on the X emission line (dot with $\Delta_{s\text{-}p}$=16.97 meV). The scale of the horizontal axis is set by the energy relative to the X emission line. The spectra are normalized to the most intense peaks and shifted for clarity purpose.

The comparison between these three set of spectra leads to the following conclusions:

- The patterns of resonant peaks detected on the X emission lines and measured on three different dots are very similar. All resonant peaks depicted in Fig. 6.19 exhibit the same type of the magnetic-field evolution. This type of dependence is typical for emission lines associated with the recombination of multiexcitons from the *s*-shell (see Fig. 5.4). The main difference manifests itself in the energy position of the resonant peaks. As a result of striking similarities between the patterns observed for various micro-PLE spectra, the resonant peaks can be organized into two groups:
  - The first group consists of three well-separated resonant peaks that for zero magnetic field occur at ∼11 meV, ∼12.3 meV and ∼14.1 meV (see Fig. 6.19). Those peaks are labelled $R_1$, $R_2$ and $R_3$ in ascending order of their central energy.
  - The second group includes two pairs of "interacting" resonant peaks (note the crossings and anticrossings between them that develop with

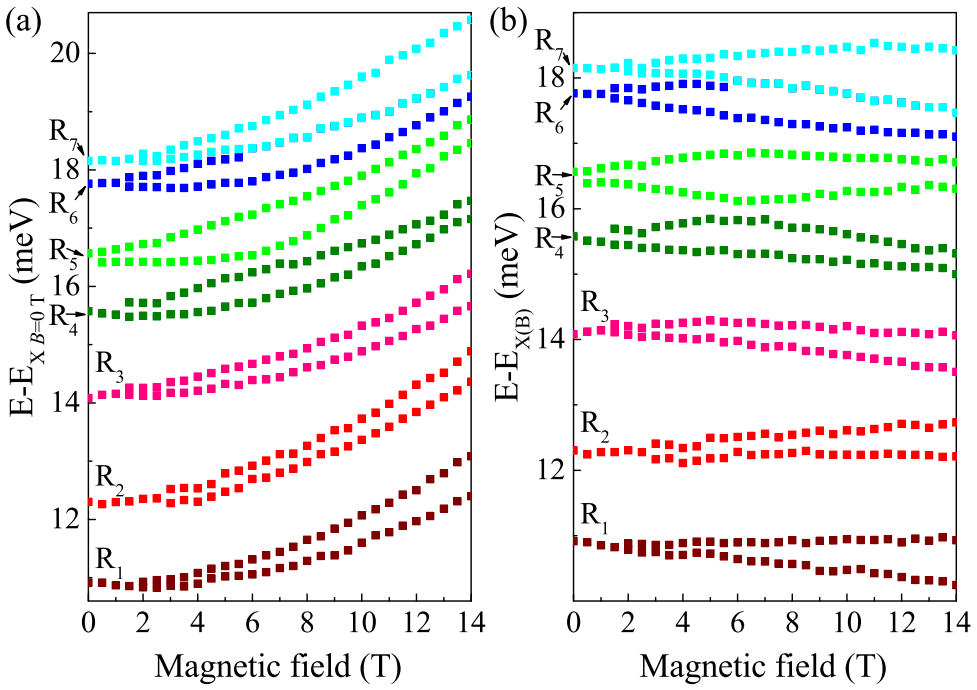


Figure 6.22: A fan chart of the magneto-absorption transitions of the neutral exciton (dot with $\Delta_{s\text{-}p}$=14.30 meV). The relative energy is calculated with reference to the energy of the X emission line at zero magnetic field. The diamagnetic shift of this line is not corrected in panel (a) and extracted from the data in panel (b).

the increasing magnetic field), which for zero magnetic field occur at ∼15.6 meV, ∼16.5 meV and slightly below and above ∼18 meV (see Fig. 6.19). Those peaks are labelled $R_4$, $R_5$, $R_6$ and $R_7$, respectively.

Fig. 6.22 displays the fan chart of the magneto-absorption transitions of the neutral exciton, labelled above with $R_1$, $R_2$, $R_3$, ... and measured on the dot for which the micro-PLE spectra are presented in Fig. 6.19. The division of the resonant peaks into two groups is observed. It has to be mentioned that the zero-field splitting between the $R_1$, $R_2$ and $R_3$ lines is substantially above 1 meV (typically 2 meV), when in the case of the "interacting" peaks it falls below 1 meV. The presence of (anti)crossings between the peaks belonging to the first group can not be definitively excluded and they probably do appear at higher magnetic fields. The (anti)crossings of emission lines are likely related to the anticrossings of levels, that result from the interaction induced by the HH-LH mixing of the valence band levels of the investigated QDs.

The diamagnetic shift and the Zeeman splitting of the first group of resonant peaks ($R_1$, $R_2$, $R_3$) is presented in Fig. 6.23(a) and (b). As can be seen, for all the lines the magnitude of the diamagnetic shift is essentially the same (small red-shifts appear in the low-magnetic-field evolution of the $R_1$ and $R_2$ peaks). The Zeeman splitting looks very similar for all the resonant peaks, but is about two

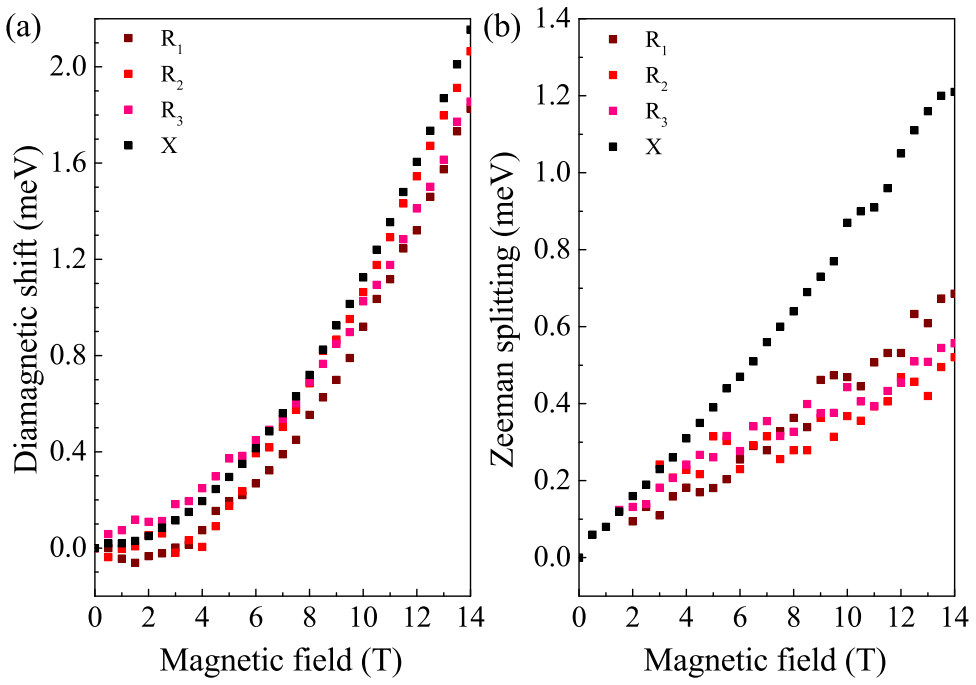


Figure 6.23: (a) The diamagnetic shift and (b) the Zeeman splitting of three resonant peaks: $R_1$, $R_2$, $R_3$ and the X emission line (dot with $\Delta_{s\text{-}p}$=14.30 meV).

times smaller than for the X emission line. It suggests a significant difference of Zeeman splitting between the electron and/or (holes) hole levels that are involved in the transitions under study.

Based on the results and the discussion presented above, the origin and the properties of the resonant peaks are studied in what follows.

### 6.4.2 Origin of PLE peaks

The identification of the resonant peaks observed in the micro-PLE spectra of the neutral exciton (see Fig. 6.19) is not a trivial task because of, *e.g.*, the number of peaks that occur in the spectra. First of all, it has to be clearly said that the structure of levels in the conduction and valence bands of the studied GaAlAs/AlAs QDs is more complex than in the case of the InAs/GaAs dots and can not be characterized in terms of the Fock-Darwin diagram (compare Fig. 2.5 and 5.4). Further remarks about the structure of levels in both bands are as follows:

- The structure of the conduction band levels of the QDs investigated within the framework of this PhD thesis is not much different from the structure established for the InAs dots. The SP levels attributed to the $s$- and $p$-shells can be distinguished. Nonetheless, as a consequence of the presence of an in-plane anisotropy and due to the electron-electron interactions, the degeneracy between the $p_-$ and $p_+$ states is lifted. It results in the emergence of both the $p_x$ and $p_y$ states, which evolve into the $p_-$ and $p_+$ states at high magnetic fields (refer to Section 5.3 for more information). Previously in this work, the two lowest-lying energy levels in the conduction band have been called the $s$- and $p$-shells in accordance with a popularly used nomenclature. Due to the splitting of the $p$-subshells, however, the energetically lower one of them should be identified from now on as a $p_-$-shell.

- Due to the occurrence of the heavy and light hole mixing, as it has been discussed in Section 6.3, the $J_h$ and $m_h$ are no longer proper quantum numbers for the hole levels. In consequence, new quantum numbers: the total angular momentum - $F_h = J_h + m_h$ and its $z$ projection - $F_{h,z} = J_{h,z} + m_{h,z}$, have been defined. A state characterized by a given value of $F_{h,z}$ consists of all the possible combinations of $J_{h,z}$ and $m_{h,z}$, but the main contribution comes from the heavy holes ($J_{h,z} = \pm 3/2$) and the orbital momentum ($m_{h,z} = 0, \pm 1, \pm 2, \ldots$) corresponding to the consecutive hole shells ($s$-, $p$-, $d$-,...shell). The effect of the in-plane anisotropy on the hole levels is omitted.

Fig. 6.24 displays the presumed ladders of levels in the conduction and valence bands of the studied dots and the possible absorption transitions of a single $e$-$h$

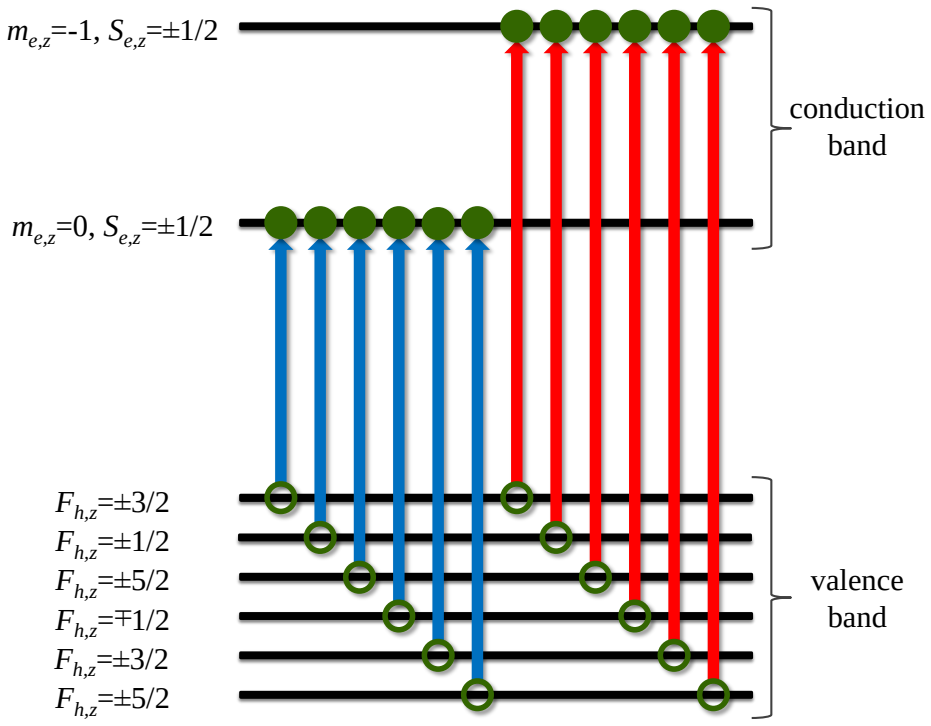


Figure 6.24: Black horizontal lines illustrate the ladders of levels in the conduction and valence bands. The blue (red) arrows indicate the possible absorption transitions between the valence band levels and the $s$-shell ($p_-$-shell), respectively.

(pairs) pair between them. Due to the symmetry breaking, resulting from the HH-LH mixing, the absorption transitions between levels of the different symmetry, *e.g.* the $s$- and $p$-shells, are also allowed [11, 16, 61, 114].

The $s$-shell-like resonant peaks of the neutral exciton are related to the transitions between the consecutive levels in the valence band and the $s$-shell level in the conduction band - see the transitions marked in red in Fig. 6.24. This behaviour of peaks can be explained as a result of the magnetic field effect on the spatial confinement. It is expected that the ladder of electrons in the conduction band should be affected by such a phenomenon to a larger extent than the ladder of holes in the valence band [49]. Based on the presented origin of the resonant peaks, the energetic separation between the hole levels is estimated to be on the order of 1-2 meV. Unfortunately, such a small energetic distance makes it impossible to register the transitions associated with the lowest-lying energy levels, such as: $F_{h,z} = \pm 3/2 \rightarrow m_{e,z} = 0$, $F_{h,z} = \pm 1/2 \rightarrow m_{e,z} = 0$, ... [11, 16]. This in turn disables the attribution of the resonant peaks to a specific transition (the laser could not be tuned closer to the detection range, for the sake of available long-pass filter that was placed in front of the monochromator when performing the experiments).

We expect that resonant peaks due to the process involving the $p$-shell-like electron should appear in the high-energy part of the micro-PLE spectrum (above ~21 meV in Fig. 6.18). However, in this energy range a big number of resonant peaks emerges, out of which only one around 26 meV exhibits a $p$-shell-like evolution in the magnetic field. The high intensity of this peak suggests that it is associated with a transition between levels of similar symmetries. The most probable transition is the excitation of an electron from the "$p$-shell" level of the valence band ($F_{h,z} = \pm 1/2$) to the $p_-$-shell levels in the conduction band ($m_{e,z} = -1$).

The presented results shed some new light on the issue of both ladders of the electron and hole levels in the QDs. In particular, the ladder of hole levels in the valence band is more complex as a result of the HH-LH mixing and can not be discussed in terms of the Fock-Darwin diagram ($s$-, $p$-, ... shells), as it has been done so far in the literature [11, 16].

## 6.5 Conclusions

In conclusion, the properties of four emission lines from the *s*- and *p*-shell that are attributed to the transitions within the neutral charge states, such as: X, 2X, 3X, and 4X are presented and discussed. The fine structure splitting of the X and 3X excitonic states is analysed and the diagram of the cascade decay of the quadexciton in the single QDs is postulated. Moreover, the two effects on the X and 3X emission lines induced by an external magnetic field: the diamagnetic shift and the Zeeman splitting, are described. Due to the non-linearity observed for the Zeeman splitting of the X emission line and the large Zeeman splitting of the 3X emission line, the effect of the HH-LH mixing is considered. The magnetic-field-dependent photoluminescence excitation spectra detected on the X emission line are also presented and the origin of the resonant peaks is discussed. In general, the resonant peaks follow one type of evolution in the magnetic field, the *s*-shell-like. The *s*-shell-related resonant peaks are attributed to the transition between the excited hole levels in the valence band and the ground *s*-shell level in the conduction band. As compared to a typical model of the hole shells known in the literature, the hole ladder in the valence band is described in the present thesis within a more complex framework, which takes into account also the HH-LH mixing.

# Chapter 7

# Positively charged excitonic states

There are significant differences in the spin states of charged excitonic complexes as compared to neutral ones. As charged complexes have total spins of half-integer values, a double degeneracy remains in the absence of magnetic field in accordance with the Kramer theorem [34]. In addition, the exchange interaction between the inter-sublevel spins becomes pronounced due to the presence of an excess carrier. As a result, several split peaks that originate from the recombination of charged excitonic complexes have been observed so far in the micro-PL spectra [38, 118, 119].

In this Chapter, the properties of five emission lines attributed to the recombination process of the positively charged states between the *s*- and *p*-shell levels are discussed. Especially, the fine structure splitting, the diamagnetic shift and the Zeeman splitting of these lines are studied. Moreover, the magnetic-field-dependent photoluminescence excitation spectra of the singly charged excitons are presented and analysed.

## 7.1 Optical recombination of the positively charged excitons

The micro-PL spectra of a single dot, excited quasi-resonantly (see Section 5.2) and measured as a function of the excitation power are shown in Fig. 6.1. In the low excitation power range (below $P_0$=10 μW), a single emission line, labelled $X^+$, is observed. This line is attributed to the recombination of a single *e*-*h* pair and an additional hole - the positively charged exciton, which forms

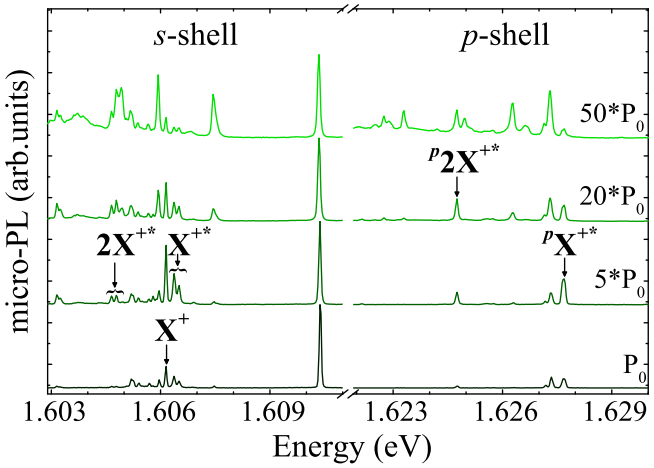


Figure 7.1: The excitation-power evolution of the micro-PL spectra of a single GaAlAs/AlAs QD measured at $T$= 4.2 K. The spectra are excited quasi-resonantly ($E_{exc}$=1.71 eV). $P_0$=10 µW and indicates the excitation power. The spectra are normalized to the intensity of the X emission line and vertically shifted for clarity purpose.

the spin-singlet state. At higher excitation power, several peaks appear on the low energy side of X. They are related to the emission of the multiexcitons in the QD. Among those peaks, the $X^{+*}$ and $2X^{+}$ emission lines occur which are identified as originating from the emission of a singly positively charged exciton (a single $e$-$h$ pair and an additional hole) forming a spin-triplet state and a positively charged biexciton (two $e$-$h$ pairs and an additional hole) forming a spin-singlet state, respectively. A broad group of features, which include the $X^{+}$, $X^{+*}$ and $2X^{+}$ emission lines, is associated with the recombination of $e$-$h$ pairs occupying the $s$-shell levels.

A further increase in the excitation power leads to the emergence of another set of lines at higher energies (∼12 meV above the energy of the X line), ascribed to the emission that takes place within the $p$-shell (see Fig. 6.1). Two emission lines denoted by $^{p}2X^{+*}$ and $^{p}X^{+*}$ occur in this energy range. The former one is recognized as resulting from the recombination of a positively charged biexciton (two $e$-$h$ pairs and an additional hole) forming a spin-triplet state. The attribution of the latter one is analysed in the next Section 7.3. Emission lines which are not labelled in Fig. 6.1 belong to neutral and negatively charged states, and have been discussed in Chapter 6 and 8.

The emission lines due to the recombination of positively charged multiexcitons have more complex fine structure than the lines related to the neutral multiexcitons (to compare see Section 6.2). Fig 7.2(a) shows the effect of the linear polarization on a typical micro-PL spectrum of the positively charged GaAlAs QD (as a function with the linear polarization-resolution). Based on results of

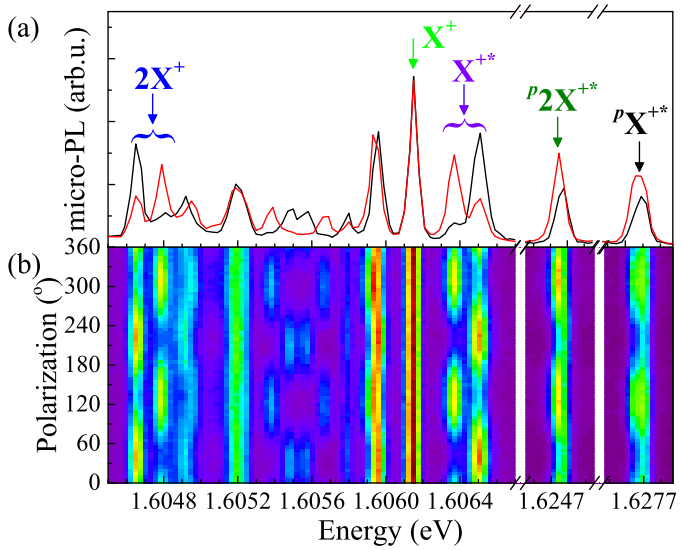


Figure 7.2: (a) The micro-PL spectra of a single GaAlAs QD recorded for two different linear polarizations: $\pi_x$ (violet curve) and $\pi_y$ (red curve) oriented along the crystallographic directions [110] and [1$\bar{1}$0], respectively. (b) Color plot presenting the micro-PL spectra of the same QD measured using different linear polarizations of detection. The 45 ° and 135 ° correspond to the crystallographic directions [110] and [1$\bar{1}$0], respectively.

the correlation experiment one can conclude that pairs of the emission lines: $X^+$, $^p2X^{+*}$ and $X^{+*}$, $2X^+$ belong to separate cascade pathways. The cross-correlation measurements between the $^pX^{+*}$ and other emission lines exhibit antibunchings, which make the identification of this line more difficult. This subject will be addressed in Section 7.3.

The emission lines: $X^{+*}$, $2X^+$,and $2X^{+*}$ split into doublets, which are partially linearly polarized along the two principal crystallographic directions: [110] and [1$\bar{1}$0] (see Fig. 7.2), previously identified for the X emission line and discussed in Section 6.2.1. In order to analyse the energy structure of the two cascade pathways involving the singlet and triplet states of charged excitons and biexcitons, the many-carrier Hamiltonian equation for QDs given in Ref. 38 is applied. This equation is used to describe the splitting of levels involved in the cascades under investigation that is caused by the exchange interaction.

Theoretical description of the fine structure of the investigated states is schematically presented in Fig. 7.3. Two separate cascade pathways for emission involving the $X^{+*}$ and $2X^+$ lines (Fig. 7.3(a)) and the $X^+$ and $^p2X^{+*}$ lines (Fig. 7.3(b)) are identified. The fine structure of the emission lines shown in Fig. 7.2(a), involving the $X^{+*}$ and $2X^+$ lines are related to the fine structure of the spin-triplet state of the singly positively charged exciton. The structure of $2X^+$ emission line results from the splitting of the final state of an *s*-shell

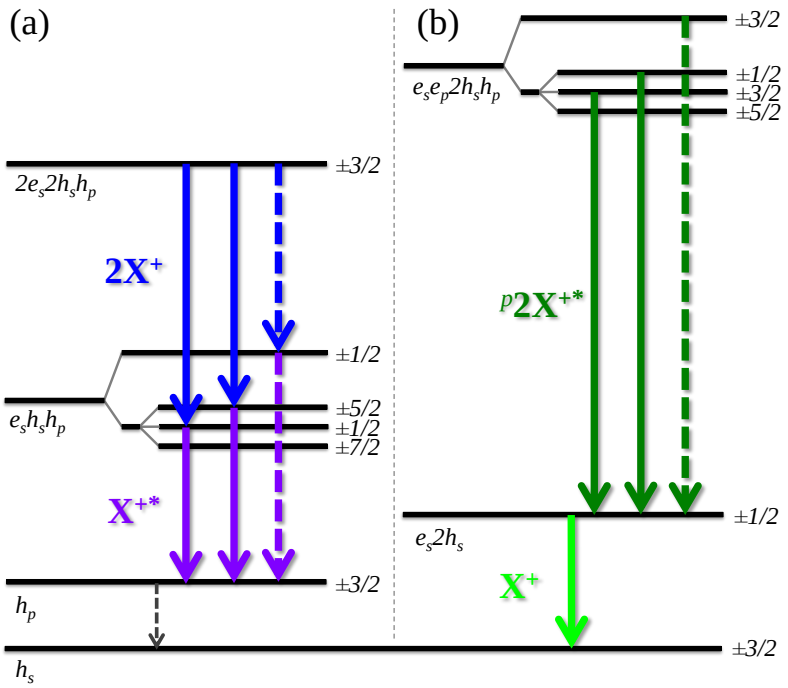


Figure 7.3: Theoretical structure (not to scale) of various transitions that can be observed for a positively charged single QD. Two separate cascade pathways are shown in parts (a) and (b). The symbols $e_s$ ($h_s$) and $e_p$ ($h_p$) denote the electron (hole) occupying the $s$- and $p$-shell, respectively. The half-integers are the projections $J_z = J_z^e + J_z^h$ of the total spins.

electron ($e_s$), an $s$-shell hole ($h_s$), and a $p$-shell hole ($h_p$). The final state consists of three interacting carriers: $e_s$, $h_s$ and $h_p$. The two holes form a spin-singlet ($J_h = 0$) and a spin-triplet ($J_h = 3$) states split by the $hh$ exchange energy $V_{s,p}^{hh}$. In addition, the $eh$ exchange interaction splits the triplet states into three doublets separated by $\tilde{V}_{s,sp}^{eh} = (V_{s,s}^{eh} + V_{s,p}^{eh})/2$, which includes the $eh$ exchange energies between the respective holes and the electron $e_s$. It is known, that the $hh$ ($ee$) isotropic exchange energy is larger than the $eh$ exchange energy by one order of magnitude [81, 118]. In optical transitions, the lowest-lying triplet state $J_z = \pm 7/2$ in which the three particles have parallel spins, is forbidden. In contrast to the case of the $2X^+$ emission, the $X^{+*}$ emission line structure results from the splitting of the initial state (no interaction is present in the final state due to $h_p$). The anisotropic part of the $eh$ exchange interaction leads to partial linear polarization of both visible emission lines ($2X^+$, $X^{+*}$) in this cascade pathway (see Fig. 7.3(a)).

In the second cascade pathway that is schematically presented in Fig. 7.3(b), the fine structure of the triplet-spin state of the positively charged biexciton re-

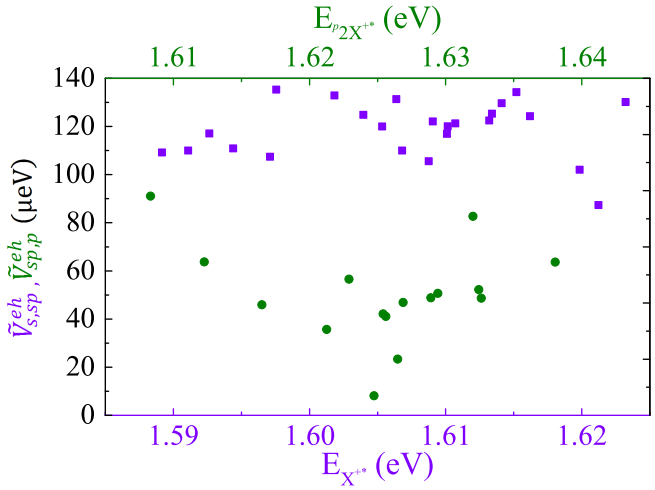


Figure 7.4: The measured values of $\tilde{V}^{eh}_{s,sp}$ ($\tilde{V}^{eh}_{sp,p}$) as a function of the $X^{+*}$ ($^p2X^{+*}$) emission line energy for a series of single QDs.

lated to the $p$-shell emission is also analysed. The initial state of the $^p2X^{+*}$ emission line, which is responsible for the observed fine structure, consists of five carriers: $e_s$, $e_p$, $2h_s$ and $h_p$. The final state related to the $^p2X^{+*}$ emission line is the initial state that underlies the $X^+$ emission for which no splitting is observed (see Fig. 7.2). The observed fine structure of the $2X^{+*}$ emission line is similar to the fine structure occurring in the $2X^+ \rightarrow X^{+*}$ cascade pathway. The energy separation between the singlet-triplet configurations of both states is given by the $ee$ exchange energy $V^{ee}_{s,p}$. The energy difference between the triplet states is given by the $eh$ exchange energy $\tilde{V}^{eh}_{sp,p} = (V^{eh}_{s,p} + V^{eh}_{p,p})/2$ for the $2X^{+*}$ emission line.

Note that the $X^{+*}$,$2X^+$ and $^p2X^{+*}$ emission lines which are related to recombination of the spin-singlet states (transitions presented in Fig. 7.3(a) with dashed arrows) have not yet been experimentally observed. These lines should be shifted with respect to the spin-triplet state recombination due to the $ee$ and $hh$ exchange interaction.

The analysis of the fine structure splitting of the $X^{+*}$ and $^p2X^{+*}$ emission lines as a function of their energy has been performed for a series of single GaAlAs QDs. The results are presented in Fig. 7.4. No dependence of the FSS of the emission lines on their emission energy can be observed (in Fig. 7.4). This suggests that the FSS splitting due to the $ee$ and $hh$ interaction is independent on the QD size, what contrasts with the effect of the $eh$ interaction as it takes place in the X and 3X emission lines - compare Fig. 7.4 and Fig. 6.3. Furthermore, the comparison between the FSS magnitude of the $X^{+*}$ emission line (∼131 μeV) and the FSS of the X emission line (∼16 μeV) confirms that the $hh$ ($ee$) isotropic exchange energy is one magnitude larger than the anisotropic $eh$ exchange energy. This is

in agreement with the results that have been previously published in Ref. 81,118.

The average value of $\tilde{V}^{eh}_{s,sp}$ equals to 119 µeV and is similar to what has already been reported for GaAs QDs [81]. In the case of $\tilde{V}^{eh}_{sp,p}$, the average energy splitting is equal to 57 µeV which is nearly 50% lower than the splitting observed for GaAs dots in the former studies [81]. This lower value could be due to different confining potentials and alloy composition of the investigated GaAlAs/AlAs QDs as compared to previously studied GaAs/GaAlAs QDs [81]. The difference most likely results from the differences in the ladders of excitonic states.

## 7.2 The effect of magnetic field

As it was discussed earlier in this Chapter, the charged excitonic complexes have a total spin of half-integer value. This is in contrast to neutral excitonic complexes whose total spin is integer-valued. Because of this, the fine structure of the former states is more complicated, especially if the carriers form the spin-triplet state [38,118,119]. The external magnetic field introduces an inter-play between the spatially and the magnetically induced confinement, and therefore lifts the spin degeneracy and modifies the energies of the states due to the Zeeman interaction with the orbital momentum of the carriers involved [58,120].

The magnetic-field evolution of the emission lines corresponding to the positively charged excitons is presented in Fig. 7.5. A complex behaviour of all these lines is a consequence of the zero-field splitting they experience due to the *eh*, *ee* and *hh* exchange interaction (refer to Section 7.1 for details).

In the case of the emission lines attributed to the recombination of the neutral states, two effects of the magnetic field has been noticed (see Section 6.3). The diamagnetic shift, characteristic for the SP levels of zero orbital momentum (the *s*-shell) as well as the energy shift due to the Zeeman interaction between the magnetic field and the SP states of orbital momentum equal to 1 (the *p*-shell) is analysed in detail for the X and 3X emission lines, respectively. No new information about the positively charged excitons is expected to result from the diamagnetic shift of the emission lines they give rise to. According to Eq. 2.13, the diamagnetic coefficient reflects the magnetic-field evolution of the size of the electron and hole wave functions as well as of the magnitude of the *eh* Coulomb interaction. Thus, the analysis presented in Section 6.3.1 for the X emission line can also be applied to the emission lines related to a positively charged dot.

The magnetic-field evolution of the emission lines related to the positively charged excitons can be summarized as follows:

- **$X^+$ emission line** - The excitonic effective $g^*$ factor results from the $g$-factor of the initial state (the *s*-shell electron) and the $g$-factor of the final

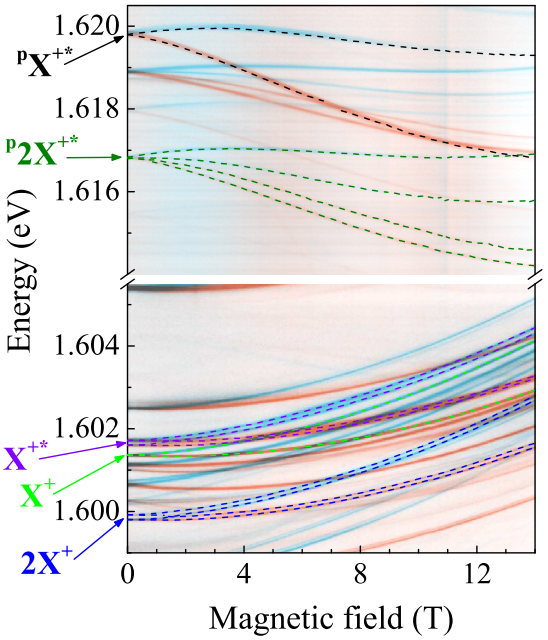


Figure 7.5: The energy evolution of the emission lines attributed to the recombination of the positively charged excitons (dashed lines) superimposed on the colour-scale map of the QD emission in the magnetic field up to 14 T. The results of measurements performed with the $\sigma_+$ and $\sigma_-$ polarizations are shown with blue and red, respectively.

state (the *s*-shell hole). As a consequence, the splitting of the emission line should be identical with the splitting of the X emission line.

- **$X^{+*}$ emission line** - The initial triplet configuration is split into three levels as a result of the *eh* interaction between the *s*-shell electron and the holes occupying the *s*- and *p*-shell (see Fig. 7.2 in Section 7.1). Thus in the presence of the magnetic field, all zero-field levels are split into additional two because of lifting the spin degeneracy. In the final state, the splitting is that of the *p*-shell hole. Whereas only two transitions are identified in the absence of magnetic field - Fig. 7.3, four transitions are allowed when the magnetic field is turned on.

- **$2X^{+}$ emission line** - The origin of the splitting is in this case the same as for the $X^{+*}$ emission line, only the initial and final states have to be reversed (see above). Therefore, four components of the $2X^{+}$ emission line appear in the spectrum.

- **$^{p}2X^{+*}$ emission line** - Due to the *eh* interaction between the *p*-shell hole and the electrons occupying the *s*- and *p*-shells, the initial triplet state is split into three levels. The final state is the initial state of the $X^{+}$ emission

line, the splitting of which is given by the $s$-shell electron. The zero-field two-component structure is observed (two optically active transitions - see Fig. 7.3). Furthermore, like in the case of the $X^{+*}$ and $2X^{+}$ emission lines, the presence of magnetic field causes the ${}^{p}2X^{+*}$ emission line to split into four components.

- **${}^{p}X^{+*}$ emission line** - The origin and the scheme of the energy levels occupied by carriers confined in the dot and involved in this emission line is presented and analysed in Section 7.3.3. Based on the results displayed in Fig. 7.2 and 7.5, the zero-field splitting of the ${}^{p}X^{+*}$ emission line is present and only two split components are observed in the magnetic field. As it is discussed in Section 7.3.3, the ${}^{p}X^{+*}$ emission line split into four components when the magnetic field is turned on (each circularly polarized branch of the line consists of two components).

Based on the above analysis, Fig. 7.6 schematically illustrates the theoretical structure of investigated states and studied transitions. It is shown in Ref. 58,118,120 that the magnetic-field evolution of the $2X^{-}$ emission line results from the two inner spin-split components that approach each other. Moreover, the inspection of the circular polarization and the high-magnetic-field behaviour of both components lead to the prediction of the anticrossing between them. The anticrossing that arises from the anisotropic $eh$ exchange interaction [58] is indeed observed. A corresponding effect is expected for the recombination of the spin-triplet state of the singly positively charged exciton. The magnetic-field evolution of emission lines which have at zero-field a double structure as a result of the $eh$ exchange interaction, such as: $X^{+*}$, $2X^{+}$, ${}^{p}2X^{+*}$, should also contain anticrossings, as has been previously observed for the negatively charged QDs [58,118,120].

Unfortunately, the linear polarization cannot be exchanged in the experimental setup employed which relies on the usage of optical fibers (see Section 4.1.2). Nevertheless, the anticrossing (a crossing in the case of the applied procedure) for all the investigated emission lines is clearly observed (the circular polarization is determined by a specific detection, in which the intensity of one split component of the X emission line is maximized while at the same time the other component of this line is minimized). For the $X^{+*}$ and $2X^{+}$ emission lines, the anticrossing is observed around 1.8 T. The analysis of the magnetic-field dispersion of the ${}^{p}2X^{+*}$ emission line shows, that the anticrossing appears at extremely low magnetic field (below 1 T).

The Zeeman splitting, defined as $\Delta E_Z = E(\sigma_+) - E(\sigma_-)$, of the emission lines related to the positively charged excitons is shown in Fig. 7.7. The magnitude of the Zeeman splitting, described by the effective $g^*$ factor, is determined for different studied emission lines on the basis of transition-specific equations. In particular, for the $X^{+}$ line, an appropriate equation reads: $g^* = g_e^0 + g_h^0$ (if the HH-LH

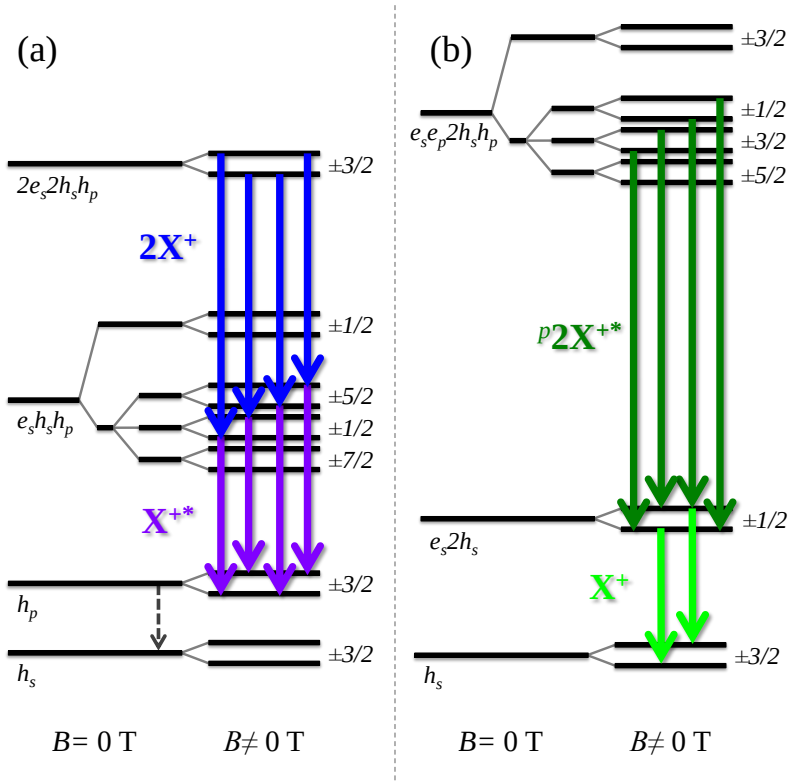


Figure 7.6: Theoretical structure (not to scale) of various positively charged transitions observed in a studied single QD in the presence of external magnetic field. The parts (a) and (b) describe two separate cascade pathways. The symbols $e_s$ ($h_s$) and $e_p$ ($h_p$) denote the electron (hole) occupying the $s$- and $p$-shell, respectively. The half-integers are the projections $J_z = J_z^e + J_z^h$ of the total spins.

mixing is not considered - see Section 6.3.2). The values of $\Delta E_Z$ for all emission lines ascribed to the recombination of the positively charged excitons and related to the $s$-shell, $X^+$, $X^{+*}$ and $2X^+$, are similar (only the small changes are observed) and they are also similar to the $g^*$ factor of the neutral exciton - see Fig. 7.7. The most intriguing effect appears for pairs of components of the $X^{+*}$ and $2X^+$ lines. The values of $\Delta E_Z$ for both components of the $X^{+*}$ emission lines are different, while in the case of $2X^+$ line they are almost the same (compare the solid and dashed lines corresponding to each of these transitions in Fig. 7.7). The difference might be induced by the HH-LH mixing, as a consequence of the same origin of the Zeeman splitting of both emission lines (see the description above).

The dependence of $\Delta E_Z$ on the magnetic field for the $p$-shell related emission lines, $^p2X^{+*}$ and $^pX^{+*}$, is analogous to the one obtained for the 3X emission line in Section 6.3.2). The slope of the Zeeman splitting changes for each transition. Moreover, the Zeeman splitting of both the split components of the $^p2X^{+*}$ emis-

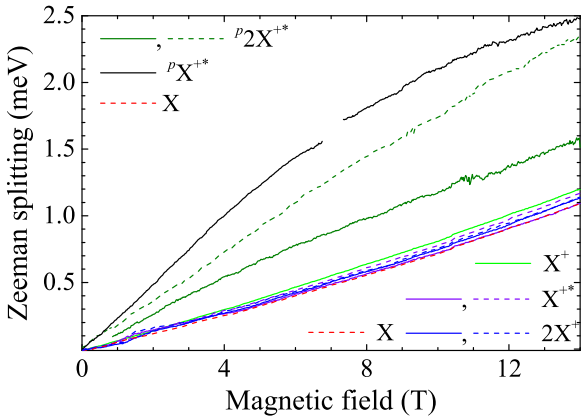


Figure 7.7: The Zeeman splitting of the emission lines attributed to the recombination of the positively charged excitons in magnetic field up to 14 T.

sion line associated with the $p$-shell, exhibits a completely opposite behaviour when compared to the case of the $X^{+*}$ and $2X^{+}$ emission lines. The difference in the value of $\Delta E_Z$ for both split components is huge. The origin of these effects is not clear and requires theoretical studies to be fully understood.

## 7.3 Photoluminescence excitation

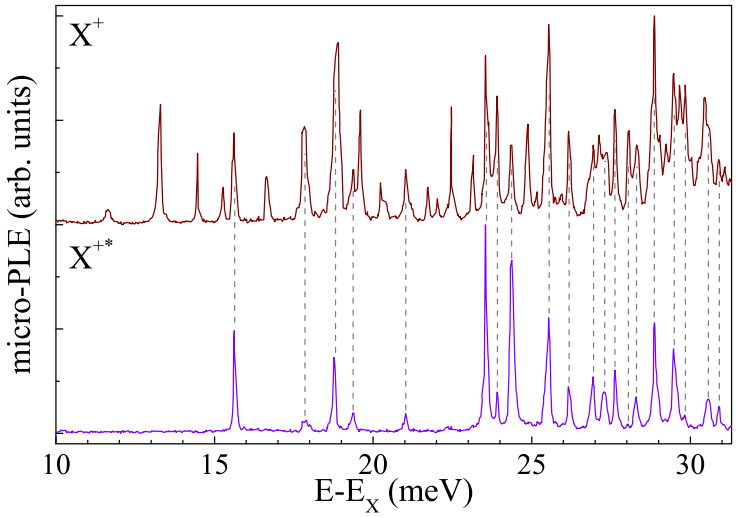


Figure 7.8: Micro-PLE spectra of a single dot detected on the $X^{+}$ and $X^{+*}$ emission lines (dot with $\Delta_{s\text{-}p}$=14.30 meV). The grey vertical dashed lines indicate the energy of resonant peaks associated with the $X^{+*}$ line. The scale of the horizontal axis is set by the energy relative to the X emission line. The spectra are normalized to the most intense peaks and vertically shifted for clarity purpose.

In order to get insight into the energy structure of the positively charged excitons, the measurements of the micro-PLE spectra have been performed [11, 61, 114, 121, 122].

The micro-PLE spectra of a single QD detected on the $X^+$ and $X^{+*}$ emission lines and measured in a broad range of the excitation energy are presented in Fig. 7.8. Note the energy scale is set by the energy relative to the X line. Several resonant peaks occur in the spectra. The number of peaks appearing in the micro-PLE spectra of the singly positively charged exciton is significantly larger when it forms the spin-singlet state and not the spin-triplet state. The origin of this difference is not clear at the moment, however, it may result from the complex character of the PLE processes, which involve the absorption, the relaxation, and finally the emission. Moreover, it can be seen that the number of observed resonant peaks per energy unit substantially increases above 23 meV. This value is consistent with the previously determined energy of 25 meV which corresponds to the micro-PLE spectra of the neutral exciton (refer to Section 6.4).

In the first step, the micro-PLE spectra presented in Fig. 7.9 and 7.10 have been measured for a number of single QDs. The spectra are systematised in

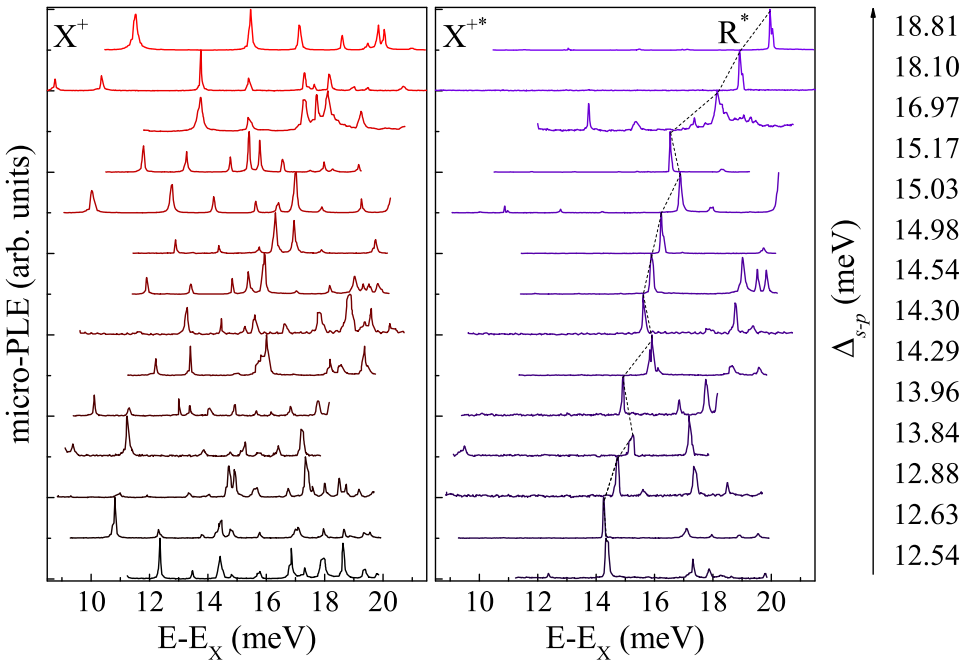


Figure 7.9: Micro-PLE spectra detected on the $X^+$ and $X^{+*}$ emission lines, measured for a series of QDs characterized by different amplitude of $\Delta_{s\text{-}p}$. The scale of the horizontal axis is set by the energy relative to the X emission line. The black dashed lines indicate the evolution of the energy position of the resonant peak R*. The spectra are normalized to the most intense peaks and vertically shifted for clarity purpose.

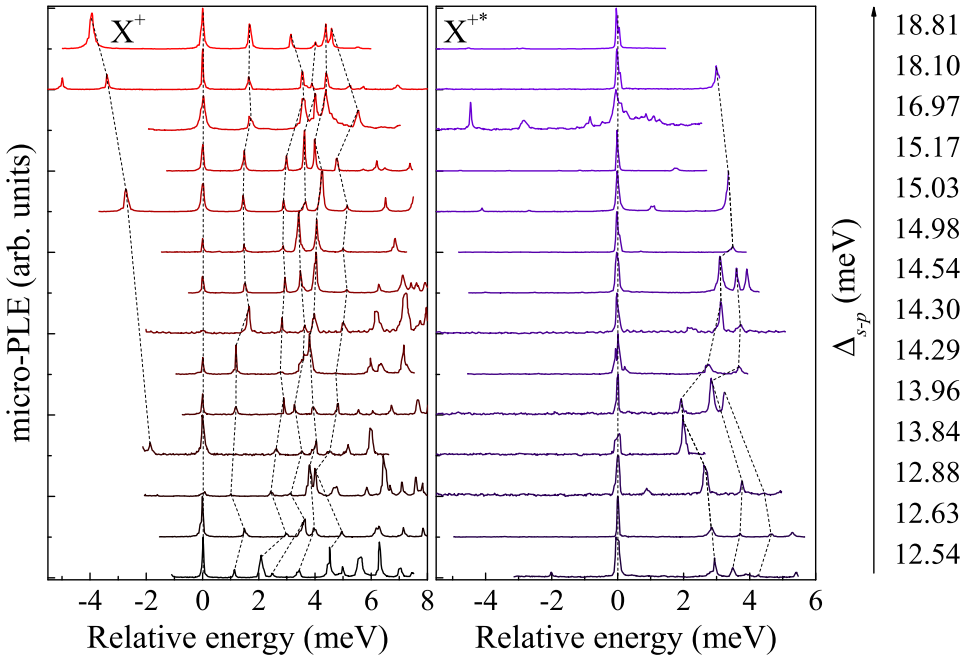


Figure 7.10: Micro-PLE spectra of different series of QDs detected on the $X^+$ and $X^{+*}$ emission lines, measured for a series of QDs characterized by different amplitude of $\Delta_{s\text{-}p}$. The scale of the horizontal axis is set by the energy relative to: (left panel) the arbitrary chosen resonant peak and (right panel) the resonant peak R*. The black dashed lines indicate the evolution of the energy position of a given resonant peak. The spectra are normalized to the most intense peaks and vertically shifted for clarity purpose.

the order of increasing energy separation between the *s*- and *p*-shells, previously defined as the energy difference between the X and 3X emission lines - $\Delta_{s\text{-}p}$ (see Section 5.3). It can be seen that for the $X^+$ emission line, they all exhibit a similar pattern of resonant peaks - Fig. 7.9. In Fig. 7.10 the energy scale has been shifted and set by the energy relative to an arbitrary chosen resonant peak. With this arrangement, the similarities between various micro-PLE spectra are emphasized. Based on them, the corresponding resonant peaks in each spectrum are connected with the black dashed lines. Due to smaller number of resonant peaks in the micro-PLE spectrum detected on the $X^{+*}$ line, the pattern of resonances can be discerned more easily - see Fig. 7.9. The micro-PLE spectra are dominated by the resonance denoted with R*, which is studied in more detail in Section 7.3.3. The resonances in the spectra recorded on different dots are connected by black dashed lines. One can notice that the energy of the peak R* systematically increases with increasing value of $\Delta_{s\text{-}p}$ (Fig. 7.9). This suggests that the *p*-shell electron is involved in the initial and/or final state of the transition. Moreover, a few resonant peaks of smaller intensity, marked with black dashed lines in Fig. 7.10,

behave in an analogous way, what further supports the conclusion of the $p$-shell electron participation in these transitions.

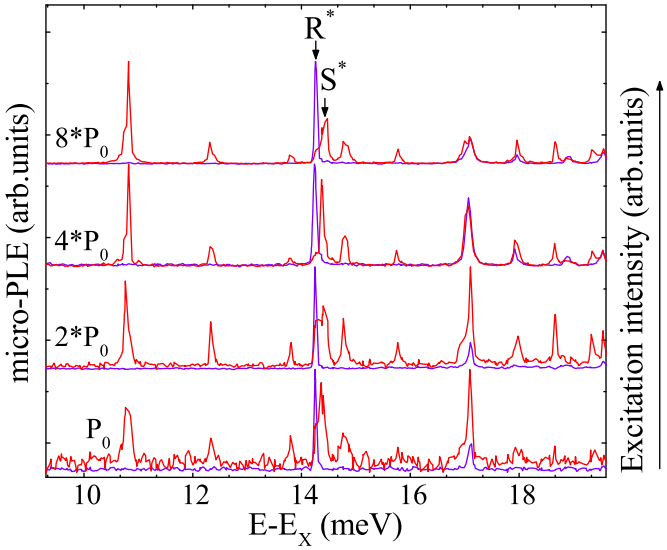


Figure 7.11: The excitation-power evolution of micro-PLE spectra detected on the $X^+$ (red curves) and the $X^{+*}$ (violet curves) emission lines (dot with $\Delta_{s\text{-}p}$=12.63 meV). The scale of the horizontal axis is set by the energy relative to the X emission line. The spectra are normalized to the most intense peaks and vertically shifted for clarity purpose.

The micro-PLE spectra only slightly depend on the excitation power, what can be noticed in Fig. 7.11. This behaviour is similar to the dependence observed for the neutral exciton (compare with Fig. 6.17). It confirms that the resonant peaks under study are related to elementary excitations, in which a valence-band electron is excited to the conduction-band and an $e$-$h$ pair is created in the presence of an extra hole in the QD (for more information see Section 6.4). It can also be seen in Fig.7.11, where the previously mentioned resonant peak $R^*$ is present in both the ground (spin-singlet) and the excited (spin-triplet) states of the singly positively charged exciton, while the ground-state emission can be as well excited with a different resonance $S^*$ of slightly larger energy.

The presence of an extra hole in the singly positively charged exciton makes the possible configuration of its excited states more complicated than in the case of the neutral exciton (see Section 6.4). This additional hole may occupy a number of states in the valence band, out of which the $s$-shell levels have the highest probability of occupation. The spin-singlet and spin-triplet states can be formed by an $e$-$h$ pair (as it is observed in the micro-PL spectra detected on the $X^+$ and $X^{+*}$ emission lines). The excited state spectrum of the spin-singlet (spin-

triplet) state of the singly positively charged exciton, which is the initial state of the $X^+$ ($X^{+*}$) line should consist of the excited spin-singlet (spin-triplet) states, respectively. For instance, when both holes are in the spin-singlet or spin-triplet state, then the first one occupies the $s$-shell and the second one the higher excited shell, such as: $d$, $f$,... shell [11].

The resonant peaks in the micro-PLE spectra detected on the $X^+$ and $X^{+*}$ lines are discrete and separate in the energy range of 10...20 meV above the X emission line. The micro-PLE spectra observed at zero field hardly support any unquestionable attribution of the resonant peaks. Thus, in order to acquire wider knowledge about their origin, the studies involving the application of external magnetic field were undertaken.

### 7.3.1 PLE spectra in magnetic field

The magnetic-field evolution of micro-PLE spectra of three single QDs detected on the $X^+$ and $X^{+*}$ emission lines is presented in Figs 7.12, 7.13, 7.14, 7.15, 7.16, and 7.17. By careful inspection of the experimental data collected for both charged excitons the following conclusions may be drawn:

- In the micro-PLE spectra detected on the $X^+$ emission line, presented in Figs 7.12, 7.13 and 7.14, two types of resonant peaks can be distinguished. The first type exhibits the $s$-shell-like magnetic-field evolution, which is similar to the behaviour previously reported for the resonant peaks detected on the X line (see Fig. 6.19 for comparison). The second type (comprising *e.g.* the peak R*) shows the $p$-shell-like magnetic-field dispersion. The number of the resonant peaks observed is relatively large, what makes tracing the magnetic-field evolution of a given peak a rather difficult task.

- The micro-PLE spectra detected on the $X^{+*}$ line (see Figs 7.15, 7.16 and 7.17) are dominated by the peak R* of the $p$-shell-like magnetic-field dispersion (the magnetic-field evolution of emission lines related to different shells is analysed in Section 5.3). The resonant peaks associated with the $s$-shell-like evolution are also found in the spectra (*e.g.* at ~14.5 meV at zero-field in Fig. 7.17) but their intensities are relatively small.

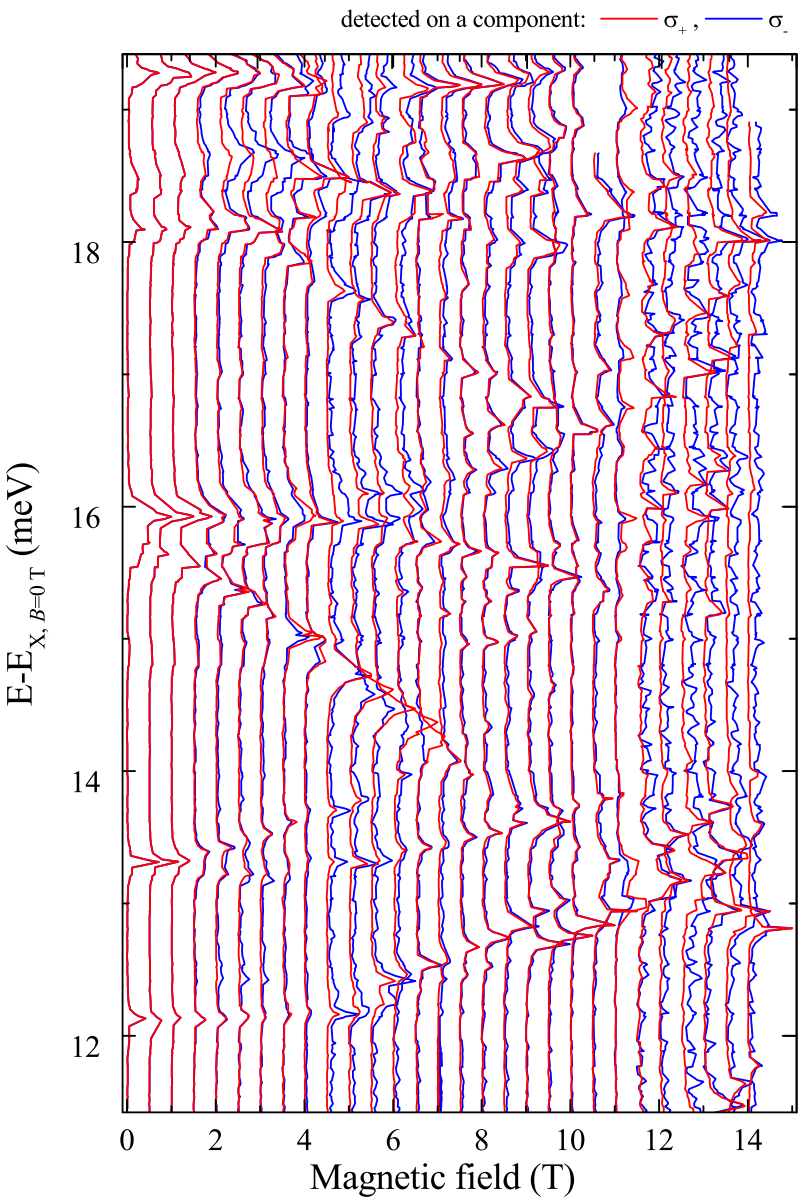


Figure 7.12: The magnetic-field evolution of micro-PLE spectra detected on the $X^+$ emission line (dot with $\Delta_{s\text{-}p}$=14.29 meV). The scale of the horizontal axis is set by the energy relative to the X emission line. The spectra are normalized to the most intense peaks and shifted for clarity purpose.

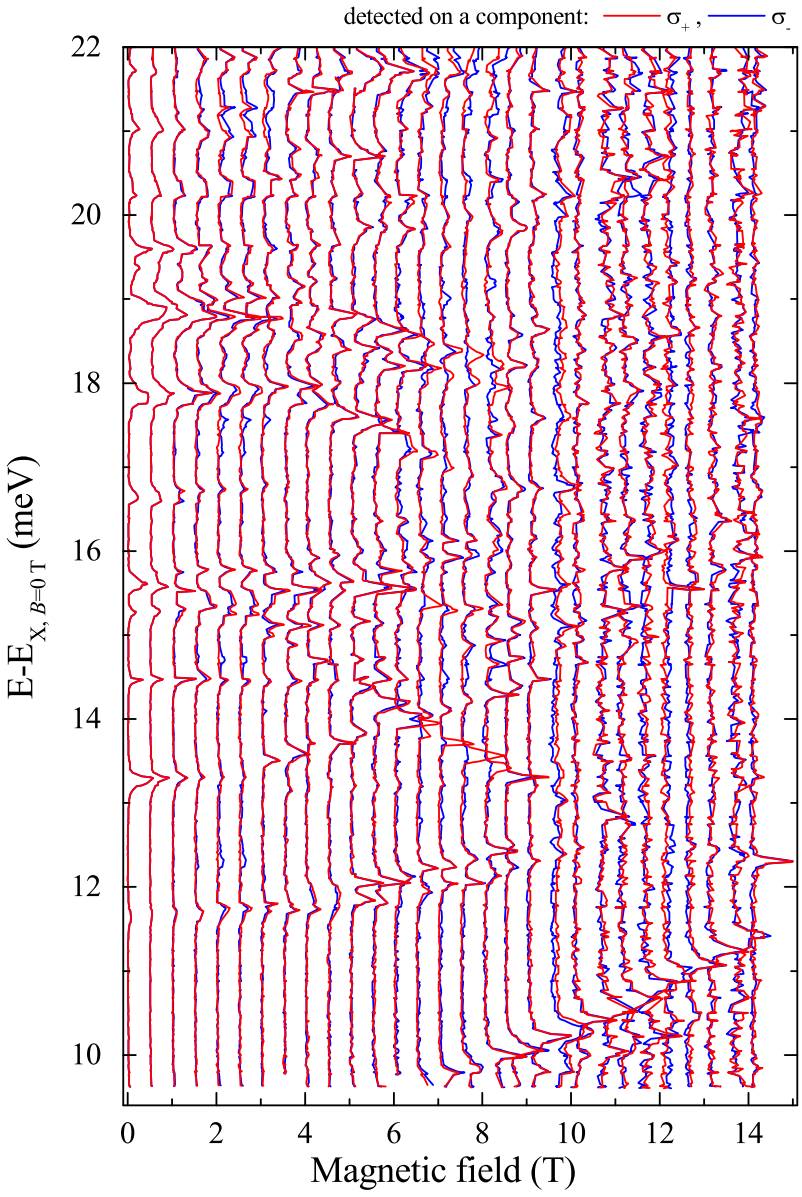


Figure 7.13: The magnetic-field evolution of micro-PLE spectra detected on the $X^+$ emission line (dot with $\Delta_{s\text{-}p}$=14.30 meV). The scale of the horizontal axis is set by the energy relative to the X emission line. The spectra are normalized to the most intense peaks and shifted for clarity purpose.

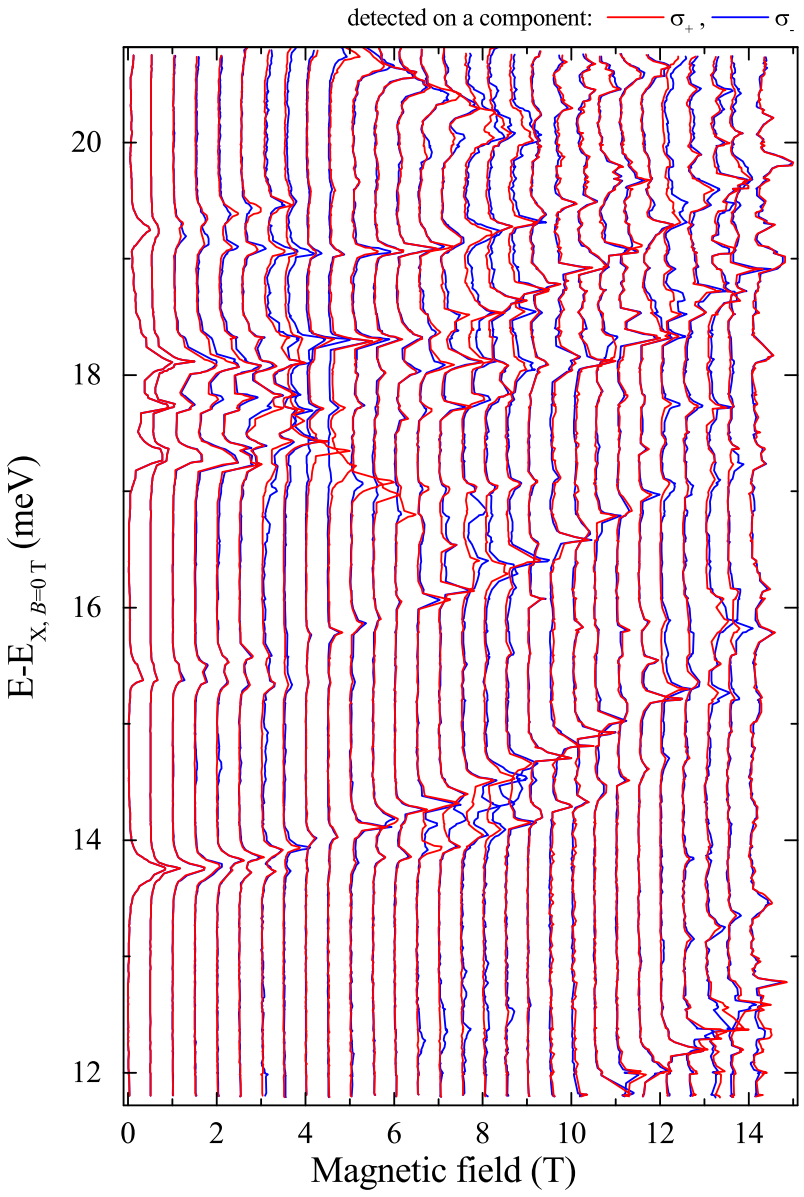


Figure 7.14: The magnetic-field evolution of micro-PLE spectra detected on the $X^+$ emission line (dot with $\Delta_{s\text{-}p}$=16.97 meV). The scale of the horizontal axis is set by the energy relative to the X emission line. The spectra are normalized to the most intense peaks and shifted for clarity purpose.

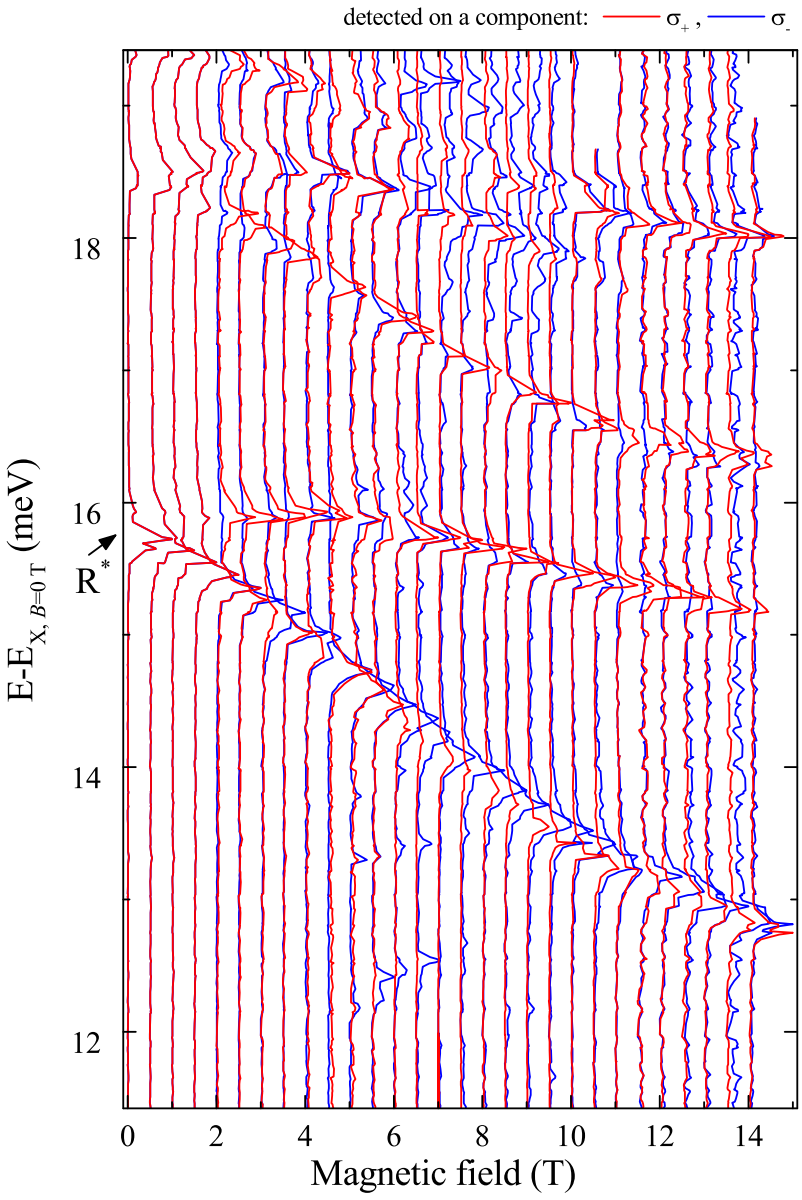


Figure 7.15: The magnetic-field evolution of micro-PLE spectra detected on the $X^{+*}$ emission line (dot with $\Delta_{s\text{-}p}$=14.29 meV). The scale of the horizontal axis is set by the energy relative to the X emission line. The spectra are normalized to the most intense peaks and shifted for clarity purpose.

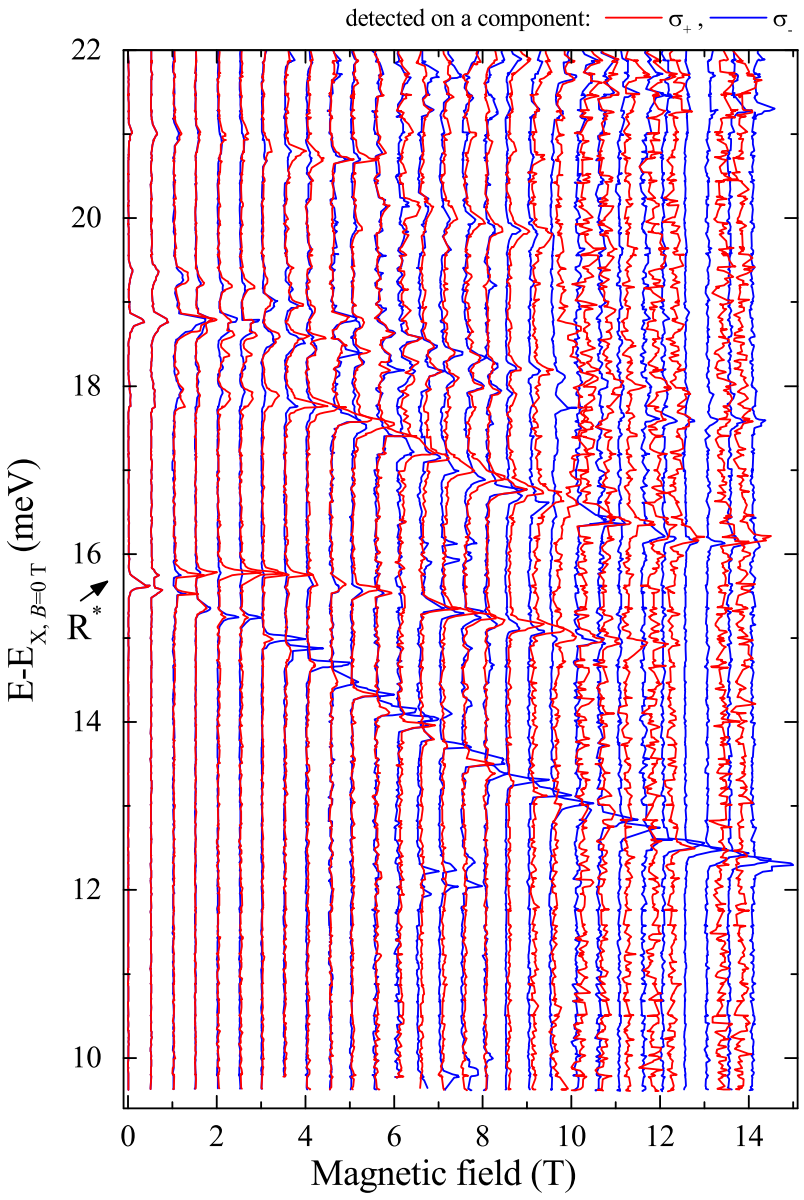


Figure 7.16: The magnetic-field evolution of micro-PLE spectra detected on the $X^{+*}$ emission line (dot with $\Delta_{s\text{-}p}$=14.30 meV). The scale of the horizontal axis is set by the energy relative to the X emission line. The spectra are normalized to the most intense peaks and shifted for clarity purpose.

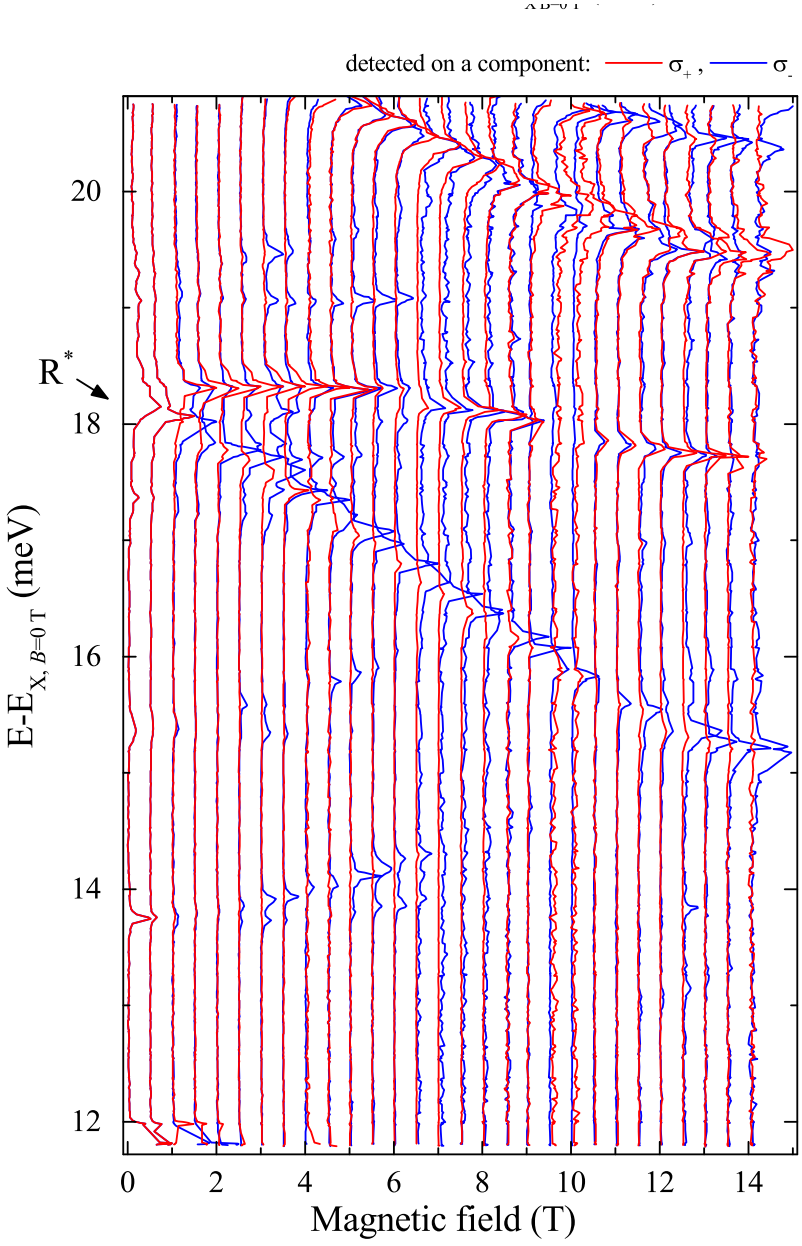


Figure 7.17: The magnetic-field evolution of micro-PLE spectra detected on the $X^{+*}$ emission line (dot with $\Delta_{s\text{-}p}$=16.97 meV). The scale of the horizontal axis is set by the energy relative to the X emission line. The spectra are normalized to the most intense peaks and shifted for clarity purpose.

The attribution of the $s$-shell-like resonant peaks, which occur in the micro-PLE spectra of the spin-singlet and the spin-triplet states of positively charged excitons (measured at the energy of the $X^+$ and the $X^{+*}$ emission lines, respectively) is analogous to the one proposed in the case of the neutral exciton. Keeping in mind, that the $e$-$h$ pair excitation process occurs in the presence of an additional hole (a "charged" QD), the studied problem is more complex than the excitation of only one $e$-$h$ pair in an empty QD (a "neutral" dot). The exact identification of a given resonance of the neutral exciton is difficult as it was discussed in Section 6.4.2. A similar analysis can also be applied to the $s$-shell-related resonances of the positively charged excitons (the next Section). In particular, the origin of the resonant peak $R^*$ is studied this way in Section 7.3.3

### 7.3.2 Origin of PLE peaks

The energy structure of the confined states in the investigated GaAlAs QDs was already discussed in Section 6.4.2. Along with the proposed line of thought, the possible excitations of electrons from the six lowest-lying energy levels in the valence band to the $s$-shell of the conduction band, that occur in the presence of an extra hole in the QD, can be considered as giving rise to the resonant peaks, as it is shown in Fig. 7.18.

The two transitions of the lowest energy: ($F_{h,z} = \pm 3/2 \rightarrow m_{e,z} = 0$ and $F_{h,z} = \pm 1/2 \rightarrow m_{e,z} = 0$), presented in Fig. 7.18, result in formation of the spin-singlet and the spin-triplet states of the singly positively charged exciton, which

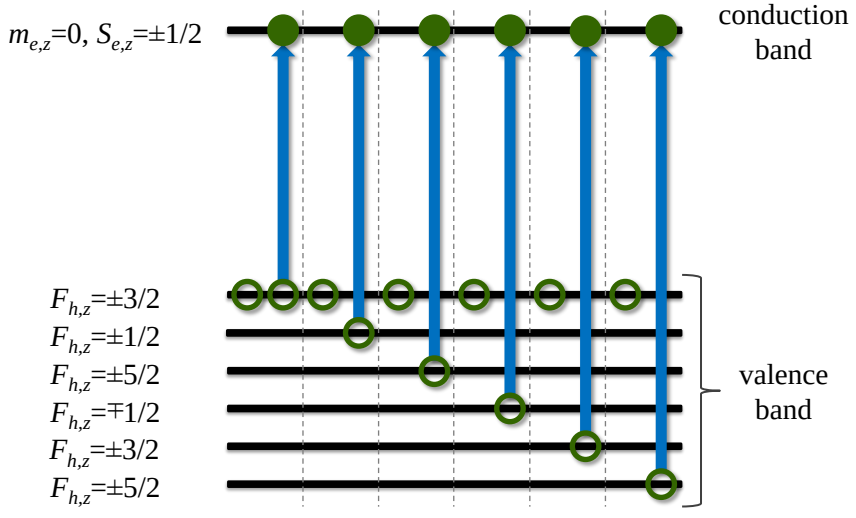


Figure 7.18: Black horizontal lines illustrate the ladders of levels in the conduction and valence bands. The blue (red) arrows indicate the possible absorption transitions between the valence band levels and the $s$-shell ($p_-$-shell), respectively.

decay by the emission of the $X^+$ and $X^{+*}$ emission lines, respectively. If the *hh* exchange interaction is not included, the excited states of both charged excitons should be the same. If two holes occupy two different levels in the valence band (*e.g.* as it seen for the $X^{+*}$ emission line in Section 7.1), then due to the *hh* exchange interaction they can form two configurations: the spin-singlet and the spin-triplet states. As it is presented in Ref. 11, both spin configurations of the excited states form two series of the excited states of charged excitons. The excited spin-singlet and the spin-triplet states should therefore lead to different final states and the expected spectrum of resonant peaks for both configurations should be in principle different. However, it is observed that all resonant peaks of the spin-triplet state of the positively charged exciton (detected on $X^{+*}$) are also present in the PLE spectrum of the spin-singlet state of the positively charged exciton (detected on $X^+$). Moreover, the number of the resonant peaks in the micro-PLE spectrum of the spin-singlet state of the positively charged exciton is significantly larger than in the case of its spin-triplet state (see Fig. 7.8). The origin of this asymmetry is not yet completely understood. It might be related to the relaxation process of the excited hole. In general, two scenarios can be conceived:

(a) If the spin flip time - $\tau_s$ is larger than the relaxation time of excited hole to the ground level - $\tau_r$, the $m_{h,z}$ value of the excited hole is conserved. This gives rise to a resonant peak in the micro-PLE spectra detected on the $X^+$ or $X^{+*}$ emission lines, depending on the total angular momentum of the photogenerated *e*-*h* pair.

(b) In the opposite case, $\tau_s \ll \tau_r$, the $m_{h,z}$ value of the excited hole is not conserved (+3/2 or -3/2). This means, that the same excited state may underlie a resonant peak for both (the singlet and triplet) configurations of the positively charged exciton.

In Ref. 11 dedicated to InGaAs/GaAs QDs, the micro-PLE spectra detected on the $X^+$ and $X^{+*}$ emission lines follow the scenario (a). In the case of the studied QDs, some of the resonant peaks in the micro-PLE spectra registered on the $X^+$ and $X^{+*}$ emission lines, *e.g.* at ∼14.5 meV at zero-field in Fig. 7.14 and 7.17, occur at the same energy. This observation agrees with the scenario (b), which is thus considered as a correct one for the present work.

As it is discussed in Section 6.4.2, due to small energetic distance between the hole levels in the valence band (around 1-2 meV), the access to the transitions involving the lowest-lying energy states, such as: $F_{h,z} = \pm 3/2 \rightarrow m_{e,z} = 0$, $F_{h,z} = \pm 1/2 \rightarrow m_{e,z} = 0$, ... [11,16] is unavailable and the attribution of the resonant peaks to given transitions can not be done.

The obtained results show that description of the micro-PLE spectra related to the positively charged excitons is more complex than in the case of the neutral

exciton. In particular, the second type of resonant peaks - the *p*-shell-like, *e.g.* R*, requires further elaboration, which is presented in the next Section.

### 7.3.3 The resonant peak corresponding to the emission line

As it is depicted in Figs 7.9(b), 7.15 7.16 and 7.17, the resonant peak R* dominates over the micro-PLE spectrum detected on the $X^{+*}$ emission line. A careful inspection of the micro-PL and micro-PLE spectra from the same dots reveals one more striking property of this peak (see Fig. 7.19). Surprisingly the resonant peak R* occurs at the same energy as the ${}^{p}X^{+*}$ emission line ascribed to the recombination of the positively charged excitonic complex.

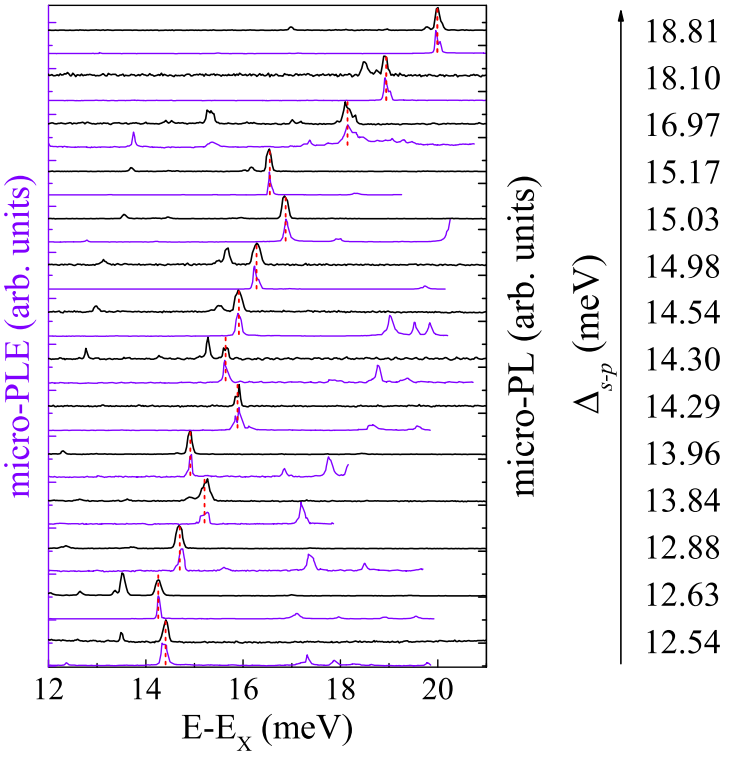


Figure 7.19: The micro-PLE spectra detected on the $X^{+*}$ emission line (purple curves) and the micro-PL spectra (black curves) of a series of different QDs. The red dashed vertical lines indicate the energy of the resonant peak R* and the ${}^{p}X^{+*}$ emission line. The scale of the horizontal axis is set by the energy relative to the X emission line. The spectra are normalized to the most intense peaks and vertically shifted for clarity purpose.

Moreover, the magnetic field evolution of the resonant peak R* follows exactly the evolution of the ${}^{p}X^{+*}$ emission line (see Fig. 7.20). This suggests that the final

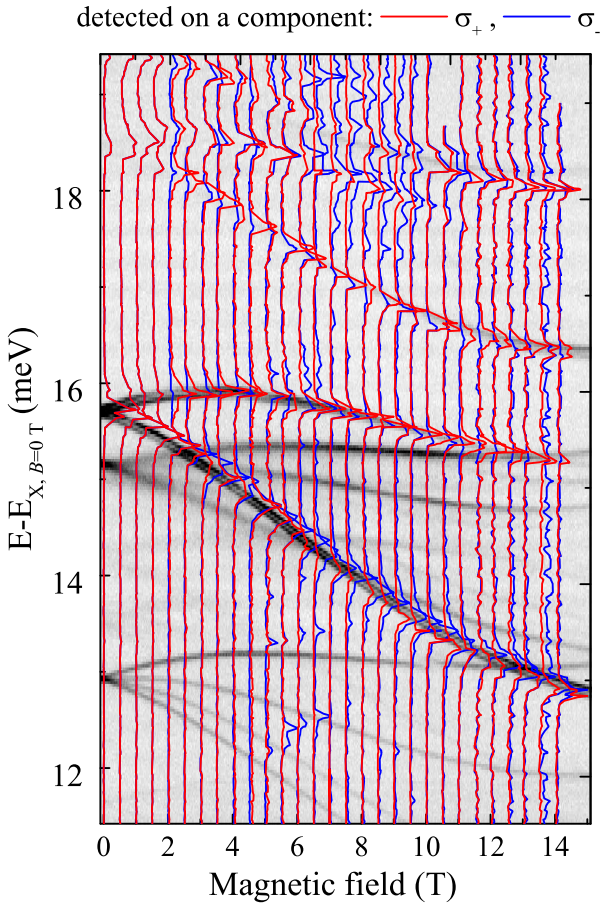


Figure 7.20: The magnetic-field evolution of the micro-PLE spectra detected on the $X^{+*}$ emission line (the blue and red curves), superimposed on a gray-scale map displaying the micro-PL spectra of the same dot, plotted as a function of the magnetic field. $\Delta_{s\text{-}p}$=14.29 meV. The scale of the horizontal axis is set by the energy relative to the X emission line. The spectra are normalized to the most intense peaks and vertically shifted for clarity purpose.

state of the absorption process associated with the peak $R^*$ is the initial state for the ${}^{p}X^{+*}$ emission line. This result is unexpected and according to the best knowledge of the Author, no similar behaviour has been observed so far.

In order to find the initial and the final state, which are involved in both the ${}^{p}X^{+*}$ emission line and the *p*-shell-like resonant peak $R^*$, one needs to scrupulously combine the properties of both these features:

- All the obtained histograms of the cross-correlation measurements between the ${}^{p}X^{+*}$ emission line and other lines related to the recombination of the positively charged excitons show the antibunching - see Fig. 5.9. This means that the ${}^{p}X^{+*}$ emission line does not belong to any identified cascade path-

ways, in which the positively charged exciton forms either the spin-singlet or the spin-triplet state (see Section 7.1 for more information).

- The ${}^{p}X^{+*}$ emission line is excited with the same excitation power as the $X^{+}$ and $X^{+*}$ emission lines. The excitation-power dependence of all three lines is also similar. Taking into account that the initial states of both singly positively charged excitons are formed by three carriers: an electron and two holes, the initial state of the ${}^{p}X^{+*}$ line should also involve the same number of carriers.

- The FSS of the resonant peak $R^{*}$ and the ${}^{p}X^{+*}$ emission line correspond to the observed fine structure of the $X^{+*}$ emission line (Fig. 7.20). At zero field, the splitting into two components which are partially linearly polarized is observed. The application of the magnetic field leads to further splitting into four components, which come in pairs like in the case of the $X^{+*}$ line.

- Due to the fact that the resonant peak $R^{*}$ appears in the micro-PLE spectra detected on the $X^{+}$ and $X^{+*}$ emission lines, the state it is associated with, has to be the excited state of the positively charged exciton (in both configurations) no matter what the spin configuration is.

Based on the analysis of the results of various experiments, the resonant peak $R^{*}$ (the ${}^{p}X^{+*}$ emission line) can be attributed to the absorption (emission) as-

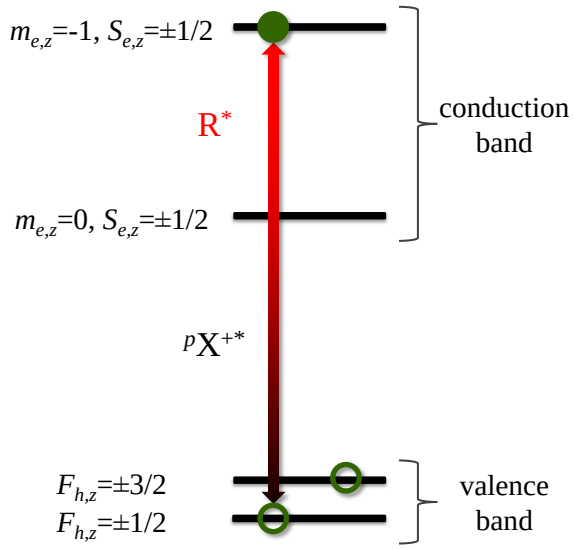


Figure 7.21: Black horizontal lines illustrate the ladders of levels in the conduction and valence bands. The green solid (open) circles represent the electrons (holes). The red-black vertical arrow indicates the absorption-emission process of the $e$-$h$ pair.

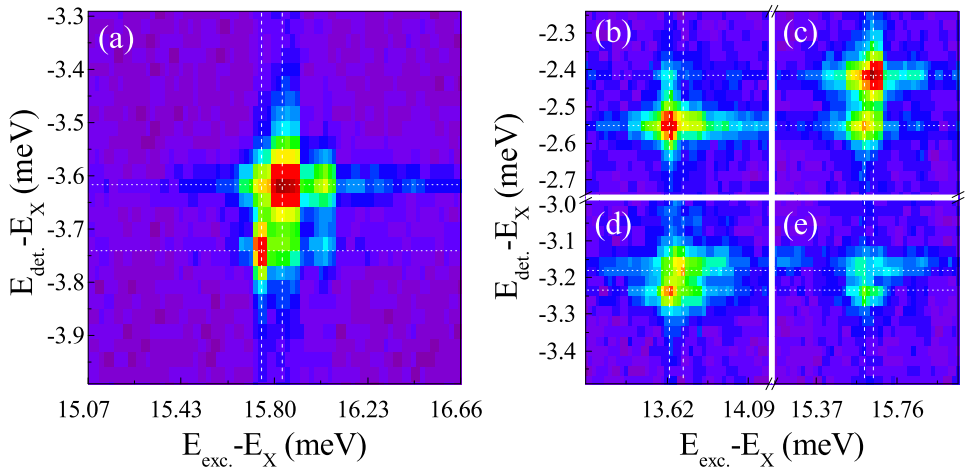


Figure 7.22: The micro-PLE maps measured at: (a) 0 T, (b) - (e) 9 T. The white dashed horizontal (vertical) lines indicate the position of the split components of the $X^{+*}$ emission line (the resonant peak R*). The excitation/detection polarizations are: (b) $\sigma_-/\sigma_+$, (c) $\sigma_+/\sigma_+$, (d) $\sigma_-/\sigma_-$, (e) $\sigma_+/\sigma_-$.

sociated with the positively charged exciton comprising the $p$-shell electron and two holes of "parallel" total momentum: the $s$- and $p$-shell hole - see Fig. 7.21. The resonant peak R* is the main one, which occurs in the micro-PLE spectrum of the spin-triplet state of the positively charged exciton. It is also observed (although its intensity is much lower) in the micro-PLE spectrum of the spin-singlet state of the positively charged exciton. To get to the initial state of the $X^{+*}$ emission line, the $p$-shell electron relaxes to the $s$-shell. In the next step, the $p$-shell hole relaxes to the $s$-shell level in the time-scale longer than $\tau_s$. Then the spin-singlet state is formed and the initial state of the $X^+$ emission line is reached.

Fig. 7.21 shows a simplified model, which does not include the exchange interaction between the carriers. The micro-PLE maps excited in the energy range of the resonant peak R* and detected in the energy range corresponding to the $X^{+*}$ emission line are presented in Fig. 7.22. The maps exhibit a non-trivial FSS of both transitions (the absorption peak and the emission line) at zero- and non-zero-magnetic field. The analysis of Fig. 7.22(a) leads to the conclusion, that the lower (higher) energy split-component of the peak R* is the excited state of the lower (higher) energy split-component of the $X^{+*}$ line. This means that during the relaxation process of the electron, the configuration of carriers is preserved - see Fig. 7.23. A similar situation is also seen in the magnetic field, especially, when the polarizations of the excitation light and the detected signal are the same (*e.g.* $\sigma_+/\sigma_+$ and $\sigma_-/\sigma_-$) - Fig. 7.23(c) and (d). In the orthogonal configuration of the polarisation, the excitation of the lower energy split-component is more

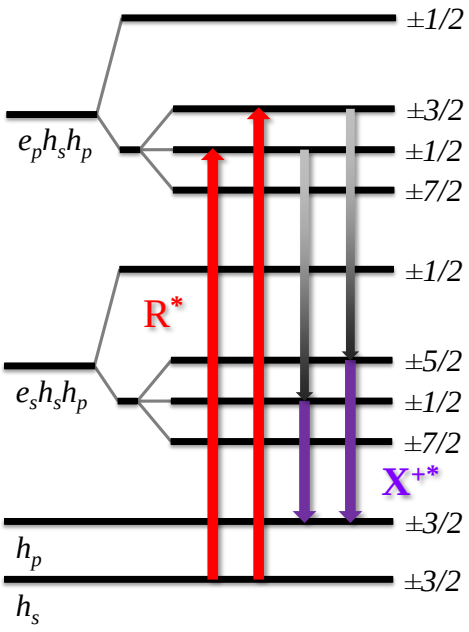


Figure 7.23: Theoretical structure (not to scale) of two states related to the resonant peak R* and the $X^{+*}$ emission line. The symbols $e_s$ ($h_s$) and $e_p$ ($h_p$) denote the electron (hole) occupying the $s$- and $p$-shell, respectively. The half-integers are the projections $J_z = J_z^e + J_z^h$ of the total momentum.

pronounced than the higher energy one - Fig. 7.23(b) and (e).

An analogous analysis in the case of the $X^+$ emission line shows that the detected signal is insensitive to the selected split component of the peak R*. To reach the initial state of the $X^{+*}$, the electron on the $p$-shell needs to relax to the $s$-shell. In the next step, due to the finite spin flip time of holes, the $p$-shell hole relaxes to the $s$-shell and the holes form the spin-singlet state (the total momentum of holes equals zero). Because the $X^+$ emission does not exhibit any fine structure (refer to Section 7.1 for details), the emission related to the spin-singlet state of the positively charged exciton is insensitive to the polarized split components of the peak R*.

The most important issue is the origin of the ${}^pX^{+*}$ emission line. A long enough lifetime of the spin-triplet state of two holes is attributed to a long spin-flip time. This is the reason why two spin configurations (singlet and triplet) of the emission of the singly positively charged excitons, such as the $X^+$ and the $X^{+*}$, are observed [81, 123]. The presence of resonant peaks, like R*, in micro-PLE spectra has been previously studied in Ref. 122. This state can be treated as a metastable due to long relaxation time of the electron from the $p$-shell level to an empty $s$-shell level. In the QDs under investigation, the relaxation time of the electron needs to be comparable with or even longer than the lifetime

of the excitonic complex associated with the ${}^{p}X^{+*}$ emission line. The electron relaxation time from the $p$- to the $s$-shell level in the InGaAs/GaAs QDs has been theoretically predicted to be on the order of single ps [124]. For instance, in n-doped InGaAs/GaAs QDs the low-temperature $p \rightarrow s$ relaxation time has been extracted from the pump-probe infrared spectroscopy and it falls in the range of 20 - 70 ps [125,126]. Due to this fact, the two hole spin-configuration is responsible for the long enough relaxation time, which allows for the optical recombination of the excitonic complex related to the ${}^{p}X^{+*}$ emission line. It has to be mentioned that a similar pair of the resonant peak and the emission line does not appear in the micro-PLE spectrum of the neutral exciton (see Section 6.4 for comparison). Several relaxation mechanisms have been proposed to explain the fast inter-shell relaxation: the emission of multiple acoustic phonons [125,127], the Auger carrier-carrier scattering [128], and the polaron relaxation [129]. Neither of them is, however, fully satisfactory.

Moreover, it should also be noted that in a single plane of self-assembled CdTe/ZnTe QDs, the inter-dot coupling have been observed [74,80]. The coupling occurs between the neutral exciton state of the absorbing QD and various excitonic states of the emitting QD. This transfer is realized via tunnelling of whole excitons between the dots with high inter-dot spin transfer efficiency. If the $e$-$h$ pair occupying the $p$-shell can only relax to the $s$-shell as a whole exciton (not as independent the electron and the hole - see the paragraph above), the long spin flip time of holes determines this relaxation process. As it has been discussed, the spin flip time of holes in the investigated GaAlAs QDs is very long (the $X^{+*}$ emission line attributed to the recombination of the triplet-state of the positively charged exciton is detected), the observation of the ${}^{p}X^{+*}$ emission line is also possible, because the spin flip time of holes blocks the relaxation of the whole exciton to the $s$-shell.

The obtained results shine new light on the issue of the excited states of electrons and holes confined in the single QD. The micro-PLE spectra of positively charged excitons are more complex than in the case of the neutral exciton. To the best knowledge of the Author, it is the first time, when the micro-PL signal is observed from the excited state, in which an electron occupy the $p$-shell while the $s$-shell in the conduction band is empty.

## 7.4 Conclusions

To conclude, the properties of five emission lines from the $s$- and $p$-shell attributed to the transitions within the positively charged excitons, such as: $X^+$, $X^{+*}$, $2X^+$, ${}^p2X^{+*}$, and ${}^pX^{+*}$ are presented and discussed. The FSS of the excitonic states, involved in these transitions is analysed and two cascade pathways are identified. Moreover, the magnetic field effect is presented, and the fine structure is described, showing the complex structure of these states. The magnetic-field-dependent micro-PLE spectra detected at the $X^+$ and $X^{+*}$ recombination energies are investigated. Two types of resonant peaks, the $s$- and $p$-shell-like, appear in the spectra. The former one is attributed to the transitions between the consecutive levels in the valence band and the $s$-shell level in the conduction band, as discussed in the case of the X emission line. Due to the isotropic $hh$ exchange interaction, the description of these resonant peaks is sophisticated and depends on the ratio of the hole relaxation time to the spin flip time. In the latter case, the attribution of the $p$-shell like resonant peak is proposed that relates them to the excitonic state, occupied by the $p$-shell electron and the $s$- and $p$-shell holes. A comparison between the micro-PL and micro-PLE spectra shows an unexpected result, that the emission energy of the ${}^pX^{+*}$ line coincides with the excitonic excited state energy (the magnetic field dispersions are also the same). Based on the results of a few different experiments, this emission line is attributed to the complex comprising an electron in the $p$-shell and two holes forming the spin triplet configuration in the $s$ and $p$ shells of the valence band.

# Chapter 8

# Negatively charged excitonic states

In order to have a comprehensive picture of the accessible charged families in the studied QDs (detailed information in Section 5.4), the negatively charged states are briefly investigated in this Chapter. The attribution of the emission lines, belonging to this family, and the fine structure of the excitonic states, which are involved in the observed emission lines, is presented and analysed. Moreover, the origin of the negatively charged states is considered in relation to the obtained micro-PLE spectrum of the negatively charged exciton.

## 8.1 Identification and properties of emission lines

The micro-PL spectra of a single dot, excited quasi-resonantly (see Section 5.2), as a function of an excitation power are shown in Fig. 8.1. In the low excitation power range (below $P_0$=10 µW), no emission lines related to negatively charged excitons are observed. The increase of the excitation power results in appearance of the $X^-$ emission line. This line is attributed to the recombination process of a singly negatively charged exciton (the complex consisting of a single $e$-$h$ pair and an additional electron, in which the electrons form a spin-singlet state), which is an elementary representative of the negatively charged excitonic family. At higher excitation power, the $X^{2-}$ emission line emerges, which is associated with the recombination of a doubly negatively charged exciton (an $e$-$h$ pair and two extra electrons; two of them are in the spin-singlet state on the $s$-shell level (and $s$-shell) and the third one occupies the $p$-shell level). The attribution of

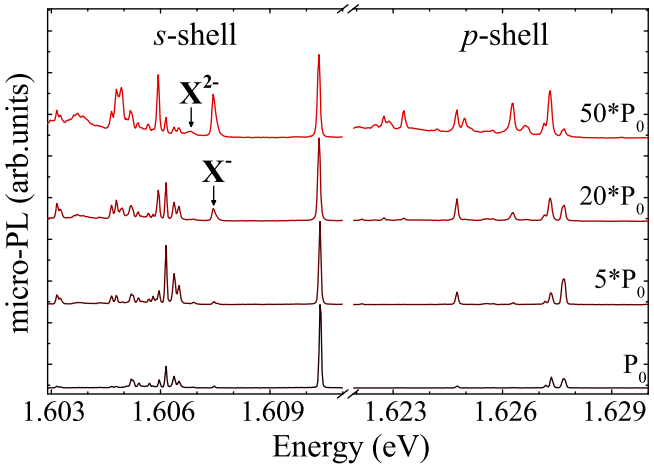


Figure 8.1: The excitation-power evolution of the micro-PL spectra of a single GaAlAs/AlAs QD measured at $T$= 4.2 K. The spectra are excited quasi-resonantly ($E_{exc}$=1.71 eV). $P_0$=10 µW and indicates the excitation power. The spectra are normalized to the intensity of the X emission line and vertically shifted for clarity purpose.

the $X^-$ and $X^{2-}$ emission lines to the singly and doubly negatively charged excitons is confirmed by the polarization-resolved micro-PL and photon correlation measurements (refer to Section 5.4 for further information), discussed in detail in what follows. [11,38,58,118]

Fig. 8.2 shows the energy of the $X^-$ and $X^{2-}$ emission lines as a function of the angle of a polarization analyser. The $X^-$ line does not exhibit any noticeable

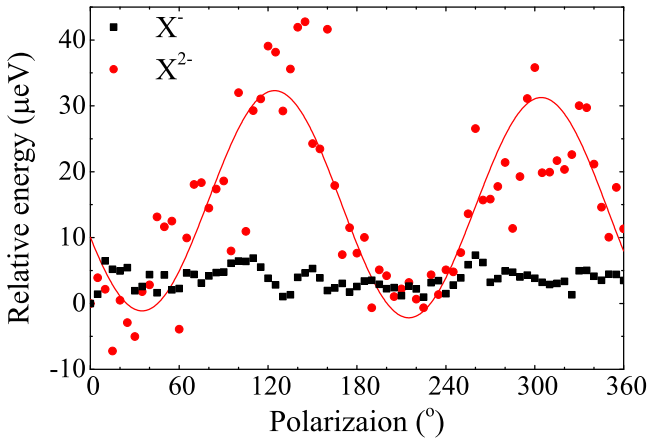


Figure 8.2: The energy of the $X^-$ and $X^{2-}$ emission lines as a function of the angle of a polarization analyser (points). The FSS of the $X^{2-}$ emission line is determined by means of fitting the cosine-squared function (a red solid curve).

fingerprint of the in-plane anisotropy. This is expected since the *eh* exchange interaction influences neither the initial (where the two electrons form the spin-singlet state) nor the final state (only one electron left) - see Fig. 8.2. The histogram of the photon correlation measurement between the $X^{-}$ and $X^{2-}$ emission lines exhibit a narrow antibunching peak (see Fig. 5.9). It confirms that both lines belong to the same excitonic family (the negatively charged one). The $X^{2-}$ emission line is tentatively attributed to the transition of the doubly negatively charged exciton, the fine structure of which is similar to that of the neutral exciton, but with the *eh* exchange interaction taking place between a *p*-shell electron and an *s*-shell hole. In the final state of the $X^{2-}$ emission line, two electrons occupying the *s*- and *p*-shell level form a spin-singlet or spin-triplet state. It results in four components of the $X^{2-}$ emission line [11,58]. In the investigated case, only two of them (orthogonally linearly polarized) are observed. Since the excitation regime (above-barrier or quasi-resonant) does not affect to any noticeable extent the FSS of the emission lines (compare Figs 6.7 and 8.2), see also characteristic of these lines in Section 6.2.1.

## 8.2 Photoluminescence excitation

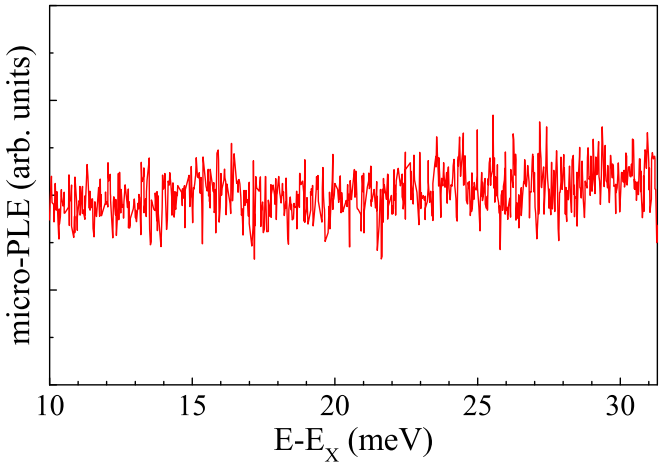


Figure 8.3: Micro-PLE spectrum detected at the energy of the recombination of the negatively charged exciton. $\Delta_{s\text{-}p}$=14.30 meV. The scale of the horizontal axis is set by the energy relative to the X emission line.

A typical micro-PLE spectrum measured at the energy of the recombination of the negatively charged exciton, because the related emission line is absent in the used range of excitation powers, is presented in Fig. 8.3. Although the spectrum is measured in the broad range of the excitation energy (up to $\sim$ 30 meV), it does not exhibit any resonant peaks. Moreover, the increase of the excitation

power does not affect the shape of the micro-PLE spectrum. These results confirm the analysis of the origin of the negatively charged excitons discussed in Section 5.5. The emission of negatively charged excitons is related to the neutralisation of the charged impurities (acceptor centres present in the system under study) by the photogenerated carriers. It excludes the possibility of observing the resonant peaks in the micro-PLE spectrum of the singly negatively charged exciton. It should also be noted that the origin of the positively charged excitons is associated with the presence of charged impurities and that the micro-PLE spectra of them consist a number of resonant peaks (see Section 7.3).

## 8.3 Conclusions

In this Chapter, the negatively charged states are studied. Two emission lines attributed to the recombination of the singly and doubly negatively charged excitons, the $X^{-}$ and $X^{2-}$ emission lines, are identified. The fine structure of these excitonic states is analysed. Moreover, the obtained micro-PL spectra detected at the energy of the recombination of the negatively charged exciton confirm the origin of the negatively charged excitons in the investigated QDs, as it has been presented in Section 5.5.

# Chapter 9

# Conclusions

The thesis presents the experimental results and the analysis of the multiexciton phenomena in single semiconductor GaAlAs/AlAs QDs. The main goal of the work was to study the excited states of (the) excitonic complexes, such as the neutral and charged excitons, by means of the comparison of results of two types of basic optical experiments: the photoluminescence and the photoluminescence excitation spectroscopy.

The most important results obtained in the work are:

- The energy of the excitation laser strongly affects the lineshape of the micro-PL spectra of a single QD. Particularly, two excitation regimes, the above-barrier and quasi-resonant, are identified and the respective mechanisms of carrier trapping active in both of them are discussed.

- The magnetic-field dispersion of the multiexcitonic emission from a highly excited QD is analysed in terms of the Fock-Darwin model. Despite the fact that the shells emission does not follow a typical Fock-Darwin-like evolution in a magnetic field, three groups of emission lines are attributed to the $s$-, $p_-$-, and $p_+$-shell in the QD.

- Three *families* of excitonic lines (the neutral, positively and negatively charged ones) are identified on the basis of respective charge states of a QD. The number of electrons and holes confined in the dot in a particular configuration was found using the single photon correlation experiment.

- The properties of four emission lines (X, 2X, 3X, and 4X) related to the neutral charge state of a QD are discussed. The FSS of the emission lines is analysed and the diagram of the cascade decay of the neutral quadexciton in QDs is postulated. It is shown that while the polarization of the 4X and

3X (2X and X) emission is correlated, there is no correlation between the 3X and X emission. Moreover, the effect of magnetic field on the $p$-shell-related emission, the diamagnetic shift of the $s$-shell-related emission as well as the Zeeman splitting of both the $s$-shell- and the $p$-shell-related emission are investigated. The observed non-linear Zeeman splitting of the X emission line and large Zeeman splitting of the 3X emission line strongly suggest the substantial effect of the HH-LH mixing in the studied QDs.

- Five emission lines associated with the positively charged states of a QD are identified: $X^{+}$, $X^{+*}$, $2X^{+}$, ${}^{p}2X^{+*}$, and ${}^{p}X^{+*}$. Based on the results of the correlation experiment, two cascade pathways are identified which involve the spin-singlet and spin-triplet states of the positively charged exciton and biexciton. Moreover, their fine structure is described, showing a more complex structure of these states than for the neutral states. The effect is attributed to the exchange interaction between electrons or holes, occupying different excitonic energy levels. The influence of magnetic field on the related complexes is also presented.

- Two emission lines ascribed to the recombination of the singly and doubly negatively charged excitons, the $X^{-}$ and $X^{2-}$ emission lines, are identified. The fine structure of these excitonic states is analysed.

- Two types of the magnetic field evolution of resonant peaks in the micro-PLE of the neutral exciton and the positively charged excitons, the $s$- and $p$-shell-like, are observed.

    - The $s$-shell-related resonant peaks are attributed to the transition between the excited hole levels in the valence band and the ground $s$-shell level in the conduction band. As compared to a typical model of the hole shells known in the literature, the hole ladder in the valence band is described in the present thesis within a more complex framework, which takes into account also the HH-LH mixing.

    - The $p$-shell-related resonant peak is also found. It originates from the transition of carriers between the $p$-shells of both bands. The comparison of the micro-PL and micro-PLE spectra shows an unexpected result: the energy of the emission line $pX^{+*}$ coincides with the energy of this excitonic excited state (the magnetic field dispersions are also the same). Based on the results of a few different experiments, this emission line is attributed to the complex comprising an electron in the $p$-shell and two holes forming the spin triplet configuration in the $s$ and $p$ shells of the valence band.

# Appendix A

# List of publications

During the Phd studies the Author has published as a co-author few publications.

**List of publications related to this work**

- M. R. Molas, A. A. L. Nicolet, A. Babiński, and M. Potemski, "Quadexciton cascade and fine structure splitting of the triexciton in a single quantum dot," *to be published.*
- M. R. Molas, A. A. L. Nicolet, B. Piętka, A. Babiński, and M. Potemski, "Magnetic field effect on the excitation spectrum of a neutral exciton in a single quantum dot," *accepted to publish in Acta Physica Polonica A.*
- M. R. Molas, A. A. L. Nicolet, M. Potemski, and A. Babiński, "Intershell Exchange Interaction in Charged GaAlAs Quantum Dots," *Acta Physica Polonica A*, vol. 124, p. 785, 2013.
- M. Molas, K. Gołasa, B. Piętka, M. Potemski, and A. Babiński, "Fine Structure of Neutral Excitons in Single GaAlAs Quantum Dots," *Acta Physica Polonica A*, vol. 122, p. 988, 2012.

**List of publication basing on the research of single InGaAs QDs**

- K. Gołasa, M. Molas, M. Goryca, T. Kazimierczuk, T. Smoleński, M. Koperski, A. Golnik, P. Kossacki, M. Potemski, Z. R. Wasilewski, and A. Babiński, "Properties of Excitons in Quantum Dots with a Weak Confinement," *Acta Physica Polonica A*, vol. 124, p. 781, 2013.
- M. Molas, K. Gołasa, M. Furman, J. Lapointe, Z.R. Wasilewski, M. Potemski, and A. Babiński, "The Fine Structure of a Triexciton in Single InAs/GaAs Quantum Dots," *Acta Physica Polonica A*, vol. 122, p. 991, 2012.

- M. Molas, K. Gołasa, K. Kuldova, J. Borysiuk, A. Babiński, J. Lapointe, and Z. R. Wasilewski, "The effect of In-flush on the optical anisotropy of InAs/GaAs quantum dots," *Journal of Applied Physics*, vol. 111, p. 033510, 2012.

- M. Molas, K. Gołasa, K. Kuldova, J. Borysiuk, A. Babiński, J. Lapointe, and Z. R. Wasilewski, "The effect of In-flush on the optical anisotropy of InAs/GaAs quantum dots," *Journal of Applied Physics*, vol. 111, p. 033510, 2012.

# Bibliography


[1] M. Grundmann, ed., *Nano-Optoelectronics Concepts, Physics, and Devices*. Berlin: Springer-Verlag, 2002. (cited at p. 1)

[2] L. Jacak, P. Hawrylak, and A. Wojs, *Quantum dots*. Berlin: Springer-Verlag Berlin, 1998. (cited at p. 1)

[3] M. Grundmann, D. Bimberg, and N. N. Ledentsov, *Quantum Dot Heterostructures*. New York: John Wiley & Sons Ltd., 1998. (cited at p. 1)

[4] P. Michler, A. Imamoğlu, M. D. Mason, P. J. Carson, G. F. Strouse, and S. K. Buratto, "Quantum correlation among photons from a single quantum dot at room temperature," *Nature*, vol. 406, p. 968, 2000. (cited at p. 1 and 38)

[5] J. Urayama, T. B. Norris, J. Singh, and P. Bhattacharya, "Observation of Phonon Bottleneck in Quantum Dot Electronic Relaxation," *Physical Review Letter*, vol. 86, p. 4930, 2001. (cited at p. 1)

[6] E. A. Zibik, T. Grange, B. A. Carpenter, N. E. Porter, R. Ferreira, G. Bastard, D. Stehr, S. Winnerl, M. Helm, H. Y. Liu, M. S. Skolnick, and L. R. Wilson, "Long lifetimes of quantum-dot intersublevel transitions in the terahertz range," *Nature Materials*, vol. 8, p. 803, 2009. (cited at p. 1)

[7] Y. Wei, W. Ma, J. Huang, Y. Zhang, Y. Huo, K. Cui, L. Chen, and Y. Shi, "Very long wavelength quantum dot infrared photodetector using a modified dots-in-a-well structure with AlGaAs insertion layers," *Applied Physics Letters*, vol. 98, p. 103507, 2011. (cited at p. 1)

[8] P. Hawrylak, "Excitonic artificial atoms: Engineering optical properties of quantum dots," *Physical Review B*, vol. 60, p. 5597, 1999. (cited at p. 1, 5, 10, 12, 32, 45, 48, 49, and 129)

[9] M. Bayer, O. Stern, P. Hawrylak, S. Fafard, and A. Forchel, "Hidden symmetries in the energy levels of excitonic 'artificial atoms'," *Nature*, vol. 405, p. 923, 2000. (cited at p. 1, 2, 8, 11, 31, 45, and 129)

[10] A. Babiński, M. Potemski, S. Raymond, J. Lapointe, and Z. R. Wasilewski, "Emission from a highly excited single InAs/GaAs quantum dot in magnetic fields: An excitonic Fock-Darwin diagram," *Physical Review B*, vol. 74, p. 155301, 2006. (cited at p. 1, 5, 9, 10, 11, 23, 31, 33, 57, 58, 60, and 129)

[11] Y. Benny, Y. Kodriano, E. Poem, D. Gershoni, T. A. Truong, and P. M. Petroff, "Excitation spectroscopy of single quantum dots at tunable positive, neutral, and negative charge states," *Physical Review B*, vol. 86, p. 085306, 2012. (cited at p. 1, 36, 43, 60, 63, 71, 72, 85, 88, 96, 106, and 107)

[12] U. Banin, Y. Cao, D. Katz, and O. Millo, "Identification of atomic-like electronic states in indium arsenide nanocrystal quantum dots," *Nature*, vol. 400, p. 542, 1999. (cited at p. 1)

[13] O. Benson, C. Santori, M. Pelton, and Y. Yamamoto, "Regulated and Entangled Photons from a Single Quantum Dot," *Physical Review Letters*, vol. 84, p. 2513, 2000. (cited at p. 2, 14, and 45)

[14] E. Moreau, I. Robert, L. Manin, V. Thierry-Mieg, J. M. Gérard, and I. Abram, "Quantum Cascade of Photons in Semiconductor Quantum Dots," *Physical Review Letters*, vol. 87, p. 183601, 2001. (cited at p. 2 and 38)

[15] M. Bayer, T. Gutbrod, A. Forchel, V. D. Kulakovskii, A. Gorbunov, M. Michel, R. Steffen, and K. H. Wang, "Exciton complexes in $In_xGa_{1-x}As/GaAs$ quantum dots," *Physical Review B*, vol. 58, p. 4740, 1998. (cited at p. 2)

[16] Y. Benny, Y. Kodriano, E. Poem, S. Khatsevitch, D. Gershoni, and P. M. Petroff, "Two-photon photoluminescence excitation spectroscopy of single quantum dots," *Physical Review B*, vol. 84, p. 075473, 2011. (cited at p. 3, 24, 60, 63, 71, 72, and 96)

[17] S. Awirothananon, S. Raymond, S. Studenikin, M. Vachon, W. Render, A. Sachrajda, X. Wu, A. Babinski, M. Potemski, S. Fafard, S. J. Cheng, M. Korkusinski, and P. Hawrylak, "Single-exciton energy shell structure in InAs/GaAs quantum dots," *Physical Review B*, vol. 78, p. 235313, 2008. (cited at p. 5)

[18] K. H. Schmidt, G. Medeiros-Ribeiro, M. Oestreich, P. M. Petroff, and G. H. Döhler, "Carrier relaxation and electronic structure in InAs self-assembled quantum dots," *Physical Review B*, vol. 54, p. 11346, 1996. (cited at p. 5)

[19] H. Drexler, D. Leonard, W. Hansen, J. P. Kotthaus, and P. M. Petroff, "Spectroscopy of Quantum Levels in Charge-Tunable InGaAs Quantum Dots," *Physical Review Letters*, vol. 73, p. 2252, 1994. (cited at p. 5)

[20] S. Löttjohann, C. Meier, A. Lorke, D. Reuter, and A. D. Wieck, "Screening effects in InAs quantum-dot structures observed by photoluminescence and capacitance-voltage spectra," *Applied Physics Letters*, vol. 87, p. 163117, 2005. (cited at p. 5)

[21] A. Wojs, P. Hawrylak, S. Fafard, and L. Jacak, "Electronic structure and magneto-optics of self-assembled quantum dots," *Physical Review B*, vol. 54, p. 5604, 1996. (cited at p. 5)

[22] M. Korkusiński, M. Zieliński, and P. Hawrylak, "Multiexciton complexes in InAs self-assembled quantum dots," *Journal of Applied Physics*, vol. 105, p. 122406, 2009. (cited at p. 5, 7, 10, and 129)

[23] Z. R. Wasilewski, S. Fafard, and J. P. McCaffrey, "Size and shape engineering of vertically stacked self-assembled quantum dots," *Journal of Crystal Growth*, vol. 201, p. 1131, 1999. (cited at p. 7 and 129)

[24] V. Fock, "Bemerkung zur quantelung des harmonischen oszillators in magnet-feld," *Zeitschrift für Physik*, vol. 47, p. 446, 1928. (cited at p. 8)

[25] C. G. Darwin, "The Diamagnetism of the Free Electron," *Mathematical Proceedings of the Cambridge Philosophical Society*, vol. 27, p. 86, 1930. (cited at p. 8)

[26] G. Bester and A. Zunger, "Cylindrically shaped zinc-blende semiconductor quantum dots do not have cylindrical symmetry: Atomistic symmetry, atomic relaxation, and piezoelectric effects," *Physical Review B*, vol. 71, p. 045318, 2005. (cited at p. 8 and 32)

[27] L. He and A. Zunger, "Multiple charging of InAs/GaAs quantum dots by electrons or holes: Addition energies and ground-state configurations," *Physical Review B*, vol. 73, p. 115324, 2006. (cited at p. 8 and 32)

[28] W. Sheng, S.-J. Cheng, and P. Hawrylak, "Multiband theory of multiexciton complexes in self-assembled quantum dots," *Physical Review B*, vol. 71, p. 035316, 2005. (cited at p. 10)

[29] R. J. Warburton, B. T. Miller, C. S. Dürr, C. Bödefeld, K. Karrai, J. P. Kotthaus, G. Medeiros-Ribeiro, P. M. Petroff, and S. Huant, "Coulomb interactions in small charge-tunable quantum dots: A simple model," *Physical Review B*, vol. 58, p. 16221, 1998. (cited at p. 11)

[30] S.-J. Cheng, W. Sheng, and P. Hawrylak, "Theory of excitonic artificial atoms: InGaAs/GaAs quantum dots in strong magnetic fields," *Physical Review B*, vol. 68, p. 235330, 2003. (cited at p. 11 and 60)

[31] A. Zrenner, L. V. Butov, M. Hagn, G. Abstreiter, G. Böhm, and G. Weimann, "Quantum dots formed by interface fluctuations in AlAs/GaAs coupled quantum well structures," *Physical Review Letters*, vol. 72, p. 3382, 1994. (cited at p. 11, 27, and 28)

[32] D. Gammon, E. S. Snow, and D. S. Katzer, "Excited state spectroscopy of excitons in single quantum dots ," *Applied Physics Letters*, vol. 67, p. 2391, 1995. (cited at p. 11 and 28)

[33] S. Raymond, S. Studenikin, A. Sachrajda, Z. Wasilewski, S. J. Cheng, W. Sheng, P. Hawrylak, A. Babiński, M. Potemski, G. Ortner, and M. Bayer, "Excitonic Energy Shell Structure of Self-Assembled InGaAs/GaAs Quantum Dots," *Physical Review Letters*, vol. 92, p. 187402, 2004. (cited at p. 11, 31, and 33)

[34] M. Bayer, G. Ortner, O. Stern, A. Kuther, A. A. Gorbunov, A. Forchel, P. Hawrylak, S. Fafard, K. Hinzer, T. L. Reinecke, S. N. Walck, J. P. Reithmaier, F. Klopf, and F. Schafer, "Fine structure of neutral and charged excitons in self-assembled In(Ga)As/(Al)GaAs quantum dots," *Physical Review B*, vol. 65, p. 195315, 2002. (cited at p. 14, 16, 23, 35, 36, 45, 46, 47, 48, and 75)

[35] K. Kowalik, O. Krebs, A. Golnik, J. Suffczyński, P. Wojnar, J. Kossut, J. A. Gaj, and P. Voisin, "Manipulating the exciton fine structure of single CdTe/ZnTe quantum dots by an in-plane magnetic field," *Physical Review B*, vol. 75, p. 195340, 2007. (cited at p. 14)

[36] H. W. van Kesteren, E. C. Cosman, W. A. J. A. van der Poel, and C. T. Foxon, "Fine structure of excitons in type-II GaAs/AlAs quantum wells," *Physical Review B*, vol. 41, p. 5283, 1990. (cited at p. 14)

[37] E. Blackwood, M. J. Snelling, R. T. Harley, S. R. Andrews, and C. T. B. Foxon, "Exchange interaction of excitons in GaAs heterostructures," *Physical Review B*, vol. 50, p. 14246, 1994. (cited at p. 14)

[38] E. Poem, J. Shemesh, I. Marderfeld, D. Galushko, N. Akopian, D. Gershoni, B. D. Gerardot, A. Badolato, and P. M. Petroff, "Polarization sensitive spectroscopy of charged quantum dots," *Physical Review B*, vol. 76, p. 235304, 2007. (cited at p. 14, 36, 43, 75, 77, 80, and 106)

[39] V. K. Kalevich, I. A. Merkulov, A. Y. Shiryaev, K. V. Kavokin, M. Ikezawa, T. Okuno, P. N. Brunkov, A. E. Zhukov, V. M. Ustinov, and Y. Masumoto, "Optical spin polarization and exchange interaction in doubly charged InAs self-assembled quantum dots," *Physical Review B*, vol. 72, p. 045325, 2005. (cited at p. 14)

[40] E. Poem, Y. Kodriano, C. Tradonsky, N. H. Lindner, B. D. Gerardot, P. M. Petroff, and D. Gershoni, "Accessing the dark exciton with light," *Nature Physics*, vol. 6, p. 993, 2010. (cited at p. 14)

[41] R. Rinaldi, P. V. Giugno, R. Cingolani, H. Lipsanen, M. Sopanen, J. Tulkki, and J. Ahopelto, "Zeeman Effect in Parabolic Quantum Dots," *Physical Review Letters*, vol. 77, p. 342, 1996. (cited at p. 15)

[42] M. Bayer, S. N. Walck, T. L. Reinecke, and A. Forchel, "Exciton binding energies and diamagnetic shifts in semiconductor quantum wires and quantum dots," *Physical Review B*, vol. 57, p. 6584, 1998. (cited at p. 15)

[43] P. P. Paskov, P. O. Holtz, B. Monemar, J. M. Garcia, W. V. Schoenfeld, and P. M. Petroff, "Magnetoluminescence of highly excited InAs/GaAs self-assembled quantum dots," *Physical Review B*, vol. 62, p. 7344, 2000. (cited at p. 15)

[44] S. N. Walck and T. L. Reinecke, "Exciton diamagnetic shift in semiconductor nanostructures," *Physical Review B*, vol. 57, p. 9088, 1998. (cited at p. 15)

[45] G. Danan, B. Etienne, F. Mollot, R. Planel, A. M. Jean-Louis, F. Alexandre, B. Jusserand, G. Le Roux, J. Y. Marzin, H. Savary, and B. Sermage, "Optical evidence of the direct-to-indirect-gap transition in GaAs-AlAs short-period superlattices," *Physical Review B*, vol. 35, p. 6207, 1987. (cited at p. 18)

[46] H. W. van Kesteren, E. C. Cosman, P. Dawson, K. J. Moore, and C. T. Foxon, "Order of the $X$ conduction-band valleys in type-II GaAs/AlAs quantum wells," *Physical Review B*, vol. 39, p. 13426, 1989. (cited at p. 18 and 28)

[47] M. R. Teisser, "Effects electro-optiques dans les hétérostructures GaAs/AlAs de type II," *Phd thesis, Université Paris VI*, 1992. (cited at p. 18)

[48] P. Lefebvre, B. Gil, H. Mathieu, and R. Planel, "Piezospectroscopy of GaAs-AlAs superlattices," *Physical Review B*, vol. 40, p. 7802, 1985. (cited at p. 18)

[49] B. Piętka, "Excitonic Complexes in Natural Quantum Dots Formed in Type II GaAs/AlAs Structures," *Phd thesis, Joseph Fourier University, Grenoble I, and University of Warsaw, Warsaw*, 2007. (cited at p. 18, 19, 28, 31, 42, 43, 63, and 71)

[50] A. Trüby, M. Potemski, and R. Planel, "Magnetic field effects in the luminescence spectra of type II GaAs/AlAs double layer structures," *Solid-State Electronics*, vol. 40, p. 139, 1996. (cited at p. 19 and 28)

[51] A. Wysmołek, M. Potemski, and V. Thierry-Mieg, "Single-dot-like emission induced by high magnetic fields," *Physica E*, vol. 12, p. 876, 2002. (cited at p. 19 and 28)

[52] A. Wysmołek, B. Chwalisz, M. Potemski, R. Stępniewski, A. Babiński, and S. Raymond, "Emission from Mesoscopic-Size Islands Formed in a GaAs/AlAs Double Layer Structure ," *Acta Physica Polonica A*, vol. 106, p. 367, 2004. (cited at p. 19, 28, and 31)

[53] B. Chwalisz, A. Wysmołek, R. Stępniewski, A. Babiński, and V. Thierry-Mieg, "Magneto-luminescence of a single lateral island formed in the type - II GaAs/AlAs QW," *International Journal of Modern Physics B*, vol. 18, p. 3807, 2004. (cited at p. 19)

[54] B. Chwalisz-Piętka, A. Wysmołek, R. Stępniewski, S. Raymond, R. Bożek, and V. Thierry-Mieg, "Direct bandgap quantum dots embedded in a type-II GaAs/AlAs double quantum well structure ," *International Journal of Modern Physics B*, vol. 21, p. 1654, 2007. (cited at p. 19)

[55] B. Piętka, J. Suffczyński, M. Goryca, T. Kazimierczuk, A. Golnik, P. Kossacki, A. Wysmolek, J. A. Gaj, R. Stępniewski, and M. Potemski, "Photon correlation studies of charge variation in a single GaAlAs quantum dot," *Physical Review B*, vol. 87, p. 035310, 2013. (cited at p. 19, 30, 36, 37, and 39)

[56] M. D. Martín, C. Antón, L. Viña, B. Piętka, and M. Potemski, "Recombination dynamics of excitons and exciton complexes in single quantum dots," *Europhysics Letters*, vol. 100, no. 6, p. 67006, 2012. (cited at p. 19)

[57] M. Molas, K. Gołasa, K. Kuldova, J. Borysiuk, A. Babiński, J. Lapointe, and Z. R. Wasilewski, "The effect of In-flush on the optical anisotropy of InAs/GaAs quantum dots," *Journal of Applied Physics*, vol. 111, p. 033510, 2012. (cited at p. 23)

[58] T. Kazimierczuk, T. Smoleński, M. Goryca, L. Kłopotowski, P. Wojnar, K. Fronc, A. Golnik, M. Nawrocki, J. A. Gaj, and P. Kossacki, "Magnetophotoluminescence study of intershell exchange interaction in CdTe/ZnTe

quantum dots," *Physical Review B*, vol. 84, p. 165319, 2011. (cited at p. 23, 43, 80, 82, 106, and 107)

[59] A. Babiński, M. Potemski, S. Raymond, M. Korkusinski, W. Sheng, P. Hawrylak, and Z. Wasilewski, "Optical spectroscopy of a single InAs/GaAs quantum dot in high magnetic fields," *Physica E*, vol. 34, p. 288, 2006. (cited at p. 23)

[60] R. Oulton, J. J. Finley, A. I. Tartakovskii, D. J. Mowbray, M. S. Skolnick, M. Hopkinson, A. Vasanelli, R. Ferreira, and G. Bastard, "Continuum transitions and phonon coupling in single self-assembled Stranski-Krastanow quantum dots," *Physical Review B*, vol. 68, p. 235301, 2003. (cited at p. 24 and 60)

[61] T. Warming, E. Siebert, A. Schliwa, E. Stock, R. Zimmermann, and D. Bimberg, "Hole-hole and electron-hole exchange interactions in single InAs/GaAs quantum dots," *Physical Review B*, vol. 79, p. 125316, 2009. (cited at p. 24, 35, 60, 71, and 85)

[62] R. M. Stevenson, R. J. Young, P. Atkinson, K. Cooper, D. A. Ritchie, and A. J. Shields, "A semiconductor source of triggered entangled photon pairs," *Nature*, vol. 439, p. 179, 2006. (cited at p. 25 and 45)

[63] N. Akopian, N. H. Lindner, E. Poem, Y. Berlatzky, J. Avron, D. Gershoni, B. D. Gerardot, and P. M. Petroff, "Entangled Photon Pairs from Semiconductor Quantum Dots," *Physical Review Letters*, vol. 96, p. 130501, 2006. (cited at p. 25, 45, and 48)

[64] J. Persson, T. Aichele, V. Zwiller, L. Samuelson, and O. Benson, "Three-photon cascade from single self-assembled InP quantum dots," *Physical Review B*, vol. 69, p. 233314, 2004. (cited at p. 25 and 36)

[65] Y. Arashida, Y. Ogawa, and F. Minami, "Four-photon cascade from quadexcitons in a single GaAs quantum dot," *Physical Review B*, vol. 84, p. 125309, 2011. (cited at p. 25, 36, and 45)

[66] R. Hanbury-Brown and R. Q. Twist, "Correlation between Photons in two Coherent Beams of Light," *Nature (London)*, vol. 74, p. 1447, 1956. (cited at p. 25)

[67] J. Suffczyński, T. Kazimierczuk, M. Goryca, B. Piechal, A. Trajnerowicz, K. Kowalik, P. Kossacki, A. Golnik, K. P. Korona, M. Nawrocki, J. A. Gaj, and G. Karczewski, "Excitation mechanisms of individual CdTe/ZnTe quantum dots studied by photon correlation spectroscopy," *Physical Review B*, vol. 74, p. 085319, 2006. (cited at p. 25, 29, and 37)

[68] L. V. Butov, A. Zrenner, G. Abstreiter, G. Böhm, and G. Weimann, "Condensation of Indirect Excitons in Coupled AlAs/GaAs Quantum Wells," *Physical Review Letters*, vol. 73, p. 304, 1994. (cited at p. 27)

[69] M. Molas, K. Gołasa, B. Piętka, M. Potemski, and A. Babiński, "Fine Structure of Neutral Excitons in Single GaAlAs Quantum Dots," *Acta Physica Polonica A*, vol. 122, p. 988, 2012. (cited at p. 28, 42, and 48)

[70] S. W. Brown, T. A. Kennedy, D. Gammon, and E. S. Snow, "Spectrally resolved Overhauser shifts in single GaAs/$Al_xGa_{1-x}$As As quantum dots," *Physical Review B*, vol. 54, p. 17339, 1996. (cited at p. 28)

[71] B. Lita, S. Ghaisas, R. Goldman, and M. Melloch, "Nanometer-scale studies of Al-Ga interdiffusion and As precipitate coarsening in nonstoichiometric AlAs/GaAs superlattices," *Applied Physics Letters*, vol. 75, p. 4082, 1999. (cited at p. 28)

[72] J. Behrend, M. Wassermeier, W. Braun, P. Krispin, and K. H. Ploog, "Formation of GaAs/AlAs(001) interfaces studied by scanning tunneling microscopy," *Physical Review B*, vol. 53, p. 9907, 1996. (cited at p. 28)

[73] W. Braun, A. Trampert, L. Däweritz, and K. H. Ploog, "Nonuniform segregation of Ga at AlAs/GaAs heterointerfaces," *Physical Review B*, vol. 55, p. 1689, 1997. (cited at p. 28)

[74] T. Kazimierczuk, J. Suffczyński, A. Golnik, J. A. Gaj, P. Kossacki, and P. Wojnar, "Optically induced energy and spin transfer in nonresonantly coupled pairs of self-assembled CdTe/ZnTe quantum dots," *Physical Review B.*, vol. 79, p. 153301, 2009. (cited at p. 29 and 102)

[75] A. Lemaître, A. D. Ashmore, J. J. Finley, D. J. Mowbray, M. S. Skolnick, M. Hopkinson, and T. F. Krauss, "Enhanced phonon-assisted absorption in single InAs/GaAs quantum dots," *Physical Review B*, vol. 63, p. 161309, 2001. (cited at p. 29)

[76] E. S. Moskalenko, K. F. Karlsson, P. O. Holtz, B. Monemar, W. V. Schoenfeld, J. M. Garcia, and P. M. Petroff, "Acceptor-induced threshold energy for the optical charging of InAs single quantum dots," *Physical Review B*, vol. 66, p. 195332, 2002. (cited at p. 29)

[77] W.-H. Chang, H.-S. Chang, W.-Y. Chen, T. M. Hsu, T.-P. Hsieh, J.-I. Chyi, and N.-T. Yeh, "Optical control of the exciton charge states of single quantum dots via impurity levels," *Physical Review B*, vol. 72, p. 233302, 2005. (cited at p. 29 and 43)

[78] H. Nakajima, H. Kumano, H. Iijima, S. Odashima, and I. Suemune, "Carrier-transfer dynamics between neutral and charged excitonic states in a single quantum dot probed with second-order photon correlation measurements," *Physical Review B*, vol. 88, p. 045324, 2013. (cited at p. 30, 36, 37, and 39)

[79] T. Kazimierczuk, T. Smoleński, M. Goryca, L. Kłopotowski, P. Wojnar, K. Fronc, A. Golnik, M. Nawrocki, J. A. Gaj, and P. Kossacki, "Magnetophotoluminescence study of intershell exchange interaction in CdTe/ZnTe quantum dots," *Physical Review B*, vol. 84, p. 165319, 2011. (cited at p. 35 and 36)

[80] T. Kazimierczuk, J. Suffczyński, A. Golnik, J. A. Gaj, P. Kossacki, and P. Wojnar, "Optically induced energy and spin transfer in nonresonantly coupled pairs of self-assembled CdTe/ZnTe quantum dots," *Physical Review B*, vol. 79, p. 153301, 2009. (cited at p. 36, 37, and 102)

[81] Y. Arashida, Y. Ogawa, and F. Minami, "Polarization-correlated three-photon emission from charged triexcitons in a single quantum dot," *Physical Review B*, vol. 85, p. 235318, 2012. (cited at p. 36, 78, 80, and 101)

[82] A. Kiraz, S. Fälth, C. Becher, B. Gayral, W. V. Schoenfeld, P. M. Petroff, L. Zhang, E. Hu, and A. Imamoğlu, "Photon correlation spectroscopy of a single quantum dot," *Physical Review B*, vol. 65, p. 161303, 2002. (cited at p. 37)

[83] M. H. Baier, A. Malko, E. Pelucchi, D. Y. Oberli, and E. Kapon, "Quantum-dot exciton dynamics probed by photon-correlation spectroscopy," *Physical Review B*, vol. 73, p. 205321, 2006. (cited at p. 37 and 39)

[84] A. Malko, M. Baier, E. Pelucchi, D. Chek-al-kar, D. Y.Oberli, and E. Kapon, "Correlated photon emission from semiconductor quantum dots grown in inverted pyramids," *Physica E*, vol. 26, p. 194, 2005. (cited at p. 37)

[85] V. Zwiller, H. Blom, P. Jonsson, N. Panev, S. Jeppesen, T. Tsegaye, E. Goobar, M.-E. Pistol, L. Samuelson, and G. Björk, "Single quantum dots emit single photons at a time: Antibunching experiments," *Applied Physics Letters*, vol. 78, p. 2476, 2001. (cited at p. 38)

[86] D. V. Regelman, U. Mizrahi, D. Gershoni, E. Ehrenfreund, W. V. Schoenfeld, and P. M. Petroff, "Semiconductor Quantum Dot: A Quantum Light Source of Multicolor Photons with Tunable Statistics," *Physical Review Letters*, vol. 87, p. 257401, 2001. (cited at p. 38)

[87] R. J. Warburton, C. Schäflein, D. Haft, F. Bickel, A. Lorke, K. Karrai, J. M. Garcia, W. Schoenfeld, and P. M. Petroff, "Optical emission from a charge-tunable quantum ring," *Nature*, vol. 405, p. 926, 2000. (cited at p. 41)

[88] M. Baier, F. Findeis, A. Zrenner, M. Bichler, and G. Abstreiter, "Optical spectroscopy of charged excitons in single quantum dot photodiodes," *Physical Review B*, vol. 64, p. 195326, 2001. (cited at p. 41)

[89] D. Hessman, J. Persson, M.-E. Pistol, C. Pryor, and L. Samuelson, "Electron accumulation in single InP quantum dots observed by photoluminescence," *Physical Review B*, vol. 64, p. 233308, 2001. (cited at p. 41)

[90] A. S. Bracker, E. A. Stinaff, D. Gammon, M. E. Ware, J. G. Tischler, A. Shabaev, A. L. Efros, D. Park, D. Gershoni, V. L. Korenev, and I. A. Merkulov, "Optical Pumping of the Electronic and Nuclear Spin of Single Charge-Tunable Quantum Dots," *Physical Review Letters*, vol. 94, p. 047402, 2005. (cited at p. 41)

[91] M. Abbarchi, T. Kuroda, T. Mano, K. Sakoda, C. A. Mastrandrea, A. Vinattieri, M. Gurioli, and T. Tsuchiya, "Energy renormalization of exciton complexes in GaAs quantum dots," *Physical Review B*, vol. 82, p. 201301, 2010. (cited at p. 42)

[92] "Spectroscopy of positively and negatively charged quantum dots: wave function extent of holes and electrons, author = D.V. Regelman and D. Gershoni and E. Ehrenfreund and W.V. Schoenfeld and P.M. Petroff, journal = Physica E, volume = 13, pages = 114, year = 2002,," (cited at p. 43)

[93] J. Gomis-Bresco, G. Muñoz-Matutano, J. Martínez-Pastor, B. Alén, L. Seravalli, P. Frigeri, G. Trevisi, and S. Franchi, "Random population model to explain the recombination dynamics in single InAs/GaAs quantum dots under selective optical pumping," *New Journal of Physics*, vol. 13, p. 023022, 2011. (cited at p. 43)

[94] R. Heitz, F. Guffarth, I. Mukhametzhanov, M. Grundmann, A. Madhukar, and D. Bimberg, "Many-body effects on the optical spectra of InAs/GaAs quantum dots," *Physical Review B*, vol. 62, p. 16881, 2000. (cited at p. 43)

[95] A. K. Nowak, E. Gallardo, H. P. van der Meulen, J. M. Calleja, J. M. Ripalda, L. González, and Y. González, "Band-gap renormalization in InP/$Ga_xIn_{1-x}P$ quantum dots," *Physical Review B*, vol. 83, p. 245447, 2011. (cited at p. 43)

[96] N. Gisin, G. Ribordy, W. Tittel, and H. Zbinden, "Quantum cryptography," *Reviews of Modern Physics*, vol. 74, p. 145, Mar 2002. (cited at p. 45)

[97] T. Jennewein, G. Weihs, J.-W. Pan, and A. Zeilinger, "Experimental Nonlocality Proof of Quantum Teleportation and Entanglement Swapping," *Physical Review Letters*, vol. 88, p. 017903, 2001. (cited at p. 45)

[98] D. Gammon, E. S. Snow, B. V. Shanabrook, D. S. Katzer, and D. Park, "Fine Structure Splitting in the Optical Spectra of Single GaAs Quantum Dots," *Physical Review Letters*, vol. 76, p. 3005, 1996. (cited at p. 45)

[99] I. Favero, G. Cassabois, C. Voisin, C. Delalande, P. Roussignol, R. Ferreira, C. Couteau, J. P. Poizat, and J. M. Gérard, "Fast exciton spin relaxation in single quantum dots," *Physical Review B*, vol. 71, p. 233304, 2005. (cited at p. 45 and 48)

[100] T. Flissikowski, A. Hundt, M. Lowisch, M. Rabe, and F. Henneberger, "Photon Beats from a Single Semiconductor Quantum Dot," *Physical Review Letters*, vol. 86, pp. 3172–3175, 2001. (cited at p. 45 and 48)

[101] K. F. Karlsson, M. A. Dupertuis, D. Y. Oberli, E. Pelucchi, A. Rudra, P. O. Holtz, and E. Kapon, "Fine structure of exciton complexes in high-symmetry quantum dots: Effects of symmetry breaking and symmetry elevation," *Physical Review B*, vol. 81, p. 161307, 2010. (cited at p. 45 and 48)

[102] D. Chithrani, M. Korkusiński, S. J. Cheng, P. Hawrylak, R.L.Williams, J. Lefebvre, P. J. Poole, and G. C. Aers, "Electronic structure of the p-shell in single, site-selected InAs/InP quantum dots," *Physica E*, vol. 26, p. 322, 2005. (cited at p. 48 and 49)

[103] M. R. Molas, A. A. L. Nicolet, A. Babiński, and M. Potemski, "Quadexciton cascade and fine structure splitting of the triexciton in a single quantum dot," *to be published*, 2014. (cited at p. 48)

[104] C. Santori, D. Fattal, M. Pelton, G. S. Solomon, and Y. Yamamoto, "Polarization-correlated photon pairs from a single quantum dot," *Physical Review B*, vol. 66, p. 045308, 2002. (cited at p. 51)

[105] T. Belhadj, T. Amand, A. Kunold, C.-M. Simon, T. Kuroda, M. Abbarchi, T. Mano, K. Sakoda, S. Kunz, X. Marie, and B. Urbaszek), "Impact of heavy hole-light hole coupling on optical selection rules in GaAs quantum dots ," *Applied Physics Letters*, vol. 97, p. 051111, 2010. (cited at p. 54)

[106] R. Seguin, A. Schliwa, S. Rodt, K. Pötschke, U. W. Pohl, and D. Bimberg, "Size-Dependent Fine-Structure Splitting in Self-Organized InAs/GaAs

Quantum Dots," *Physical Review Letters*, vol. 95, p. 257402, 2005. (cited at p. 54)

[107] M. R. Molas, A. A. L. Nicolet, M. Korkusiński, P. Hawrylak, J. Borysiuk, M. Potemski, Z. R. Wasilewski, and A. Babiński, "The effective mass in self-assembled InAs/GaAs quantum dots," *to be published.* (cited at p. 56)

[108] A. Babiński, G. Ortner, S. Raymond, M. Potemski, M. Bayer, W. Sheng, P. Hawrylak, Z. Wasilewski, S. Fafard, and A. Forchel, "Ground-state emission from a single InAs/GaAs self-assembled quantum dot structure in ultrahigh magnetic fields," *Physical Review B*, vol. 74, p. 075310, 2006. (cited at p. 57 and 58)

[109] V. Jovanov, T. Eissfeller, S. Kapfinger, E. C. Clark, F. Klotz, M. Bichler, J. G. Keizer, P. M. Koenraad, M. S. Brandt, G. Abstreiter, and J. J. Finley, "Highly nonlinear excitonic Zeeman spin splitting in composition-engineered artificial atoms," *Physical Review B*, vol. 85, p. 165433, 2012. (cited at p. 57, 58, and 59)

[110] C. Hermann and C. Weisbuch, "$\overrightarrow{k} \cdot \overrightarrow{p}$ perturbation theory in III-V compounds and alloys: a reexamination," *Physical Review B*, vol. 15, p. 823, 1977. (cited at p. 58)

[111] J. I. Climente, J. Planelles, M. Pi, and F. Malet, "Magnetic-field dependence of hole levels in self-assembled InGaAs quantum dots," *Physical Review B*, vol. 72, p. 233305, 2005. (cited at p. 58, 59, and 138)

[112] J. H. Blokland, F. J. P. Wijnen, P. C. M. Christianen, U. Zeitler, J. C. Maan, P. Kailuweit, D. Reuter, and A. D. Wieck, "Hole levels in InAs self-assembled quantum dots," *Physical Review B*, vol. 75, p. 233305, 2007. (cited at p. 58, 59, and 133)

[113] A. Manaselyan and T. Chakraborty, "Enhanced Rashba effect for hole states in a quantum dot," *Europhysics Letters*, vol. 88, p. 17003, 2009. (cited at p. 58)

[114] E. Siebert, T. Warming, A. Schliwa, E. Stock, M. Winkelnkemper, S. Rodt, and D. Bimberg, "Spectroscopic access to single-hole energies in InAs/GaAs quantum dots," *Physical Review B*, vol. 79, p. 205321, 2009. (cited at p. 60, 71, and 85)

[115] F. Findeis, A. Zrenner, G. Böhm, and G. Abstreiter, "Phonon-assisted biexciton generation in a single quantum dot," *Physical Review B*, vol. 61, p. R10579, 2000. (cited at p. 60)

[116] D. Sarkar, H. P. van der Meulen, J. M. Calleja, J. M. Meyer, R. J. Haug, and K. Pierz, "Resonant optical excitation of longitudinal-optical phonons and intermixing in InAs/AlAs single quantum dots," *Applied Physics Letters*, vol. 92, p. 18, 2008. (cited at p. 60 and 63)

[117] M. Abbarchi, C. Mastrandrea, T. Kuroda, T. Mano, A. Vinattieri, K. Sakoda, and M. Gurioli, "Poissonian statistics of excitonic complexes in quantum dots," *Journal of Applied Physics*, vol. 106, p. 053504, 2009. (cited at p. 63)

[118] I. A. Akimov, K. V. Kavokin, A. Hundt, and F. Henneberger, "Electron-hole exchange interaction in a negatively charged quantum dot," *Physical Review B*, vol. 71, p. 075326, 2005. (cited at p. 75, 78, 80, 82, and 106)

[119] R. Heitz, V. Türck, and O. Stier, "Few-Particle Effects in Self-Organized Quantum Dots," *Advances in Solid State Physics*, vol. 41, p. 39, 2001. (cited at p. 75 and 80)

[120] I. A. Akimov, A. Hundt, T. Flissikowski, and F. Henneberger, "Fine structure of the trion triplet state in a single self-assembled semiconductor quantum dot," *Applied Physics Letters*, vol. 81, p. 4730, 2002. (cited at p. 80 and 82)

[121] I. Akimov, A. Hundt, T. Flissikowski, P. Kratzert, and F. Henneberger, "Energy spectrum of negatively charged single quantum dot: trion and charged biexciton states," *Physica E*, vol. 17, p. 31, 2003. (cited at p. 85)

[122] V. Jovanov, S. Kapfinger, M. Bichler, G. Abstreiter, and J. J. Finley, "Direct observation of metastable hot trions in an individual quantum dot," *Physical Review B*, vol. 84, p. 235321, 2011. (cited at p. 85 and 101)

[123] Y. Igarashi, M. Shirane, Y. Ota, M. Nomura, N. Kumagai, S. Ohkouchi, A. Kirihara, S. Ishida, S. Iwamoto, S. Yorozu, and Y. Arakawa, "Spin dynamics of excited trion states in a single InAs quantum dot," *Physical Review B*, vol. 81, p. 245304, 2010. (cited at p. 101)

[124] G. A. Narvaez, G. Bester, and A. Zunger, "Carrier relaxation mechanisms in self-assembled (In,Ga)As/GaAs quantum dots: Efficient P->S Auger relaxation of electrons," *Physical Review B*, vol. 74, p. 075403, 2006. (cited at p. 102)

[125] E. A. Zibik, L. R. Wilson, R. P. Green, G. Bastard, R. Ferreira, P. J. Phillips, D. A. Carder, J.-P. R. Wells, J. W. Cockburn, M. S. Skolnick, M. J. Steer, and M. Hopkinson, "Intraband relaxation via polaron decay in InAs self-assembled quantum dots," *Physical Review B*, vol. 70, p. 161305, 2004. (cited at p. 102)

[126] S. Sauvage, P. Boucaud, R. P. S. M. Lobo, F. Bras, G. Fishman, R. Prazeres, F. Glotin, J. M. Ortega, and J.-M. Gérard, "Long Polaron Lifetime in InAs/GaAs Self-Assembled Quantum Dots," *Physical Review Letters*, vol. 88, p. 177402, 2002. (cited at p. 102)

[127] T. Inoshita and H. Sakaki, "Electron relaxation in a quantum dot: Significance of multiphonon processes," *Physical Review B*, vol. 46, p. 7260, 1992. (cited at p. 102)

[128] R. Ferreira and G. Bastard, "Phonon-assisted capture and intradot Auger relaxation in quantum dots," *Applied Physics Letters*, vol. 74, p. 2818, 1999. (cited at p. 102)

[129] J. Seebeck, T. R. Nielsen, P. Gartner, and F. Jahnke, "Polarons in semiconductor quantum dots and their role in the quantum kinetics of carrier relaxation," *Physical Review B*, vol. 71, p. 125327, 2005. (cited at p. 102)

# List of Figures


2.1 Shell structure of the SP energy spectrum, and associated total degeneracies including the angular momentum and spin. . . . . 6

2.2 (a) lens shaped InAs QD embedded in GaAs matrix, (b) Electron probability density isosurfaces and electron and hole energies for dot (a), (c) disk shaped InAs QD (grown by the indium-flush method [23]), (d) Hole probability density isosurfaces and electron and hole energy shells for dot (c). From Ref. 22. . . . . 7

2.3 On the left-hand side is a scheme of the dot energy levels, their occupation by carriers and the radiative transitions. Spin orientations of electrons and holes: grey triangles, spin-down; black triangles, spin-up. On the right-hand side are typical photoluminescence spectra as a function of excitation power of an ensemble of $In_{0.60}Ga_{0.40}As$ QDs. From [9]. . . . . 8

2.4 Simulated FD spectrum of the first five states in magnetic field for $\hbar\omega_0$=14 meV and $\mu^*$=0.06 $m_0$. The pairs of values in brackets correspond to the $(n, m_z)$ quantum numbers. Dashed lines present the evolution of the first three Landau levels (see Eq. 2.6). . . . . 9

2.5 Luminescence from the $s$-, $p$-, and $d$-shell of the single InAs/GaAs QD at magnetic field up to 14 T. Red lines represent the simulation based on the excitonic Fock-Darwin diagram. From Ref. 10. . . . . 10

2.6 Contributions to energy levels and oscillator strength of the triexciton complex. The $s$ and $p$ letters describe the electron and hole on the $s$- and $p$ shells, respectively. From Ref. 8. . . . . 12

2.7 A schematic diagram of a few charge states in QD: neutral exciton (X), charged excitons ($X^+$ and $X^-$), neutral biexciton (2X) and neutral triexciton (3X). Red full and blue empty arrows represent electrons and holes, respectively. Horizontal lines in the confining potential represent two lowest energy shells. . . . . 13

2.8 Scheme of the neutral exciton fine structure at zero magnetic field. The central part of the figure illustrates the situation when the *eh* exchange interaction is neglected ($M = \pm 1$ and $M = \pm 2$ are degenerate). The left panel shows the excitonic fine structure for QDs with $D_{2d}$ symmetry, while the right panel accounts for dots with a symmetry lower than $D_{2d}$. . . . . 14

3.1 The nominal structure of the investigated sample. . . . . 17
3.2 Distribution of the energy bands and the position of the confined levels, characteristic of the GaAs/AlAs type II QW structure. Red dashed line - $\Gamma$-symmetry band; blue dashed line - $X$-symmetry band. The positions of the $\Gamma$- and $X$-symmetry states in the QW are marked in red and yellow colours, respectively. . . . . 18
3.3 A characteristic macro-PL spectrum ($\sim$1 mm$^2$ of the laser spot) of the investigated sample. . . . . 19
3.4 General scheme of the main part of the sample structure. . . . . 19
3.5 The micro-PL map of the emission from the QDs in the energy range: 1.58-1.70 eV. The mapping step was the same in both direction and equal 10 µm. The map was measured using the setup presented on part (b) in Fig. 4.1. . . . . 20
3.6 Potential distribution through the GaAlAs QD formed in the GaAs/AlAs type II QW structure is marked schematically on the potential distribution of double QW structure. Red dashed line - $\Gamma$-symmetry band; blue dashed line - $X$-symmetry band; and green dotted line - distribution of the potential through the dot in the growth direction. The positions of the ground state in QD are marked in green colour. The energy of $\Gamma$- and $X$-symmetry states in the QW are marked in red and blue colours, respectively. . . . . 20

4.1 Scheme of micro-photoluminescence setups available in: (a) Faculty of Physics, University of Warsaw, (b) Grenoble High Magnetic Field Laboratory. . . . . 22
4.2 The scheme of the micro-PL setup used for measurements in magnetic fields. An inset photo comprising of a microscope objective and piezoelectric x-y-z stages with the sample. . . . . 24
4.3 Scheme of the photon correlation experimental setup. . . . . 26

5.1 The PL spectrum of a 1 mm size area of the investigated sample measured at $T$=4.2 K. . . . . 28
5.2 The micro-PL spectra of a single GaAlAs/AlAs QD as a function of the excitation power at (a) the above-barrier ($E_{exc}$=1.759 eV) and (b) the quasi-resonant excitation regime ($E_{exc}$=1.71 eV). . . . . 29

5.3 a) Color plot of the micro-PL spectra recorded as a function of the excitation energy while keeping the excitation power at approximately constant level. Dashed horizontal lines indicate the energies of the $\Gamma - \Gamma$ (red), $X_Z - \Gamma$ (orange), $X_{XY} - \Gamma$ (pink) transitions in the QW; (b)-(d) Three micro-PL spectra excited at energies equal to 1.75 eV, 1.73 eV and 1.71 eV, respectively. . . . . 30

5.4 The evolution of the micro-PL spectrum of the highly excited GaAlAs/AlAs QD ($E_{exc}$=1.71 eV) in the magnetic field up to 28 T. The background intensity variation is an artifact resulting from the procedure described at the beginning of this Section. . . . . 32

5.5 The micro-PL spectra of different single QDs excited with about the same excitation power. The spectra are normalized to the most intense emission lines and vertically shifted for clarity purpose. . . . . 34

5.6 The histogram of the $\Delta_{s\text{-}p}$ value for the series of QDs. . . . . 35

5.7 The micro-PL spectra of a single GaAlAs/AlAs QD, excited quasi-resonantly at $E_{exc}$=1.71 eV and measured at $T$= 4.2 K for two different excitation powers: $P_0$=200 µW and 2.5*$P_0$. The spectra are normalized to the intensity of the X emission line and vertically shifted for clarity purpose. . . . . 37

5.8 A set of correlation histograms: (a) an auto-correlation on the X emission line, (b)-(d) cross-correlations between the 2X and X, the $X^+$ and X, and the $X^-$ and X emission lines, respectively. The histograms (a) and (c) were measured at $P_{exc}$=50 µW whereas (b) and (d) at $P_{exc}$=500 µW. . . . . 38

5.9 The photon auto- and cross-correlation histograms of the excitonic lines related to the *s*- and *p*-shell of the single QD under quasi-resonant excitation. Colours of background indicate the cross-correlations between emissions from the same family: blue - neutral, green - positively charged, red - negatively charged. . . . . 40

5.10 The excitation-power evolution of the micro-PL spectra of a single GaAlAs/AlAs QD measured at $T$= 4.2 K. The spectra are excited quasi-resonantly ($E_{exc}$=1.71 eV). $P_0$=10 µW and indicates the excitation power. The spectra are normalized to the intensity of the X emission line and vertically shifted for clarity purpose. . . . . 41

5.11 The excitation-power dependence of the integrated intensity (a) and the relative energy (b) of three main emission lines: X, $X^-$, and $X^+$. The plots are drawn in the log-log and the semi-log scale, respectively. 43

6.1 The excitation-power evolution of the micro-PL spectra of a single GaAlAs/AlAs QD measured at $T$= 4.2 K. The spectra are excited quasi-resonantly ($E_{exc}$=1.71 eV). $P_0$=10 µW indicates the excitation power. The spectra are normalized to the intensity of the X emission line and vertically shifted for clarity purpose. . . . . 46

6.2 High-resolution polarization-resolved micro-PL spectra of the emission lines attributed to neutral exciton (a), biexciton (b), triexciton (c) and quadexciton (d) in a single GaAlAs QD measured in two polarizations: parallel (red) and perpendicular (blue) to the [110] crystallographic direction. The open circles and closed squares indicate the experimental data. The curves drawn with solid and dashed lines represent the results of fitting the data with the Gaussian function. . 47

6.3 Fine structure splitting $\delta_1$ ($\delta_1^p$) as a function of the X (3X) emission energy for a series of single QDs, respectively. Dashed lines are a guide to the eye. . . . . 49

6.4 The ratio ${\delta_1}^P/\delta_1$ as a function of the energy separation $\Delta E_{s-p}$. Dashed line is a guide to the eye. . . . . 50

6.5 Schematic diagram of the cascade decay of a quadexciton in a single QD. The solid blue (red) arrows denote the radiative transitions in two perpendicular polarizations. The $\pi_{\|}$ and $\pi_{\perp}$ are the parallel and perpendicular linear polarizations with respect to [110] crystallographic direction, respectively. . . . . 50

6.6 The histograms of all the possible photon correlation measurements between the X, 2X, 3X and 4X emission lines. The red and blue curves correspond to the $\pi_{\|}$-$\pi_{\|}$ (co-polarized) and $\pi_{\|}$-$\pi_{\perp}$ (cross-polarized) configurations of the experiment, respectively. $\pi_{\|}$ ($\pi_{\perp}$) stands for the linear polarization that is parallel (perpendicular) to the [110] crystallographic direction. The black curves represent the data obtained without the polarization resolution. A zero delay time between the start and stop beam is indicated in each panel with a black dashed line. 51

6.7 (a) The excitation-power evolution of the micro-PL spectra of a single GaAlAs QD measured at $T$= 4.2 K. The spectra are excited above the barrier ($E_{exc}$=2.54 eV). $P_0$=1 µW and indicates the excitation power. The spectra are normalized to the intensity of the X emission line and vertically shifted for clarity purpose. (b) The dependence of the X, $X^-$, and $X^{2-}$ intensities on the excitation power. The dashed lines indicate the linear and quadratic behaviours as guides to the eye. (c) The energy of the X, $X^-$, and $X^{2-}$ lines as a function of the angle of a polarization analyser (points). The FSS of the X and $X^{2-}$ emission lines is determined by means of fitting the cosine-squared function (solid curves). . . . . 52

6.8 The $\delta_X$ as a function of the X emission energy for a series of single QDs, measured in a broad energy range. Blue (dash) dashed line is a guide to the eye. . . . . 53

6.9 (a) The anisotropy axis, $\theta_X$, of the neutral exciton state as a function of its energy. (b) A histogram of the $\theta_X$ obtained for a number of single dots under investigation. $0^o$ indicates the [110] crystallographic direction. . . . . 54

6.10 The energy evolution of the X (solid squares) and 3X (solid circles) emission lines highlighted on the gray-scale map of the QD emission in the magnetic field up to 19 T. The green and blue points illustrate the $\sigma_+$ and $\sigma_-$ polarizations, respectively. . . . . 55

6.11 The evolution of the diamagnetic shift of the X (blue squares) and 3X (green circles) emission lines in the magnetic field up to 19 T. The solid and dashed black curves result from fitting the experimental data with Eq. 6.1. . . . . 57

6.12 Zeeman splitting of X (blue squares) and 3X (green circles) emission lines in the magnetic field up to 19 T. The solid and dashed black curves result from fitting the experimental data with Eq. 6.2 in the range 0<B<8 T. . . . . 58

6.13 The magnetic field evolution of the single-particle hole energy levels as obtained from the photoluminescence experiment. The diagram adapted from Ref. 112.. . . . . 59

6.14 Micro-PLE spectrum of a single dot detected on the X emission line (dot with $\Delta_{s\text{-}p}$=12.63 meV). The scale of the horizontal axis is set by the energy relative to the X emission line. . . . . 60

6.15 Micro-PLE spectrum of a single GaAlAs QD detected on the X emission line (dot with $\Delta_{s\text{-}p}$=14.30 meV). The scale of the horizontal axis is set by the energy relative to the X emission line. . . . . 61

6.16 Micro-PLE spectra detected on the X emission line, measured for a series of QDs characterized by different amplitude of $\Delta_{s\text{-}p}$. The scale of the horizontal axis is set by the energy relative to the X emission line. The spectra are normalized to the most intense peaks and vertically shifted for clarity purpose. . . . . 62

6.17 The excitation-power evolution of micro-PLE spectra detected on the X emission lines (dot with $\Delta_{s\text{-}p}$=12.63 meV). The scale of the horizontal axis is set by the energy relative to the X emission line. The spectra are normalized to the most intense peaks and vertically shifted for clarity purpose. . . . . 63

6.18 The magnetic-field evolution of micro-PLE spectra detected on the X emission line (dot with $\Delta_{s\text{-}p}$=14.30 meV). The scale of the horizontal axis is set by the energy relative to the X emission line. The spectra are normalized to the most intense peaks and shifted for clarity purpose. 64

6.19 The magnetic-field evolution of micro-PLE spectra detected on the X emission line (dot with $\Delta_{s\text{-}p}$=14.30 meV). The scale of the horizontal axis is set by the energy relative to the X emission line. The spectra are normalized to the most intense peaks and shifted for clarity purpose. 65

6.20 The magnetic-field evolution of micro-PLE spectra detected on the X emission line (dot with $\Delta_{s\text{-}p}$=12.24 meV). The scale of the horizontal axis is set by the energy relative to the X emission line. The spectra are normalized to the most intense peaks and shifted for clarity purpose. 66

6.21 The magnetic-field evolution of micro-PLE spectra detected on the X emission line (dot with $\Delta_{s\text{-}p}$=16.97 meV). The scale of the horizontal axis is set by the energy relative to the X emission line. The spectra are normalized to the most intense peaks and shifted for clarity purpose. 67

6.22 A fan chart of the magneto-absorption transitions of the neutral exciton (dot with $\Delta_{s\text{-}p}$=14.30 meV). The relative energy is calculated with reference to the energy of the X emission line at zero magnetic field. The diamagnetic shift of this line is not corrected in panel (a) and extracted from the data in panel (b). . . . . 68

6.23 (a) The diamagnetic shift and (b) the Zeeman splitting of three resonant peaks: $R_1$, $R_2$, $R_3$ and the X emission line (dot with $\Delta_{s\text{-}p}$=14.30 meV). . . . . 69

6.24 Black horizontal lines illustrate the ladders of levels in the conduction and valence bands. The blue (red) arrows indicate the possible absorption transitions between the valence band levels and the $s$-shell ($p_-$-shell), respectively. . . . . 71

7.1 The excitation-power evolution of the micro-PL spectra of a single GaAlAs/AlAs QD measured at $T$= 4.2 K. The spectra are excited quasi-resonantly ($E_{exc}$=1.71 eV). $P_0$=10 µW and indicates the excitation power. The spectra are normalized to the intensity of the X emission line and vertically shifted for clarity purpose. . . . . 76

7.2 (a) The micro-PL spectra of a single GaAlAs QD recorded for two different linear polarizations: $\pi_x$ (violet curve) and $\pi_y$ (red curve) oriented along the crystallographic directions [110] and [1$\bar{1}$0], respectively. (b) Color plot presenting the micro-PL spectra of the same QD measured using different linear polarizations of detection. The 45 ° and 135 ° correspond to the crystallographic directions [110] and [1$\bar{1}$0], respectively. . . . . 77

7.3 Theoretical structure (not to scale) of various transitions that can be observed for a positively charged single QD. Two separate cascade pathways are shown in parts (a) and (b). The symbols $e_s$ ($h_s$) and $e_p$ ($h_p$) denote the electron (hole) occupying the $s$- and $p$-shell, respectively. The half-integers are the projections $J_z = J_z^e + J_z^h$ of the total spins. . . . . 78

7.4 The measured values of $\tilde{V}_{s,sp}^{eh}$ ($\tilde{V}_{sp,p}^{eh}$) as a function of the $X^{+*}$ ($^p2X^{+*}$) emission line energy for a series of single QDs. . . . . 79

7.5 The energy evolution of the emission lines attributed to the recombination of the positively charged excitons (dashed lines) superimposed on the colour-scale map of the QD emission in the magnetic field up to 14 T. The results of measurements performed with the $\sigma_+$ and $\sigma_-$ polarizations are shown with blue and red, respectively. . . . . 81

7.6 Theoretical structure (not to scale) of various positively charged transitions observed in a studied single QD in the presence of external magnetic field. The parts (a) and (b) describe two separate cascade pathways. The symbols $e_s$ ($h_s$) and $e_p$ ($h_p$) denote the electron (hole) occupying the $s$- and $p$-shell, respectively. The half-integers are the projections $J_z = J_z^e + J_z^h$ of the total spins. . . . . 83

7.7 The Zeeman splitting of the emission lines attributed to the recombination of the positively charged excitons in magnetic field up to 14 T. 84

7.8 Micro-PLE spectra of a single dot detected on the $X^+$ and $X^{+*}$ emission lines (dot with $\Delta_{s\text{-}p}$=14.30 meV). The grey vertical dashed lines indicate the energy of resonant peaks associated with the $X^{+*}$ line. The scale of the horizontal axis is set by the energy relative to the X emission line. The spectra are normalized to the most intense peaks and vertically shifted for clarity purpose. . . . . 84

7.9 Micro-PLE spectra detected on the $X^+$ and $X^{+*}$ emission lines, measured for a series of QDs characterized by different amplitude of $\Delta_{s\text{-}p}$. The scale of the horizontal axis is set by the energy relative to the X emission line. The black dashed lines indicate the evolution of the energy position of the resonant peak R*. The spectra are normalized to the most intense peaks and vertically shifted for clarity purpose. . . 85

7.10 Micro-PLE spectra of different series of QDs detected on the $X^+$ and $X^{+*}$ emission lines, measured for a series of QDs characterized by different amplitude of $\Delta_{s\text{-}p}$. The scale of the horizontal axis is set by the energy relative to: (left panel) the arbitrary chosen resonant peak and (right panel) the resonant peak R*. The black dashed lines indicate the evolution of the energy position of a given resonant peak. The spectra are normalized to the most intense peaks and vertically shifted for clarity purpose. . . . . 86

7.11 The excitation-power evolution of micro-PLE spectra detected on the $X^+$ (red curves) and the $X^{+*}$ (violet curves) emission lines (dot with $\Delta_{s\text{-}p}$=12.63 meV). The scale of the horizontal axis is set by the energy relative to the X emission line. The spectra are normalized to the most intense peaks and vertically shifted for clarity purpose. . . . . 87

7.12 The magnetic-field evolution of micro-PLE spectra detected on the $X^+$ emission line (dot with $\Delta_{s\text{-}p}$=14.29 meV). The scale of the horizontal axis is set by the energy relative to the X emission line. The spectra are normalized to the most intense peaks and shifted for clarity purpose. 89

7.13 The magnetic-field evolution of micro-PLE spectra detected on the $X^+$ emission line (dot with $\Delta_{s\text{-}p}$=14.30 meV). The scale of the horizontal axis is set by the energy relative to the X emission line. The spectra are normalized to the most intense peaks and shifted for clarity purpose. 90

7.14 The magnetic-field evolution of micro-PLE spectra detected on the $X^+$ emission line (dot with $\Delta_{s\text{-}p}$=16.97 meV). The scale of the horizontal axis is set by the energy relative to the X emission line. The spectra are normalized to the most intense peaks and shifted for clarity purpose. 91

7.15 The magnetic-field evolution of micro-PLE spectra detected on the $X^{+*}$ emission line (dot with $\Delta_{s\text{-}p}$=14.29 meV). The scale of the horizontal axis is set by the energy relative to the X emission line. The spectra are normalized to the most intense peaks and shifted for clarity purpose. 92

7.16 The magnetic-field evolution of micro-PLE spectra detected on the $X^{+*}$ emission line (dot with $\Delta_{s\text{-}p}$=14.30 meV). The scale of the horizontal axis is set by the energy relative to the X emission line. The spectra are normalized to the most intense peaks and shifted for clarity purpose. 93

7.17 The magnetic-field evolution of micro-PLE spectra detected on the $X^{+*}$ emission line (dot with $\Delta_{s\text{-}p}$=16.97 meV). The scale of the horizontal axis is set by the energy relative to the X emission line. The spectra are normalized to the most intense peaks and shifted for clarity purpose. 94

7.18 Black horizontal lines illustrate the ladders of levels in the conduction and valence bands. The blue (red) arrows indicate the possible absorption transitions between the valence band levels and the $s$-shell ($p_-$-shell), respectively. . . . . 95

7.19 The micro-PLE spectra detected on the $X^{+*}$ emission line (purple curves) and the micro-PL spectra (black curves) of a series of different QDs. The red dashed vertical lines indicate the energy of the resonant peak $R^*$ and the ${}^pX^{+*}$ emission line. The scale of the horizontal axis is set by the energy relative to the X emission line. The spectra are normalized to the most intense peaks and vertically shifted for clarity purpose. . . . . 97

7.20 The magnetic-field evolution of the micro-PLE spectra detected on the $X^{+*}$ emission line (the blue and red curves), superimposed on a gray-scale map displaying the micro-PL spectra of the same dot, plotted as a function of the magnetic field. $\Delta_{s\text{-}p}$=14.29 meV. The scale of the horizontal axis is set by the energy relative to the X emission line. The spectra are normalized to the most intense peaks and vertically shifted for clarity purpose. . . . . 98

7.21 Black horizontal lines illustrate the ladders of levels in the conduction and valence bands. The green solid (open) circles represent the electrons (holes). The red-black vertical arrow indicates the absorption-emission process of the $e$-$h$ pair. . . . . 99

7.22 The micro-PLE maps measured at: (a) 0 T, (b) - (e) 9 T. The white dashed horizontal (vertical) lines indicate the position of the split components of the $X^{+*}$ emission line (the resonant peak R*). The excitation/detection polarizations are: (b) $\sigma_-/\sigma_+$, (c) $\sigma_+/\sigma_+$, (d) $\sigma_-/\sigma_-$, (e) $\sigma_+/\sigma_-$. . . . . 100

7.23 Theoretical structure (not to scale) of two states related to the resonant peak R* and the $X^{+*}$ emission line. The symbols $e_s$ ($h_s$) and $e_p$ ($h_p$) denote the electron (hole) occupying the $s$- and $p$-shell, respectively. The half-integers are the projections $J_z = J_z^e + J_z^h$ of the total momentum. . . . . 101

8.1 The excitation-power evolution of the micro-PL spectra of a single GaAlAs/AlAs QD measured at $T$= 4.2 K. The spectra are excited quasi-resonantly ($E_{exc}$=1.71 eV). $P_0$=10 µW and indicates the excitation power. The spectra are normalized to the intensity of the X emission line and vertically shifted for clarity purpose. . . . . 106

8.2 The energy of the $X^-$ and $X^{2-}$ emission lines as a function of the angle of a polarization analyser (points). The FSS of the $X^{2-}$ emission line is determined by means of fitting the cosine-squared function (a red solid curve). . . . . 106

8.3 Micro-PLE spectrum detected at the energy of the recombination of the negatively charged exciton. $\Delta_{s\text{-}p}$=14.30 meV. The scale of the horizontal axis is set by the energy relative to the X emission line. . . 107

# List of Tables

6.1 The $z$ projections ($m_{h,z}$) of the envelope angular momentum and the charge density weights associated with each $J_{h,z}$ component of the three lowest-lying SP hole states at $B$=0. Only the states with positive $F_{h,z}$ are shown. States with negative $F_{h,z}$ have reversed order of weights and $m_{h,z}$, as well as the opposite sign of $m_{h,z}$. All the values collected in the table are taken from Ref. 111. . . . . 58